Laboratory study on mechanical properties of frozen clay through state concept

土骨格状態概念に基づく凍結粘土の力学的挙動の実験的研究

By

Jinyuan WANG

A thesis submitted in partial fulfilment of the requirements for the degree of Doctor of Philosophy in Engineering

Soil Mechanics Laboratory
Division of Field Engineering for the Environment
Graduate School of Engineering
Hokkaido University
June, 2017

ABSTRACT

Towards development of a mechanical model that can be part of multi-physical analysis of frozen soils, a program of systematic frozen-unfrozen parallel triaxial tests at different temperatures and strain rates was conducted. The mechanical behavior of the reconstituted high-plasticity clay samples was investigated and interpreted through state concept based on Ladanyi and Morel's (1990) postulate on the unique relationship between the inter-particle "effective" stress and the strain path.

To begin with, constant-condition (i.e., constant strain rate and temperature) compression tests were conducted on frozen Kasaoka clay specimens with normal consolidation prior to freezing. With other conditions set identical, the shear strength linearly increased with a decrease in temperature for the range from -10°C to -2°C, and log-linearly increased with an increase in the strain rate for the range from 0.001%/min to 0.1%/min. Direct comparison of the strain-rate effects between frozen and unfrozen specimens with identical strain paths and states in the soil skeleton clearly indicates that the viscoplasticity derives from that of pore ice. The Critical State lines (CSLs) for clay specimens frozen undrained were mapped by referring to the shear behavior of unfrozen specimens sharing the same strain history. Moreover, reduction of confining pressure after stabilized freezing of frozen specimens turned out to have no significant effect on critical state strength of frozen clay.

By varying-temperature and varying-strain rate compression tests, consistency of stress-strain curves was observed at large strains between varying- and constant-temperature conditions, and less clearly, between varying- and constant-strain rate conditions. The latter observation, if further confirmed, may lead to isotach formulation of strain rate effects for the investigated range of strain rate (i.e. up to 0.1%/min), where the behavior is largely ductile.

Finally, a nondestructive testing method mainly focusing on measurements of stiffness is developed. Different temperatures and axial strain rates were applied in order each time after the specimen was loaded and unloaded in quasi-elastic strain ranges. In the investigated range of conditions, the shear stiffness, averaged from the multiple probes of the same condition, increased linearly with the decrease in temperature, and increased linearly with the logarithmic increase of strain rate.

The above observations of behavioral features of frozen and unfrozen soils, with further experimental work, are expected to lead to construction of a unified framework for describing the behavior under both states and transition between them.

Keywords: Frozen clay, strain rate effect, temperature effect, effective stress path, critical state, small-strain stiffness

ACKNOWLEDGEMENTS

First and foremost, I wish to extend my sincere gratitude to my PhD supervisor, Dr. Satoshi Nishimura, for his consistent support, guidance and understanding throughout my doctoral research. I have learned a lot from him. His broad knowledge and brilliant insights, his passion to scientific research, and his strict principle on details will benefit my whole life.

Thanks are also due to all members of doctoral committee, Prof. Yoshiaki Fujii and Prof. Tatsuya Ishikawa for their comments and help.

I would also like to express my sincere gratitude to Prof. Hiroyuki Tanaka and Prof. Yoichi Watabe for their advices given in this research during laboratory seminars and discussions. The help of Dr. Fumihiko Fukuda and Mr. Yutaka Kudoh in this research is also appreciated.

I wish to thank Mr. Watari Takahashi, Mr. Tsubasa Sasaki and Mr. Bhakta Raj Joshi for their assists in performing temperature-controlled triaxial compression tests.

I would also like to express my sincere gratitude to all members of students in Soil Mechanics lab for their help in this research.

I'm also grateful to the scholarship granted by Chinese Scholarship Council (CSC), which supported my PhD study and research work.

Last but not least, I wish to express my personal thanks to my family members for their consistent support and encouragement throughout this study. Especially, my wife (Ms. Shihuan Bi) accompanied me during the second half of PhD study. She looks after me well so that I can concentrate on the experimental work and research. Her considerate and encouraging words make me go through hardship and achieve great progress in the research. I'm indebted to her. This thesis is by all means dedicated to her.

TABLE OF CONTENTS

1. INTRODUCTION

1.1. BACKGROUND

For frozen soil, there is a dispute on its definition. One popular definition is that frozen soils are the soils and rocks with a temperature at or lower than 0 ^{o}C and with ice content (Zhou et al., 2001). Andersland and Ladanyi (2004) gave another definition, which regards the frozen ground as soil or rock with a temperature below 0 ^{o}C. Their definition is based entirely on temperature regardless of the existence of the water and ice content. In this study, frozen soils are understood based on the first definition and the experimental behavior of frozen soil with a certain content of water and ice was researched. A saturated frozen soil without air phase at a microscopic level is illustrated in **Figure 1-1**.

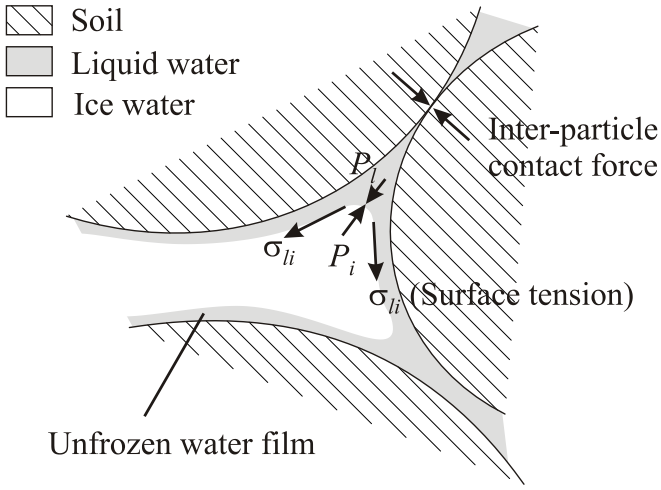

Figure 1-1 Micro-configuration of phases in water-saturated frozen soils, with pressures P and surface tension σ_{li} (after Nishimura et al., 2009)

Frozen soil is widely distributed on earth. All kinds of frozen soil and permafrost areas account for 50% and 25% of the continent area, respectively, which are mainly distributed in 48 countries, such as Russia, America, Canada, China and so on (Zhang et al., 2006). In Japan, there are continuously and discontinuously covered permafrost distributed in several mountain peaks from Chubu to Northeast of Japan and most areas of Hokkaido. The existence of permafrost in the peak of Mount Fuji and Mount Daisetsu has been confirmed (Fukuda and Kinoshita, 1974).

Due to the need of social and economical development, highway, mineral engineering and energy facility constructions have been conducted in frozen soil regions. In 1904, the 9446 kilometres long Siberia Railway was constructed in Russia. For mineral and forest exploitation, a highway going across Alaska and Canada was constructed in 1942 (Jiao, 2011).The Trans-Alaska Pipeline System

(TAPS), one of the world's largest pipeline systems, was built between 1974 and 1977 to meet the need of crude-oil after the 1973 oil crisis. The construction of the pipeline, one of the first large-scale projects to deal with problems caused by permafrost, led to developments of special construction techniques to cope with the frozen ground. On the other hand, freeze-thaw process aggravates the soil surface conditions and leads to structural failure such as slope failure caused by thawing of frozen soil, as shown in **Figure 1-2**, as well as affecting trafficability on soft soils. For example, the slope failure in the thaw season occupies 26% of the total number of slope failures in Hokkaido, Japan, for the past 14 years (Ishikawa et al., 2015). In warmer regions, useful aspects of frozen soil such as the stability, high strength and impervious conditions are utilized in geotechnical engineering projects involving shafts, tunnels, and deep foundations with poor ground conditions by artificial ground freezing, as illustrated by **Figure 1-3**.

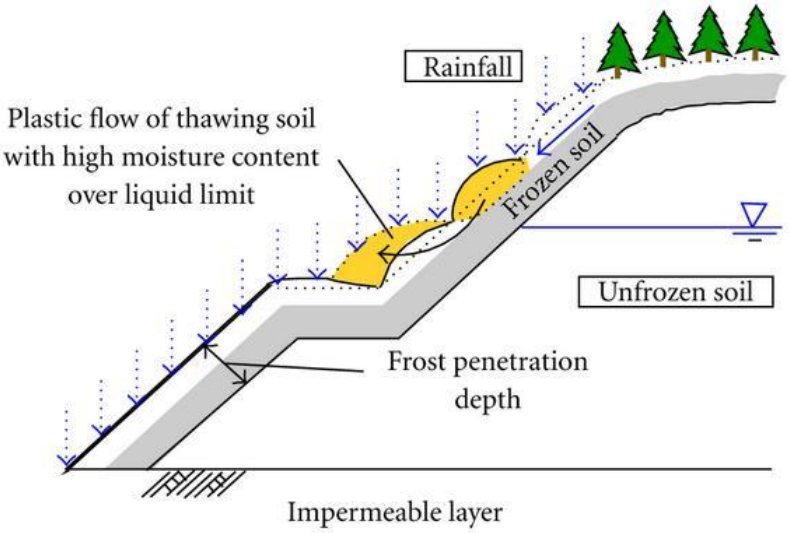

Figure 1-2 Slope failure caused by freeze-thaw process (from Kawamura et al., 2011)

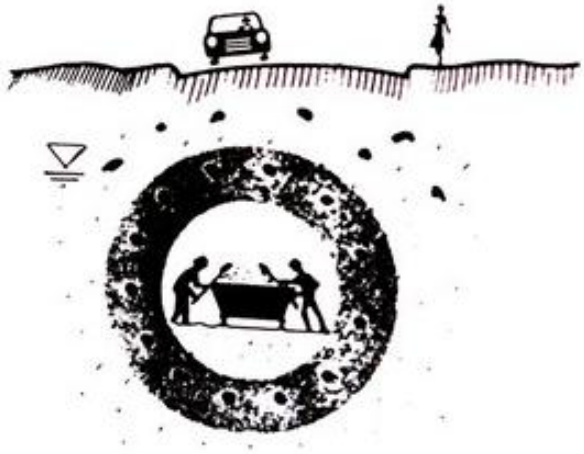

Figure 1-3 Artificial ground freezing applied in tunneling (the shaded part representing frozen wall, from Andersland and Ladanyi, 2004)

In frozen soil engineering, the safety and stability of engineering can be ensured only if the frozen soil has enough ability to resist failure and deformation under the action of external loads. The ability of frozen soil to resist failure is determined by its strength and deformation characteristics, or stress-strain relationship. Both of them are main research subjects of frozen soil mechanics, and also important information for design, construction and maintenance of frozen soil engineering (Lai et al., 2013). A further study of mechanical behavior of frozen soils is therefore crucial.

The mechanical properties of frozen soils are influenced by soil characteristics (which is determined by their components of soil particles, unfrozen water, ice content and gas) and, states and conditions (including strain rate, temperature, stress and strain history as well as confining pressure, etc.). In terms of strain rate and temperature effects on mechanical behavior of frozen soils, it has been well researched for conditions at constant strain rate and constant temperature (Andersland and Akili, 1967; Ladanyi, 1972; Hooke et al., 1972; Andersland and Ladanyi, 2004; Arenson and Springman, 2005a). But it has not been well established how frozen soils respond to general changes in the imposed strain rates ranging over different orders (Wang and Nishimura, 2015). Such rate changes are considered to be common in many geotechnical processes.

In addition to strength and stress-strain behavior at large strains, the mechanical behaviors at small and very small strain ranges are also very important. Whereas the factors controlling the small strain response are well understood for unfrozen soils, there have been few studies (Wang et al., 2007; Lee et al., 2016) dealing with the small-strain stiffness of frozen soils. In the existing studies on stiffness of frozen soils, the small-range stiffness characteristics were derived from external displacement measurement, which was prone to have errors attributed to reasons such as compliance of the load cell

and bedding-in of sample ends (Jardine et al., 1984). A new way to obtain the measurement of axial strain in small range is desired.

When studying the mechanical properties of frozen soils through experiments, many researchers in past neglect the link between frozen and unfrozen soils. Frozen soils usually form from unfrozen soils, and the stress/strain state and its history are likely to be still relevant to frozen soils. However, the consolidation history and states of soils before freezing have frequently been neglected in exploring frozen soil's behavior. A majority of triaxial tests of frozen soils reported in the literature is classified as unconsolidated-undrained tests (Andersland and Ladanyi, 2004), with a limited exceptions that include consolidation before freezing (Goodman, 1975; Ma and Chang, 2002; Wang et al., 2004). Specimens were mostly prepared in split rigid molds by compaction (for sands and sometimes clays) (Baker, 1976; Ladanyi and Morel, 1990; Wang et al., 2008; Lai et al., 2010) or pre-consolidated from slurry and then frozen under no confinement (e.g. Joshi and Wijeweera, 1990). The specimens' consolidation history before freezing, i.e. normally consolidated or over-consolidated, was not always well-defined in these tests. The effects of strain rate, temperature or confining pressure on mechanical behavior of frozen soil concluded from these tests are therefore not sufficiently convincing.

While unsaturated soil mechanics has been advanced by succeeding in experimentally measuring and controlling physical variables of multiple phases, such as pore water and air pressures (e.g. Fredlund and Rahardjo, 1993), the same approach turns out to be very difficult in frozen soils. It is technically problematic to measure the pore water and air pressure in frozen soil tests, resulting in the popularity of total stress principle applied in frozen soil mechanics though effective stress is dominant for unfrozen soil. As far as ground freezing and thawing is concerned, which involves moving freezing boundaries and soil element undergoing transition between frozen and thawed states, it is inconvenient to apply different variables and total/effective stress principle to analyze frozen and unfrozen states separately. A framework that encompasses both frozen and unfrozen soil mechanics in a unified manner through common variables is thus desired to enable proper coupled analysis of ground freezing and thawing.

1.2. OBJECTIVES AND RESEARCH APPROACHES

This study has the following four objectives:

(1) to establish a link between the behavior of unfrozen and frozen soils via common state variables.

(2) to quantify general effects of temperature and strain rate on the strength characteristics of frozen soil at well defined states.

(3) to establish laboratory experimental routines and apparatus enabling the investigation and highlight the importance of frozen-unfrozen parallel testing.

(4) to understand the stiffness characteristics of frozen soil in the above context with an newly developed, accurate measurement system.

To realize the above objectives, two out of five series were dedicated to frozen-unfrozen parallel testing, in which triaxial compression tests on Kasaoka clay in unfrozen and frozen states were conducted. The consolidation and swelling histories were deliberately controlled to be almost same for the both states and the shear was carried out at constant strain rate and constant temperature. One series of frozen soil tests with reduction of cell pressure after stabilized freezing was conducted to explore further the individual effect of pore pressure on the mechanical behavior of frozen soils. Through one series of frozen soil tests at varying-strain rate or varying-temperature condition, together with the frozen soil tests at constant strain rate and constant temperature, the general effects of temperature and strain rate on the strength behavior were quantified. Nondestructive cyclic constant strain rate test in the elastic range of frozen soil were conducted to research the stiffness characteristics of frozen soil based on a semi-local measurement of axial strain.

1.3. OUTLINE AND ORGANIZATION OF THE DISSERTATION

This dissertation is divided into seven chapters. The first chapter presented the background and objective of this study. The second chapter introduces the state of the art of mechanical study of frozen soil including factors affecting shear strength and stiffness characteristics of frozen soil, experimental methods on frozen soils and the existing models for describing frozen soil behaviors. The third chapter describes the tested material and triaxial apparatus employed in this research. The testing conditions and procedures are introduced. Nuclear magnetic resonance (NMR) measuring unfrozen water content in frozen soil is also described. The fourth chapter discusses the characteristics of unfrozen soil behavior, which lays a foundation for the following parallel frozen-unfrozen testing and interpretation. The fifth chapter shows the strength characteristics of frozen soil under the effects of strain rate and temperature. General effects of temperature and strain rate on the strength characteristics of frozen soil at well defined states are also addressed and quantified. Critical State lines (CSLs) for frozen soils are mapped by referring to the shear behavior of unfrozen specimens sharing the same strain history. Frozen soil tests with reduction of cell pressure after stabilized freezing were conducted to interpret the CSLs. The sixth chapter presents the stiffness characteristics of frozen soil. The new approach to investigate the stiffness is examined. Effects of temperature and strain rate on the initial shear stiffness are then presented. Finally, the last chapter draws conclusions for the findings in this research and proposes some recommendations for future research.

2. LITERATURE REVIEW ON MECHANICAL CHARACTERISTICS OF FROZEN SOILS

A literature review on mechanical characteristics of frozen soils is presented in this chapter. The first section addresses the experimental results exploring factors which influence the shear strength of frozen soils. The second section reviews the experimental studies on stiffness characteristics of frozen soils. A review on experimental methods is then summarized. In the end, discussions on the constitutive models for simulating the mechanical behaviors of frozen soils are presented.

2.1. FACTORS AFFECTING SHEAR STRENGTH OF FROZEN SOILS

The mechanical properties of frozen soil are largely influenced by variations in strain rate, temperature, stress path, stress/strain history, stress level and soil characteristics such as mineralogy, particle size, frozen and unfrozen water contents, salinity and organic content (Ting et al., 1983; Lai et al., 2013). The influence of these factors on mechanical properties of frozen soil will be reviewed in the following paragraphs.

With a viscoplastic constituent (ice) in their pores, frozen soils exhibit pronounced rheological behavior. Early studies on the rheological characteristics of frozen soils mainly focused on the creep behavior under sustained stresses or the stress responses against constant strain rates (Andersland and Akili, 1967; Ladanyi, 1972). The unconfined and triaxial compression tests on frozen soils confirmed the notable dependency of shear strength on strain rate (Haynes et al., 1975; Zhu and Carbee, 1984; Arenson et al., 2004). Haynes et al. (1975) found that the strength of frozen soils linearly increase with increasing strain rate. But Bragg and Andersland's (1981) uniaxial unconfined compression test results on well-graded sand demonstrated that the peak strength of frozen soil increased with increasing strain rate and then converged to a constant value at the strain rate of 0.06%/min or more, as shown in **Figure 2-1**. Choi (2011) found that the peak strength of a sand-clay mixture became independent of strain rate when it exceeded 33.33%/min. On the other hand, many researchers found that compressive strength increases linearly with an increase in strain rate on a log-log scale (e.g. Sayles and Epanchin, 1966; Baker, 1979; Parameswaran, 1980; Arenson et al., 2004). The strain rates employed in these studies were often very high, ranging from 10^{-3} to 1 %/sec, although some researchers attempted imposing lower rates (5.69×10^{-5} to 1.78×10^{-1} %/sec by Bragg and Andersland, 1981 and 9×10^{-5} to 4.07×10^{-3} %/sec by Arenson and Springman, 2005a). It has not been well established how frozen soils respond to general changes in the imposed strain rates ranging over different orders of magnitudes. Such rate changes are considered to be common in many geotechnical processes. Generalized theories have been successfully adopted to describe the time-dependent nature of unfrozen soils. For example, the isotach law describes viscous behavior that stress-strain behavior

tends to accommodate itself to the shift of strain rates (see **Figure 2-2(a)**) (Šuklje, 1957; Leroueil, 2006). Perzyna (1962) adopted the overstress concept (defined as the excess of the instantaneous stress over the stress on the quasi-static curve evaluated at the same plastic strain, illustrated in **Figure 2-2(b)**) to describe the rate effect for plastic materials. But their applicability remains largely unexplored for frozen soils, due to lack of well-established means of defining the inter-particle stress, with a few recent exceptions described later.

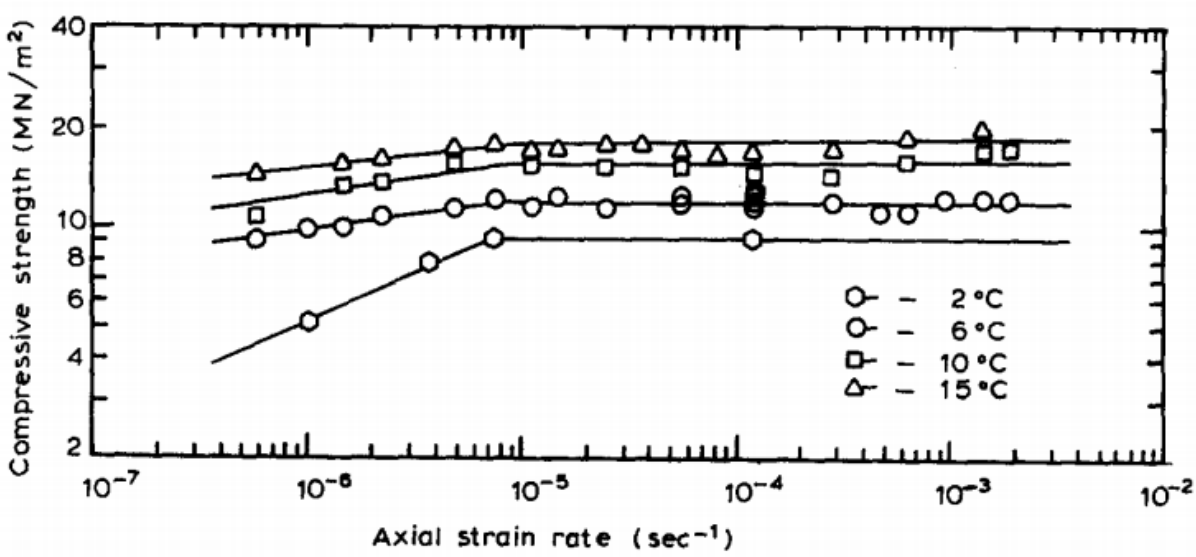

Figure 2-1 Compressive strength vs. strain rate (from Bragg and Andersland, 1981)

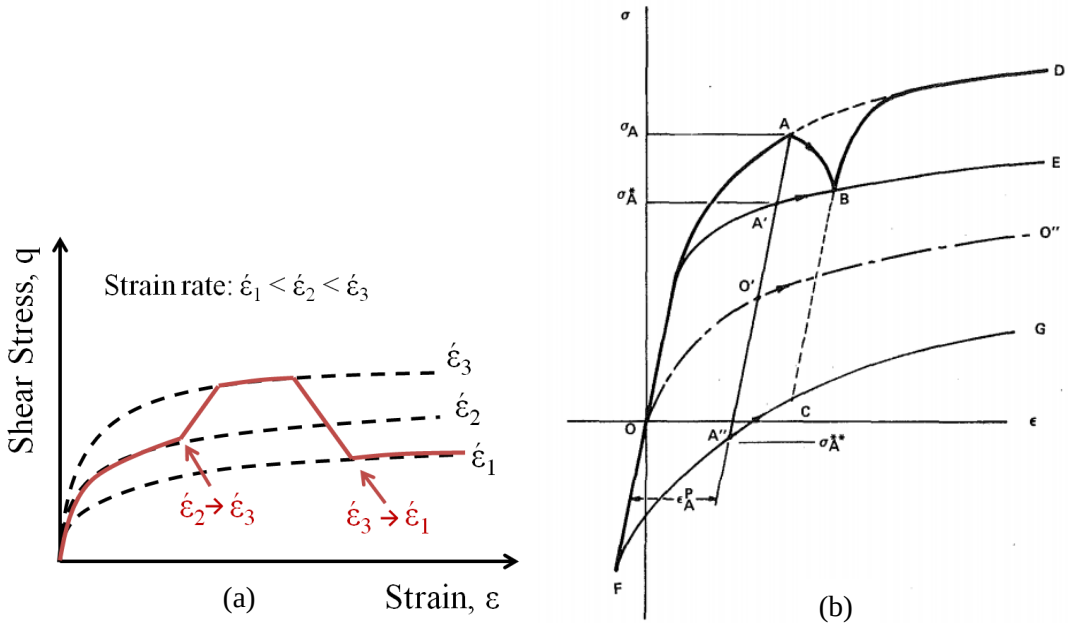

Figure 2-2 Illustrations of generalized theories describing the time-dependent nature of unfrozen soils (a) isotach law (b) overstress concept (represented by $\sigma_A - \sigma_A^*$, where σ_A and σ_A^* are both corresponding to the plastic strain ε^p_A, after Eisenberg and Yen, 1981)

The strain rate and temperature have intertwined effects; for example, Akili (1971) and Zhu and Carbee (1984) both found that the peak strength of frozen soils was very sensitive to temperature and applied strain rate simultaneously. Bragg and Andersland (1981) and Li et al. (2004) conducted unconfined compression tests on frozen sand and clay, respectively, and concluded that the unconfined compressive strength increased with increasing strain rate and descending temperature. The confining stress and the above two factors seem to have sometimes related, sometimes independent effects. Chamberlain et al. (1972) investigated the effects of confining pressure on the shear strength and found its great influence on the shear strength of frozen soils. Hohmann-Porebska (2002) noted that the temperature effects on the shear strength were mainly reflected in the cohesion rather than the frictional component. Arenson and Springman (2005b) suggested that the volumetric ice content influences both internal friction angle and apparent cohesion, but only the latter seems to be influenced by the temperature and the applied compression strain rate. Zhang et al. (2016) found that the compressive strength of ice-rich silty sand varied with confining pressure and volumetric ice content. The strength increased with increasing confining pressure for volumetric ice contents below 50.2% or larger than 75.0% but remained nearly constant at various confining pressures for volumetric ice contents ranging from 50.2% to 75.0%, as shown in **Figure 2-3**. In addition to the above, there have been many other studies investigating the individual and combined effects of strain rate, temperature, density and stress levels (Goughnour and Andersland, 1968; Sayles and Haines, 1974; Aas, 1981; Wang et al., 2004; Lai et al., 2010).

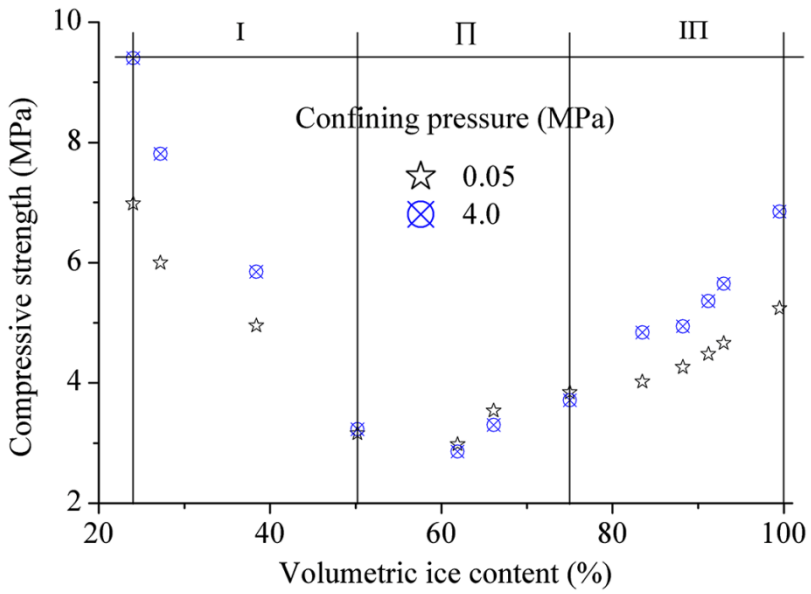

Figure 2-3 Plot of the transition zone of triaxial compressive strength as a function of volumetric ice content (from Zhang et al., 2016)

2.2. STIFFNESS CHARACTERISTICS OF FROZEN SOIL

Knowing the stiffness characteristic of soil mass is indispensable in the design of all underground excavations. It is vital in the calculation of movement of superstructures above the ground and their respective soil-structure interaction (Atkinson, 2000; Sharma and Fahey, 2003). The ground deformation in response to the load is determined by the soil stiffness. The stiffness parameter widely adopted for design is shear modulus or Young's modulus in a form of tangent or secant values at an appropriate point on a stress-strain curve. Factors such as compliance of a load cell, bedding-in of the sample and non-parallelism of sample ends result in loss of accuracy in the measurement of axial displacement, as shown in **Figure 2-4** (Jardine et al., 1984). It causes inaccurate determination of stiffness values. Therefore, various techniques have been developed to improve the strain measurement. For example, measurement of local deformation can be realized by using linearly variable differential transformers (LVDTs) (Cuccovillo and Coop, 1997), Local Deformation Transducers (LDTs) (Goto et al., 1991), gap sensors (Kokusho, 1980), etc., gauging a central part of a sample directly.

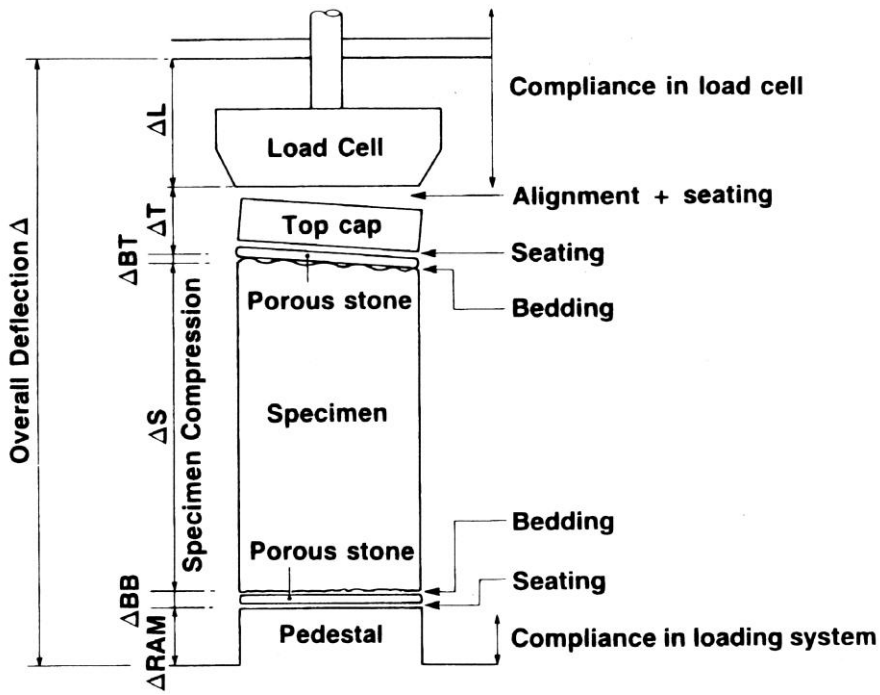

Figure 2-4 Sources of errors in the measurement of axial displacement (from Jardine et al., 1984)

Whereas the factors controlling the small strain response are well understood for unfrozen soils, there have been few studies dealing with the small strain stiffness of frozen soils. Wang et al. (2007) found that the Young's modulus (represented by secant stiffness in the strain level of 0.05%) of deep artificially frozen K_0-consolidated loess in triaxial compression tests was strongly dependent on the depth of stratum (i.e. confining pressure) and the freezing temperature, as shown in **Figure 2-5**. They

also found that higher Young's modulus was exhibited by frozen soil samples compared to unfrozen saturated soil samples under similar condition (i.e. without freezing stage after K_0 consolidation compared to frozen soil samples) and its variation with the initial confining pressure was much larger than that of unfrozen soils, as shown in **Figure 2-6**. Their study has drawbacks that the specimen was not allowed to consolidate by closing the drainage valve once the specified initial confining pressure was reached and thus not sufficiently consolidated for both frozen and unfrozen tests. The conditions of frozen and unfrozen soils were not comparable because no process in unfrozen soil tests can be analogous to the expansion caused by the freezing process in the frozen soil tests. Lee et al. (2016) researched the strain rate effects on secant deformation modulus of artificial frozen sand under the unconfined compression mode (i.e. secant Young's Modulus), E_{50}, which is determined from the secant line to the point where the stress is half of the peak stress in the stress-strain curve. They found that for all the tested temperatures the maximum and minimum E_{50} occurred at the fastest and slowest strain rate, respectively, and the increments of E_{50} tended to gradually decrease when strain rate exceeded a certain strain rate while E_{50} still presented a gradual increase with the strain rate above this level. The effects of strain rate on the deformation moduli, were more pronounced at lower temperatures for the range of -15°C and -5°C. However, E_{50} is an elasto-plastic stiffness rather than the desired small-strain initial stiffness. The above two studies describe some aspects of the stiffness characteristics from the viewpoints of confining pressure, strain rate and temperature. However, both of them adopted traditional external measurement on strain rather than on-specimen measure on local deformation, and must have inevitably underestimated the magnitude of the stiffness.

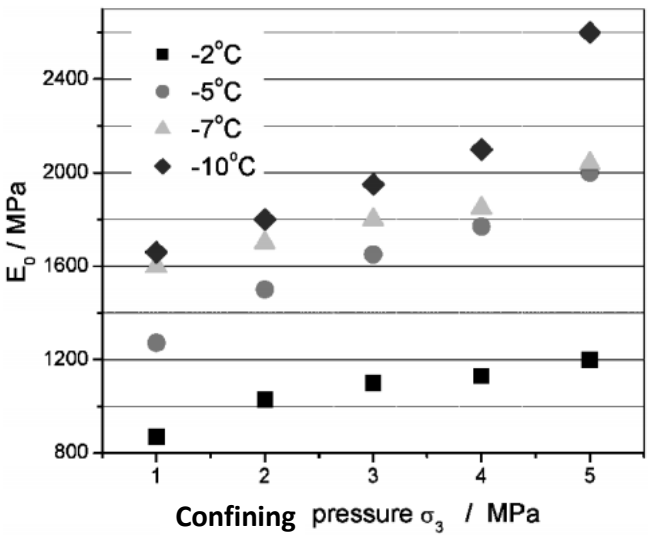

Figure 2-5 Variation of Young's Modulus (with the strain level of 0.05%) plotted against initial confining pressure at different freezing temperatures (from Wang et al., 2007; misspelling in the axis title corrected by the author)

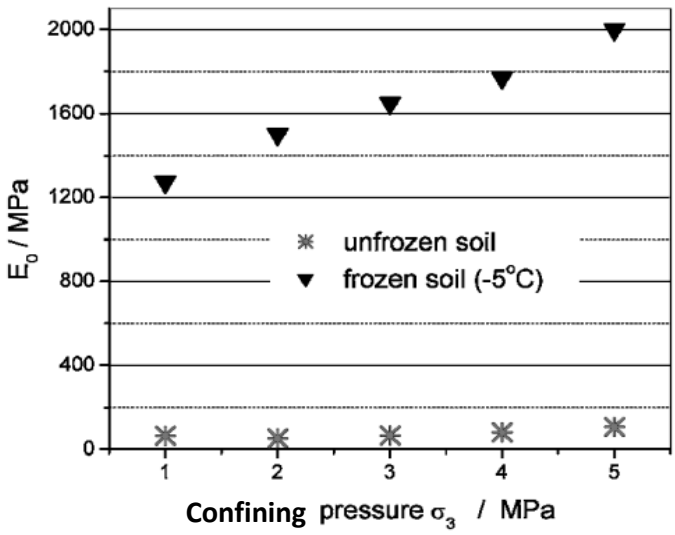

Figure 2-6 Variations of Young's Modulus (with the strain level of 0.05%) of frozen soil and unfrozen loess plotted with initial confining pressure (from Wang et al., 2007)

In addition to monotonic loading tests on frozen soils, many researchers have conducted in-situ measurements of wave speed, laboratory tests of dynamic loading, resonant-column tests, and wave-speed studies to explore the dynamic parameters of frozen soils (Liu et al., 2016). Li et al. (1979) performed strain-controlled cyclic tests on ice-saturated samples, demonstrating that the dynamic Young's modulus increased with increasing frequency, confining pressure and sand content but decreased with increasing strain and temperature. Al-Hunaidi et al. (1996) employed the resonant-column test method on frozen soil samples and found that the dynamic shear moduli of the frozen specimens were significantly greater than those of the unfrozen specimens. Wang et al. (2006) applied acoustic wave methods to investigate the physical-mechanical properties of frozen clay, frozen loess and frozen fine sand. They revealed that the dynamic shear stiffness increased with decreasing temperature and frozen soil with coarser grains had a larger increase rate of stiffness with reducing temperature.

2.3. EXPERIMENTAL METHODS ON FROZEN SOIL

A review on frozen soil experiments in past is summarized. Frozen soil experiments vary in sample preparation method, loading method, freezing method and soil type.

Naturally frozen soil sample may be tested to characterize the mechanical behavior. Watson et al. (1973) conducted a comprehensive study on strength of permafrost by using large permafrost core samples taken from the field. Arenson et al. (2003) performed triaxial compression tests on cored alpine permafrost and artificially frozen samples. The sampling and conservation of natural frozen soil turned to be expensive. Later, Arenson et al. (2004) found that artificially prepared frozen soil

exhibited very similar stress-strain behavior in triaxial tests to those of undisturbed naturally frozen samples. Therefore, artificially prepared frozen soil samples are sometimes considered acceptable to be used in the research of the mechanical characteristics through repeatable shear and creep tests (Watson et al., 1973).

Most sand samples as well as some clay or silt samples were prepared by compaction in laboratory. A pre-weighed soil fraction was mixed with water or ice. It was compacted in layers in a split mould. Then the sample was saturated with de-aired distilled water prior to freezing (e.g. Baker, 1979; Parameswaran and Jones, 1981; Landanyi and Morrel, 1990; Yamamoto and Springman, 2014). This method of preparing samples makes the initial state unknown (the void ratio can be known but the initial effective stress, over-consolidation ratio, etc. cannot be known without additional tests, due to a lack of knowledge of the consolidation history and the preconsolidation pressure. Aware of this problem, Wang et al. (2008) prepared the sample by compaction into a mould and then restored the sample to in-situ state by K_0 consolidation without lateral deformation by increasing axial and radial pressures simultaneously (as shown in **Figure 2-7**). After dropping the test temperature to a certain degree and keeping the temperature for almost 20 hours, they performed the axial loading tests until the specimen failure. Joshi and Wijeweera (1990) prepared saturated soil sample by using slurry consolidation technique in a consolidometer. They prepared samples with different water contents by consolidating the initially de-aired slurry under various vertical pressures. Before freezing, the samples were normally K_0 consolidated sample.

As previously mentioned, most tests in past froze the samples which were prepared by compaction and unclear about their consolidation history. Some researchers took into account the in-situ condition and applied K_0 consolidation to the samples before freezing (e.g. Wang et al. 2008; Joshi and Wijeweera, 1990). To avoid the anisotropy and simplify the testing method, isotropic consolidation may be desired. The freezing method can be either unidirectional freezing or isotropic freezing. Unidirectional freezing simulates the practical process in the frozen ground subjected to downward freezing from ground surface. However, unidirectional freezing is difficult to assure quick freezing on the specimen and inconvenient in triaxial compression tests. All-round isotropic freezing does not have this problem. It can also ensure the temperature of the sample uniform throughout.

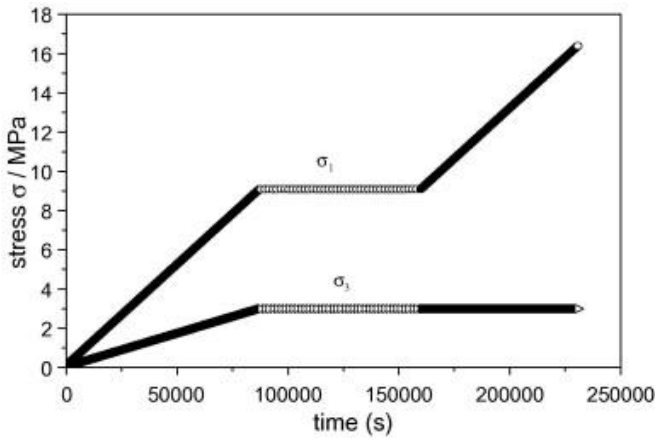

Figure 2-7 Testing procedures for triaxial testing in Wang et al. (2008)

2.4. CONSTITUTIVE MODELS DESCRIBING MECHANIC BEHAVIORS OF FROZEN SOILS

Constitutive models are needed to describe the complicated mechanical behavior of frozen soils (He et al., 2000). Total stress-based models for frozen soils (e.g. Arenson and Springman, 2005b; Lai et al., 2010; Xu, 2014) tended to attach too much importance to the confining pressure affecting the elastoplastic behavior. Due attention was not sufficiently paid to the influence of other very important factors such as temperature and ice content. Such models cannot simulate deformations under changing temperature and resultant variation of ice content during soil freezing or thawing (Ghoreishian Amiri et al. 2016). Effective stress-based models have also been proposed. The effective stress was defined as the excess of the total stress over pore pressure. Li et al. (2008) obtained the pore pressure as combination of unfrozen water pressure, ice pressure and air pressure. However, their approach becomes inexpedient when dealing with ice-rich loose frozen soils, whose strength gets drastically underestimated by their single stress variable of effective stress (Nishimura et al., 2009). Thomas et al. (2009) preferred to alternate between unfrozen water and ice pressure in partially frozen and fully frozen states, respectively, to represent pore pressure. Their approach provides practical simulation to ice segregation phenomenon during a freezing period whereas cannot yield soil strength well.

Instead of sticking to a single stress variable, Nishimura et al. (2009) firstly proposed a two-stress state variables model for describing the behavior of frozen soils by adopting the net stress (as the excess of total stress over ice pressure) and the cryogenic suction as stress variables. The model reduces to an effective stress-based critical state model by replacing ice pressure with pore water pressure when deriving net stress for unfrozen soils. Hence, continuity is achieved between this constitutive model for frozen soils and the effective-stress constitutive models applied to unfrozen

soils, which is desired in tackling with boundary value problems involving both states and transitions between them.

While the aforementioned modeling approaches have been proposed (e.g. Li et al., 2008; Nishimura et al., 2009; Casini et al., 2014; Ghoreishian Amiri et al., 2016), experimental supports to these have been severely limited. To provide such experimental supports to constitutive models encompassing frozen and unfrozen states, frozen-unfrozen parallel testing may be necessary. Noting the technical difficulty in measuring the internal variables in frozen soils, Ladanyi and Morel (1990) postulated uniqueness of the effective stress path - strain path relationship in frozen and unfrozen soils. With this postulate, the effective stress, or the inter-particle stress in frozen soils may be estimated by subjecting frozen and unfrozen soil specimens to a common strain path. Once the effective stress is estimated, albeit with the hypothesis that still needs to be tested in macro- and microscopic perspectives, it will open up a way to bridge frozen and unfrozen soil behavior descriptions.

3. MATERIAL AND TESTING METHOD

3.1. TESTED MATERIAL

Commercially available high-plasticity Kasaoka Clay was selected as sample for triaxial tests in frozen and unfrozen states. To avoid the formation of ice lensing of tested specimens during freezing, this study selected fine-grained material, clay, which has low permeability. The pore water tends to move towards the freezing front. But if the permeability is too low, no ice lens forms as the unfrozen water movement is suppressed. Although coarse-grained materials such as sand do not form ice lenses, frozen sand has been more frequently investigated than frozen clay in past and is much less sensitive to stress history and over-consolidation, therefore not the best material to appreciate the proposed objectives. Because of the uniformity, availability and fine gradation, Kasaoka Clay was selected. Its grain size distribution curve is shown in **Figure 3-1**. The main chemical components are SiO_2 (58.0%), Al_2O_3 (8.2%) and Fe_2O_3 (4.5%) (data from Kasanen Industry Co. Ltd). The specific gravity is 2.65, and the liquid limit and plastic limit are 62% and 28%, respectively. The samples were K_0 reconstituted from slurry with a water content of 100% (i.e. 1.6 times the liquid limit) under a preconsolidation pressures, σ_{v0}'=50, 100 or 200 kPa. The preconsolidation process was conducted in the consolidometer shown in **Figure 3-2**. This process takes about one week, 10 days or two weeks to reach the preconsolidation pressures, respectively. The preconsolidated cake was trimmed to form a triaxial specimen with a diameter of 30mm for frozen tests or 50mm for unfrozen tests, both with an aspect ratio of 2.

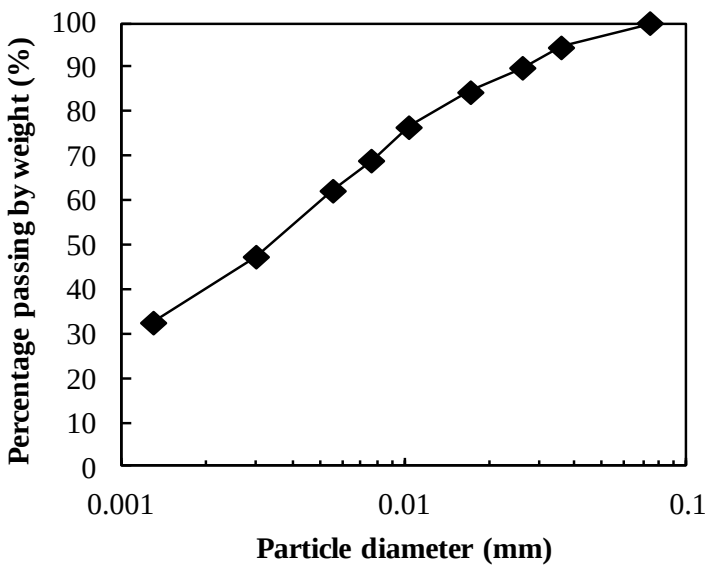

Figure 3-1 Grain size distribution curve for tested Kasaoka Clay

Figure 3-2 Sample under K_0 preconsolidation in a consolidometer (the inner diameter: 16.5cm.)

3.2. TRIAXIAL APPARATUS

The tests to obtain shear strength were conducted in temperature- and strain rate-controlled triaxial compression apparatus, as shown in **Figure 3-3**. The cell temperature was controlled by circulating cooled anti-freeze refrigerant (ethylene glycol diluted with water) by a refrigerating bath (not included in **Figure 3-3**, see **Figure 3-4**) through a spiral copper coil inside the cell (see **Figure 3-5**). The cell, initially filled with water, was eventually filled with the refrigerant as confining fluid, as described later, of which temperature was measured by thermocouples located on the inner side of the cell top and on the specimen's lateral surface. A comparison between measurements from these two thermocouples in preliminary tests is drawn in **Figure 3-6**. From **Figure 3-6**, it can be observed that the temperature on the specimen wall was 0.6^{o}C cooler than that in the cell (located in the ceiling of the cell, see **Figure 3-5**) on average. In this research, all the temperatures such as -2, -5 or -10°C were based on measurement of the thermocouple located inside the cell. An insulation jacket was placed around the cell to keep the cell temperature stable and uniform.

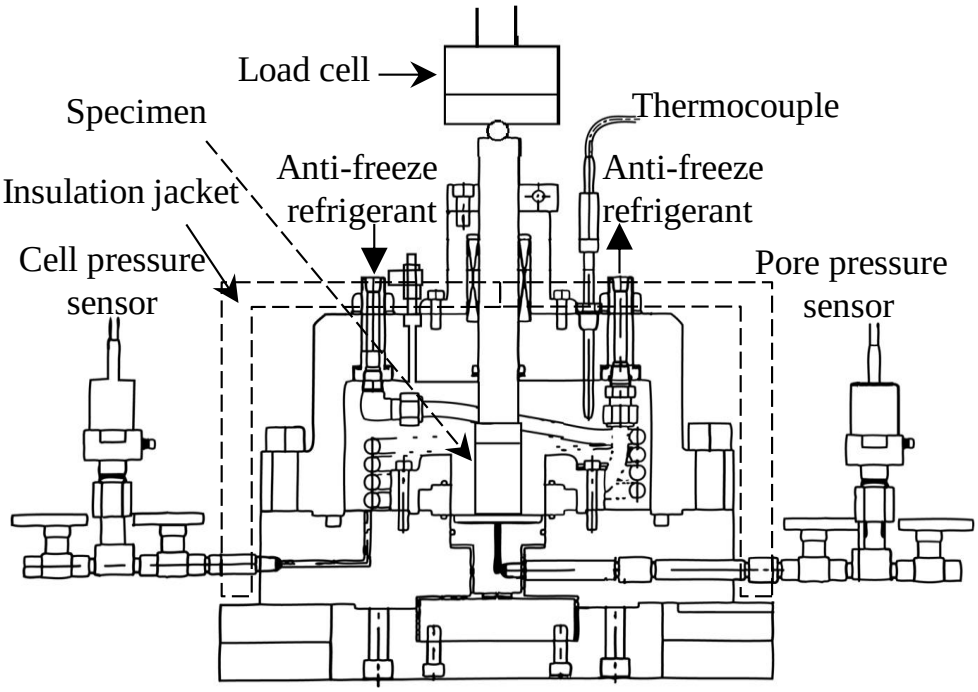

Figure 3-3 Schematic diagram of the triaxial apparatus for frozen samples

Figure 3-4 Refrigerating bath (EYELA NCB2600) for circulating low-temperature refrigerant in the triaxial apparatus

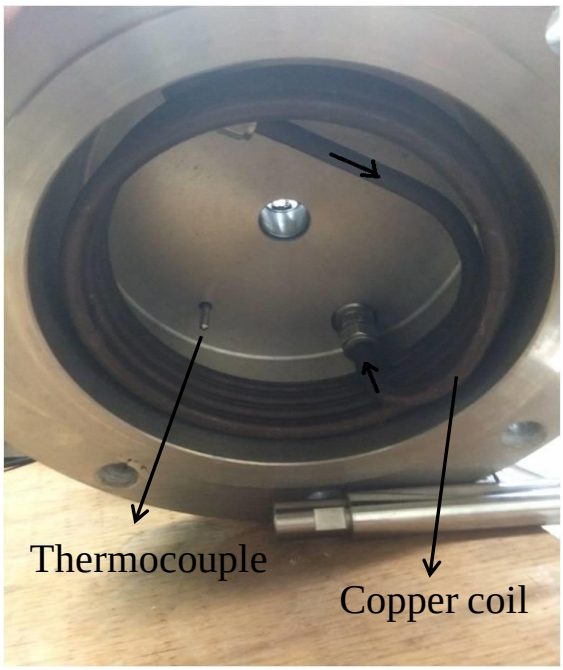

Figure 3-5 Spiral copper coil inside the cell

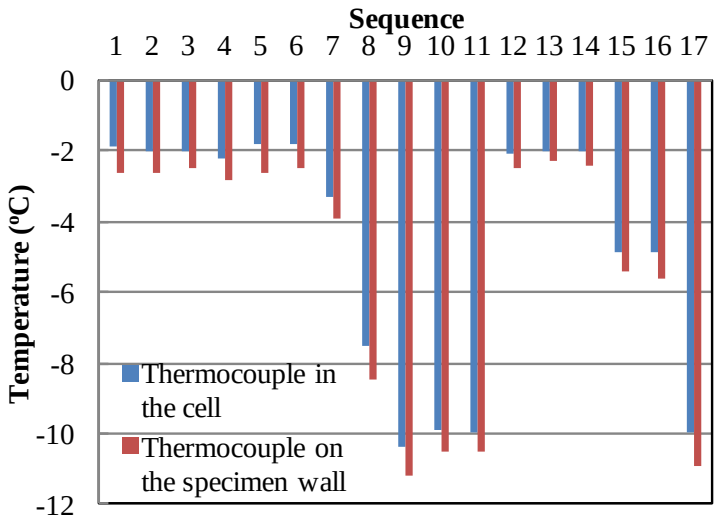

Figure 3-6 Comparison of measurements of thermocouple attached in the inner side of cell top and on the specimen with data collected in preliminary tests (The axial label of "sequence" signify individual readings after temperature equilibrium in the cell)

The adopted machine was originally a temperature-controlled oedometer (Tsutsumi and Tanaka, 2012), but modified to permit triaxial loading. A high-resolution direct-drive motor capable of applying constant strain rates was used to axially load the specimen through a loading ram. The direct-drive motor has a resolution as accurate as 2,621,440 pulses per cycle controlled by a personal computer (Tsutsumi and Tanaka, 2011), representing a resolution of 3.81×10^{-8} mm/pulse with the

gear reduction system adopted in the apparatus. The axial displacement was obtained directly by counting the number of revolutions of the motor as well as measured by a conventional dial gauge, which turned out to give consistent measurements to motor. The axial load was measured by a load cell (Minebea U381-500K-B, the capacity is 500 kg force) mounted outside the cell. The uplift force due to the cell pressure and the friction were corrected for.

Gap sensors (AEC PU-09) measuring semi-local (i.e. the sensors themselves were attached to the apparatus, sensing on-specimen targets) axial displacement were installed to overcome strain measurement errors due to imperfect coupling between the loading ram and the top cap, and other compliances, as shown in **Figure 3-7**. The measuring range of the gap sensor was 4 mm. Because the gap sensors were employed in the refrigerant at different temperatures rather than the usual medium of water, the effect of temperature and the refrigerant's electromagnetic properties on the measurement of gap sensor was investigated. The calibration factors (i.e. the ratio of measured displacement and output voltage of the gap sensor) of gap sensor were listed in **Table 3-1**. The calibration factors in the air and room-temperature refrigerant were calculated with the help of a calibrator which is capable of setting different magnitudes of distances between the head of the gap sensor and the metal target. The calibrator is inconvenient to operate when immersed in cold liquid. An indirect measurement was adopted to obtain the calculation factors for different temperatures in the refrigerant. Four magnitudes of distance between target and sensor were selected and they were fixed by a jig that keeps the selected distance. The fixed pair of gap sensor and target was immersed in the refrigerant for different temperatures (25, -2 or -10°C) and the responses of gap sensors were measured. As shown in **Table 3-1**, the temperature effect on the calibration factor of gap sensor immersed in refrigerant is negligible, so is the difference of calibration factors in the refrigerant and in air. As the semi-local measurements had a small range, and the difference from the external measurements is thought to be insignificant when large-deformation behavior is discussed, the presented results of stress-strain relationship are based on external axial displacement measurements (i.e. the measurements captured by the motor) in most parts of this thesis. Only in Chapter 6, the semi-local measurement records are presented to meaningfully discuss the small-strain stiffness characteristics.

Irregularities of the initial stress-strain curves were observed when ram-platen contact was in plane-plane form. It was attributed to the imperfect coupling in the interface between the loading ram and the top cap, which hampered the derivation of the initial small-strain stiffness characteristics even from the semi-local measurements. The imperfect coupling between the loading ram and the top cap was later greatly alleviated by replacing the plane-plane contact with a hemispherical ball point-plane contact (see **Figure 3-7(a)**). A hemispherical ball-shape head was installed to the bottom of the ram. To receive the hemispherical ball, the center of the top cap was machined to have a hemispherical groove. This new type of ram-platen contact brings about a possibility of tilting of specimens due to

the difficulty in aligning the specimen in the exact center and upright. Only if the top cap is aligned horizontal and in the exact center of the pedestal can the tilting of the specimen be prevented. A bubble level was used to assure that the upper surface of the top cap was horizontal. The position of the top cap was adjusted by measuring the horizontal distance between the edges of the top cap and the steel confining ring in two diagonal directions.

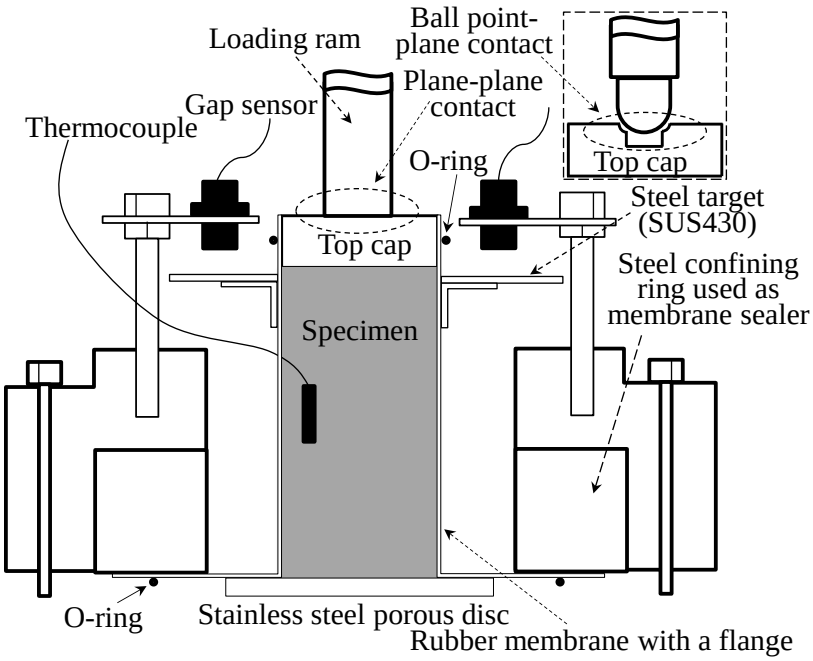

(a)

(b)

Figure 3-7 Set-up of the specimen: (a) Illustration with the gap sensors and two types of ram-platen contact (plane-plane contact and ball point-plane contact) (b) Photograph

Table 3-1 temperature effect on calibration factor (CF) of the gap sensor

Gap Sensor	CF by calibrator (mm/mV)	CF by indirect measurement (mm/mV)
in air (25 ^{o}C)	0.196	0.196
in refrigerant (25 ^{o}C)	0.198	0.206
in refrigerant (-2 ^{o}C)	-	0.207
in refrigerant (-10 ^{o}C)	-	0.210

3.3. TESTING CONDITIONS AND PROCEDURES

The whole test program consisted of five series, as shown in **Tables 3-2**, **3-3** and **3-4**. The first two are parallel tests in (i) frozen and (ii) unfrozen states at constant temperatures and strain rates. Series (iii) involved tests in frozen states with unsteady temperature and strain rate conditions. Series (iv) represents tests having a reduction of cell pressure after the specimens were put under freezing temperatures and Series (v) investigated the stiffness characteristics by loading and unloading at small strains repeatedly in a single test. In **Tables 3-2**, **3-3** and **3-4**, the maximum effective confining pressure after consolidation, $p_c^{'}$, the initial density measured after trimming the specimen and the initial water content after the pre-consolidation obtained by back calculation from the after-test water content, the void ratio before freezing, the testing temperature and axial strain rate and the resulting maximum deviator stress are listed.

Table 3-2 Frozen soil tests: Series (i), (iii) and (v)

Test No.	p_c' (kPa)	Initial density (g/cm^3)	Initial water content (%)	Void ratio before freezing	T (^{o}C)	Axial strain rate (%/min)	Maximum q (kPa)
i-1 (pl)	400	1.831	41.76	0.884	-2	0.01	813
i-2 (pl)	400	1.838	40.70	0.842	-5	0.01	1357
i-3 (pl)	400	1.833	39.85	0.841	-10	0.01	2199
i-4 (pl)	400	1.847	40.35	0.820	-2	0.1	861
i-5 (pl)	400	1.826	41.59	0.806	-5	0.1	1470
i-6 (pl)	400	1.834	41.91	0.837	-10	0.1	2442
i-7 (pl)	400	1.819	41.58	0.860	-2	0.001	752
i-8 (pt)	400	1.831	40.06	0.834	-5	0.001	1143
i-9 (pl)	400	1.837	38.88	0.823	-10	0.001	1986
i-10 (pt)	400	1.840	36.63	0.768	-2	0.01	832
i-11 (pt)	400	1.828	42.12	0.864	-2	0.01	842
i-12 (pt)*	400	1.833	40.15	0.833	-5	0.1	1396
i-13 (pl)	400	1.831	40.40	0.845	-2	0.1	846
i-14 (pt)	200	1.773	46.70	0.982	-2	0.01	648
i-15 (pt)	200	1.768	46.15	0.973	-5	0.01	1237
i-16 (pt)	200	1.772	46.41	0.972	-10	0.01	2060
i-17 (pt)	200	1.762	45.76	0.974	-5	0.1	1375
i-18 (pt)	200	1.767	46.48	0.978	-5	0.001	1228
i-19 (pt)	100	1.751	51.26	1.118	-2	0.01	616
i-20 (pt)	100	1.713	52.10	1.132	-5	0.01	1089
i-21 (pt)	100	1.733	51.04	1.116	-10	0.01	1862
i-22 (pt)	100	1.709	50.85	1.109	-5	0.1	1386
i-23 (pt)	100	1.732	51.01	1.118	-5	0.001	1152
iii-1 (pl)	400	1.837	40.70	0.838	-	0.01	-
iii-2 (pl)	400	1.848	40.64	0.850	-	0.01	-
iii-3 (pl)	400	1.832	41.10	0.841	-2	-	-
iii-4 (pt)	400	1.848	40.10	0.816	-5	-	-
v-1(pt)**	400	1.851	36.00	0.765	-	-	-

Note: (pl) in the test No. indicates plane-plane contact between loading ram and top platen while (pt) indicates ball point-plane contact between them (see **Figure 3-7**). *i-12 is a duplicate test for i-5 and not used for further presentation. **v-1(pt)'s initial water content was obtained from before-test measurement from the trimmed-off soil and the void ratio before freezing was thus derived from the before-test water content due to the lack of after-test water content data.

Table 3-3 Frozen soil tests: Series (iv)

Test No.	u (kPa)	Initial density (g/cm^3)	Initial water content (%)	Void ratio before freezing	T (^{o}C)	Axial strain rate (%/min)	Maximum q (kPa)
iv-1 (pt)	100	1.865	40.88	0.851	-2	0.01	970
iv-2 (pt)	300	1.826	41.23	0.859	-2	0.01	945
iv-3 (pt)	500	1.828	42.12	0.864	-2	0.01	842
iv-4 (pt)	100	1.834	39.32	0.837	-5	0.01	1525
iv-5 (pt)	300	1.832	37.31	0.854	-5	0.01	1471
iv-6 (pt)	500	1.857	40.44	0.827	-5	0.01	1466
iv-7 (pt)	100	1.859	41.69	0.824	-10	0.01	2465
iv-8 (pt)	300	1.848	39.99	0.824	-10	0.01	2198
iv-9 (pt)	500	1.803	37.09	0.811	-10	0.01	2365

Table 3-4 Unfrozen soil tests: Series (ii)

Test No.	p_c' (kPa)	Initial density (g/cm^3)	Intial water content (%)	Void ratio before shearing	State before shearing	Axial strain rate (%/min)	Maximum q (kPa)
ii-1	400	1.842	39.20	0.824	NC(1)	0.01	276
ii-2	400	1.836	39.19	0.824	NC	0.1	295
ii-3	400	1.832	39.85	0.830	NC	0.001	286
ii-4	400	1.860	38.63	0.889	OC(2)	0.01	195
ii-5	400	1.830	38.91	0.898	OC	0.1	190
ii-6	400	1.835	38.66	0.897	OC	0.001	192
ii-7	200	1.767	45.47	0.968	NC	0.01	158
ii-8	200	1.776	44.83	1.058	OC	0.01	101
ii-9	100	1.717	50.77	1.116	NC	0.01	84
ii-10	100	1.712	50.48	1.217	OC	0.01	52
ii-11*	400	1.813	40.77	0.914	OC	0.1	185
ii-12*	400	1.829	41.09	0.931	OC	0.01	183

Note: Symbol * indicates the unfrozen test which was conducted in the temperature-controlled apparatus. Symbol (1): "NC" indicates normally consolidated state. Symbol (2): "OC" indicates over-consolidated state; see later descriptions for the definition of NC and OC for frozen samples.

Series (i) was conducted in the following five stages, as charted in **Figure 3-8**:

(1) Isotropic consolidation was conducted at +24°C, starting from the residual effective stress in the preconsolidated specimens (around $p'=\sigma_{v0}'/3$), past σ_{v0}' and eventually to $p_c'=2\sigma_{v0}'$ in order to give an isotropic structure to the initially K_0 reconstituted specimen. The drainage was allowed from the bottom and lateral surfaces, which were in contact with the porous disc and filter paper strips, respectively. The back pressure was maintained at 200 kPa all through the consolidation and, in Series

(ii), the swelling stages. The creep after the consolidation was allowed until the volumetric compression rate became less than 0.02%/hour, which took about three days.

(2) The specimen was cooled to around +1°C by circulating a chilled refrigerant through the copper tube. 12 hours were allowed for the specimen temperature to stabilize. This pre-cooling allowed swift freezing in the next stage. This will be discussed more in detail in later paragraph describing the freezing method.

(3) The cell water was replaced with the refrigerant pre-cooled at about -18°C while keeping the cell pressure. This sudden introduction of chilled refrigerant, helped by the specimen pre-cooling, caused quick freezing of the specimen (more specific operational processes will be described later). Just after finishing the introduction of refrigerant, the temperature of the cell could be as low as -5°C and the temperature measured at the specimen surface could be about -7.5^{o}C. A trial run immersing the specimen at the refrigeration bath at -5°C with a thermocouple embedded at the specimen core confirmed that it took only about 20 minutes for the core to freeze, as shown in **Figure 3-9**. This quick freezing, along with the low permeability of the clay and the application of confining stress during freezing, led to relatively uniform specimens, as confirmed by visual observation as shown in **Figure 3-10(a)**, although local water content measurements after the tests, presented in **Table 3-5**, suggest possibility of small water migration from the core to the rim of the specimen. In case of no application of confining stress during freezing, obvious cracking caused by internal water migration was observed, as shown in **Figure 3-10(b)**. Slow freezing under no confinement would lead to minute ice lenses formed even in clays, as revealed by Viggiani et al. (2015), which would make interpretation of the specimen as an element difficult. During the freezing, the drainage valve was kept open to prevent damaging the pore water pressure transducer, but the high thermal diffusivity of the stainless steel porous metal at the specimen bottom led to quick freezing of the bottom surface and hence practically undrained conditions. The temperature was set to -15°C and kept for 12 hours.

(4) The cell temperature was raised to the testing temperature (-2, -5 or -10°C), and then kept for 24 hours.

(5) Finally, undrained shearing was conducted at a constant temperature (-2, -5 or -10°C) and a constant axial strain rate (0.1, 0.01 or 0.001%/min) until an axial strain of 20% was reached. After each test, the apparent absence of ice lenses was confirmed by the visual observation and local water content measurements. **Figure 3-11** shows the image of the triaxial compression test on frozen soil at -10°C.

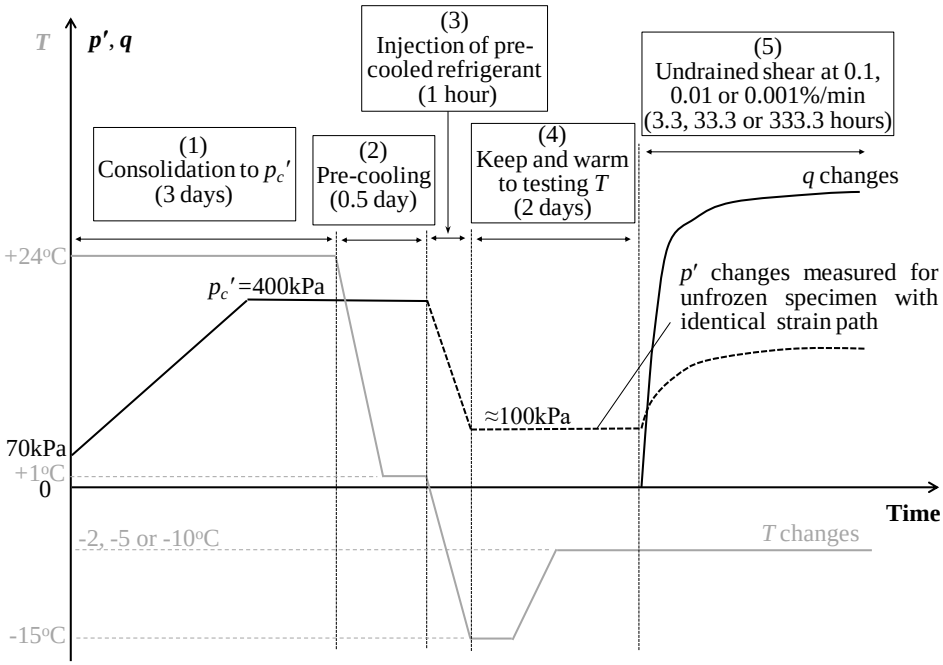

Figure 3-8 Test procedures and changes in key variables: Example of p_c' = 400kPa case in Series (i)

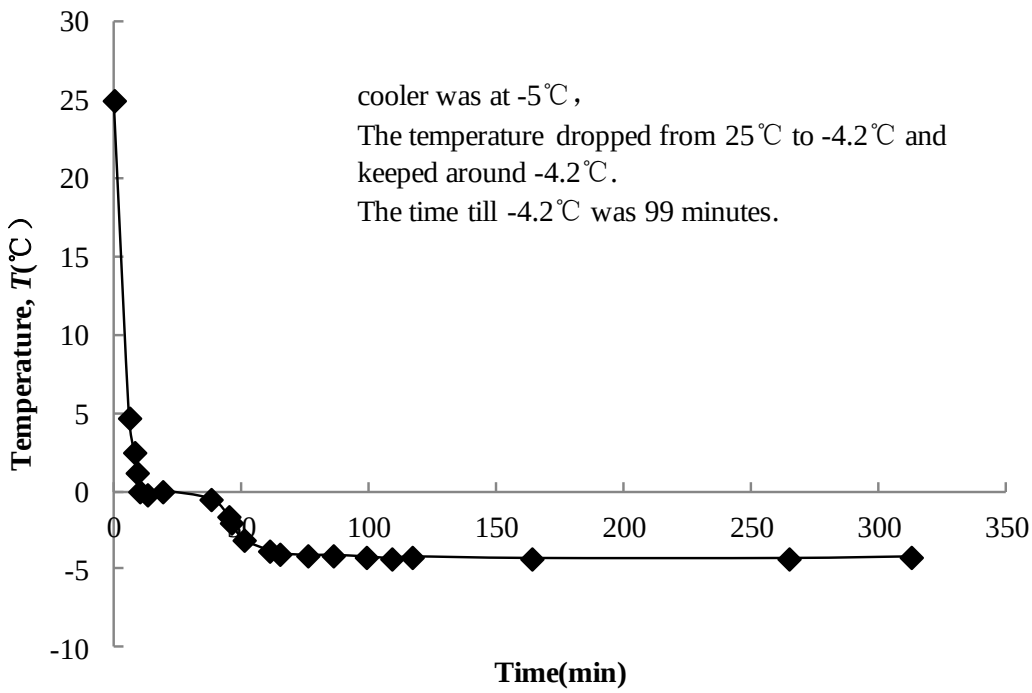

Figure 3-9 Temperature history of the core of a specimen immersed in refrigerating bath at -5°C

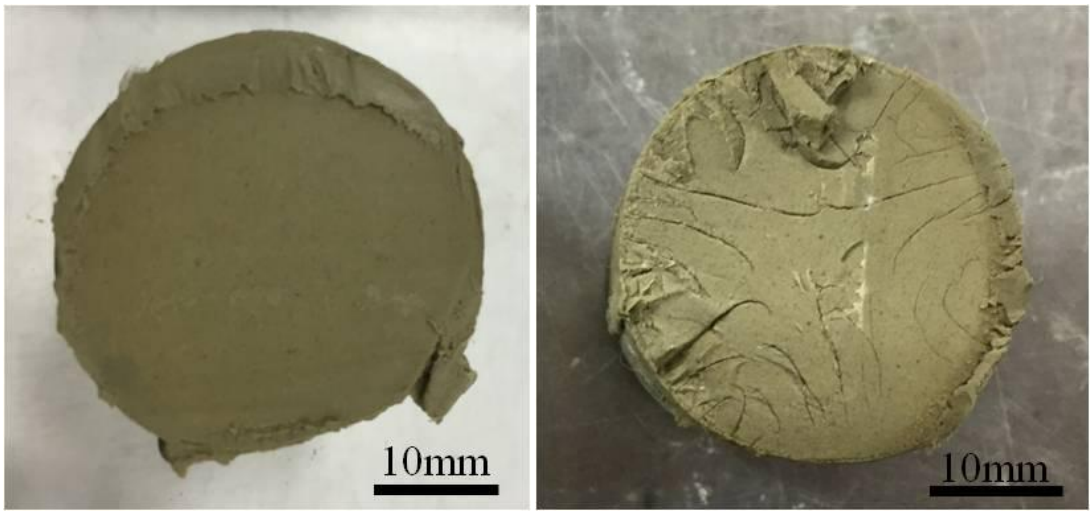

(a) (b)

Figure 3-10 Cross-section of specimen (a) At frozen state after test, showing no visible ice lens or inhomogeneity; (b) Frozen under no confinement, showing cracking caused by non-uniform deformation

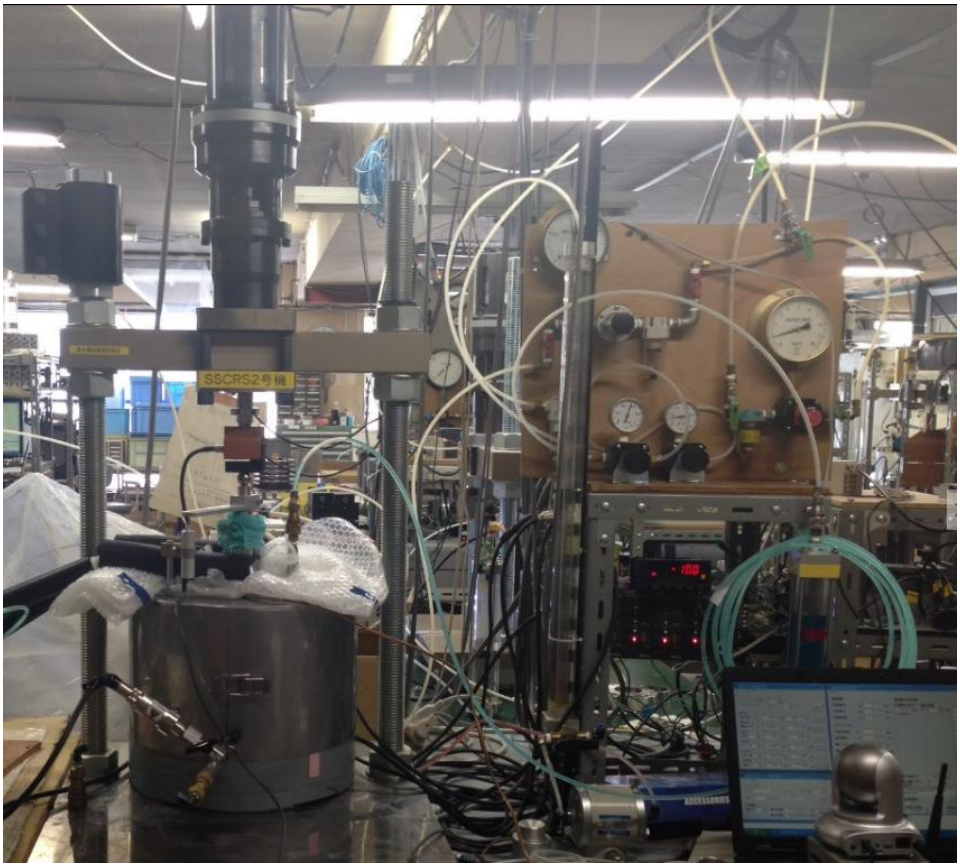

Figure 3-11 Image of the triaxial compression test on frozen soil at -10 ^{o}C

Table 3-5 Water content distribution in specimens after test (top, middle and bottom thirds of specimen: “center” refers to 10 mm-diameter core and “rim” means the rest within 30 mm-diameter specimen)

Test No.	Water content (%)					
	Top center	Top rim	Middle center	Middle rim	Bottom center	Bottom rim
i-18	38.02	37.24	35.75	36.69	36.09	36.87
i-22	40.46	42.01	39.58	41.45	40.49	42.65
i-23	42.25	42.08	40.34	42.07	40.69	42.78

Series (iii) took similar steps as above, but the strain rate and the temperature were varied stepwise during the shearing. For the varying-strain rate test, Step (5) involved switching abruptly between different strain rates (0.1, 0.01 or 0.001%/min) and keeping it constant for the axial strain of 0-5%, 5-10%, 10-15% and 15-20%. For the varying-temperature tests, the shearing was suspended at each end of the above strain intervals and a new temperature was set in the cell and kept for 24 hours. Then the shearing was resumed at the same strain rate as before for another strain interval of 5%. This was repeated until the axial strain reached 20%.

Series (iv) still took similar steps to Series (i), the cell pressure was decreased after the specimen was frozen and stabilized into a stable temperature. Frozen specimens undergoing decrease of cell pressure after frozen are defined as “Over-consolidated (OC)” frozen soil here. Since only the cell pressure varies, same effective mean stress, p' can be taken, which is 100kPa in case of p_c'=400kPa. When cell pressure p_c of 400 or 200kPa is adopted, the pore/ice pressure u equals to 300 or 100kPa (see detailed description of the principles in Section 5.4). New cell pressure was sustained for 24 hours before the specimen underwent shearing to axial strain of 20%.

Series (v) was distinguished from Series (i) in that it was focused on the measurement of stiffness of the frozen specimen for various conditions repeatedly in a single test. The specimen was at quasi-elastic stage for each time of loading. So this approach is called nondestructive method. After the specimen which had been consolidated to p_c'=400kPa froze at -15°C, it was firstly warmed up to -10°C and kept for 24 hours. Then axial compression was applied at a strain rate of 0.001%/min until an axial strain of 0.025%. The specimen was then unloaded to the original isotropic state. At least three round of loading-unloading quasi-elastic probes were carried out before another strain rate was applied, and the above 0.025%-strain probe was repeated at strain rates of 0.01, 0.1 and then 0.001%/min in order. After these loadings at -10°C were done, a new temperature was set in the cell and kept for 24 hours. Application of loading at different strain rates to the specimen and unloading

after this elastic shear was repeated for the new temperature. The order of stages was set from -10°C to -5°C and finally to -2°C, in a similar way to the earlier tests, in which the specimens warmed up from -15°C to the testing temperatures, which make the results from this test with nondestructive probes comparable to the past individual tests in Series (i). A more complete description of the loading sequences is provided in Chapter 6.

The above series of tests on frozen soil involved replacement of the cell water with pre-cooled refrigerant with cell pressure still confining the specimen as illustrated in **Figure 3-12**. After sufficient time was allowed for isotropic consolidation to p_c', the cell was cooled to around +1°C by circulating a chilled refrigerant through the copper tube as previously described. This pre-cooling allowed swift freezing in the following step. The cell water was then drained out slowly by slightly opening the valve which could ensure the cell pressure same as before draining. At the same time a bottle of pre-cooled refrigerant at -18°C was transferred into a tank as shown in **Figure 3-12**. The method of transfer from the bottle to the tank is by applying vacuum (-98kPa) to the tank in order to suck the refrigerant from the bottle. The vacuum was released after the tank was filled and a pressure of 210kPa plus p_c' which had an excess of 10kPa compared to cell pressure was then applied. By connecting the tank to the cell, the pre-cooled refrigerant flowed into the cell and started to freeze the specimen. Three or four bottles of pre-cooled refrigerant were used to reach the desired sub-zero temperature of the cell. The volumes of the bottle, tank and cell are similar. So this process also involves refilling the tank by vacuum and taking the overflow of the refrigerant once the cell was filled up with the refrigerant. At the same time as injection of pre-cooled refrigerant, the cooling bath was set at -25°C and started to circulate the refrigerant along the spiral coil inside the cell. The cell temperature was set at -15°C by the above efforts within a couple of hours. All these efforts succeeded in freezing the specimen quickly and preventing the formation of ice lensing.

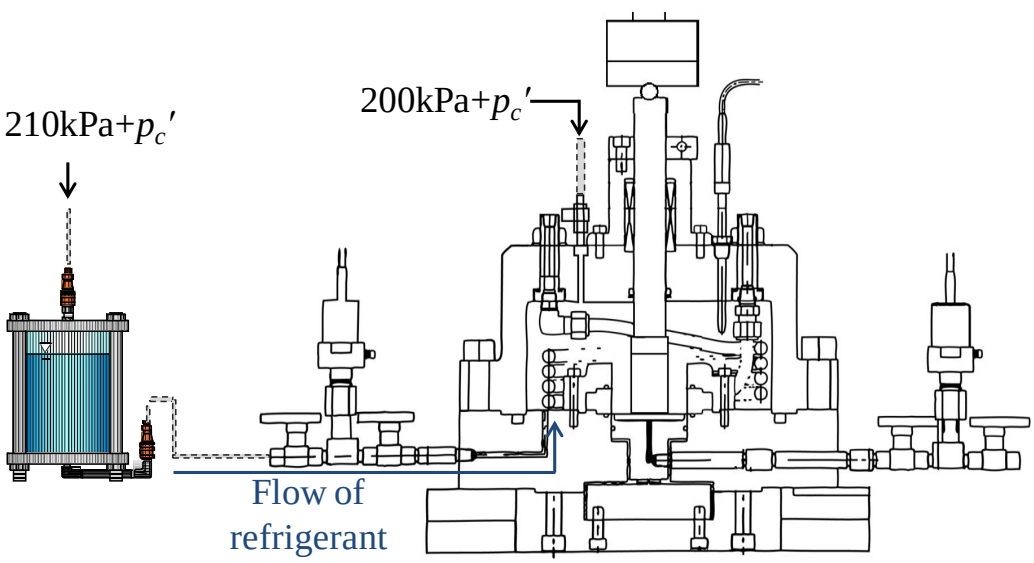

Figure 3-12 Illustration of injection of pre-cooled refrigerant

Series (ii), the unfrozen test series, was performed at +24°C separately in another conventional triaxial apparatus (see **Figure 3-13**) by following similar steps but without freezing. After the consolidation to $p_c'=2\sigma_{v0}'$, the confining pressure was decreased to unload the specimen isotropically so that the specimen was allowed to swell by the same amount as the freezing expansion, calculated based on 9% expansion of pore water. This corresponds to the whole specimen's volumetric strain of $(1+1.09e_c)/(1+e_c)$, where e_c is the void ratio after the normal consolidation. Due to the unfrozen content in the soil (Williams, 1964; Smith and Tice, 1988; Andersland and Ladanyi, 2004; Watanabe and Wake, 2009), the actual expansion of frozen specimen was slightly less than this value. The correction for this will be discussed subsequently. This path is illustrated in **Figure 3-14**. The following undrained shearing at +24°C was performed in a similar way as Series (i). Both the frozen and unfrozen specimens experienced a similar volumetric strain history in this way throughout the tests. In addition, normally consolidated (NC) specimens at unfrozen state were also tested to establish the Critical State Line (CSL) accurately.

The present study limits the confining pressure range to low to medium levels (100-400 kPa), relevant to construction activities such as tunneling and temporary excavation. Pressure melting and ice fracturing are not considered to be dominant at such stress levels.

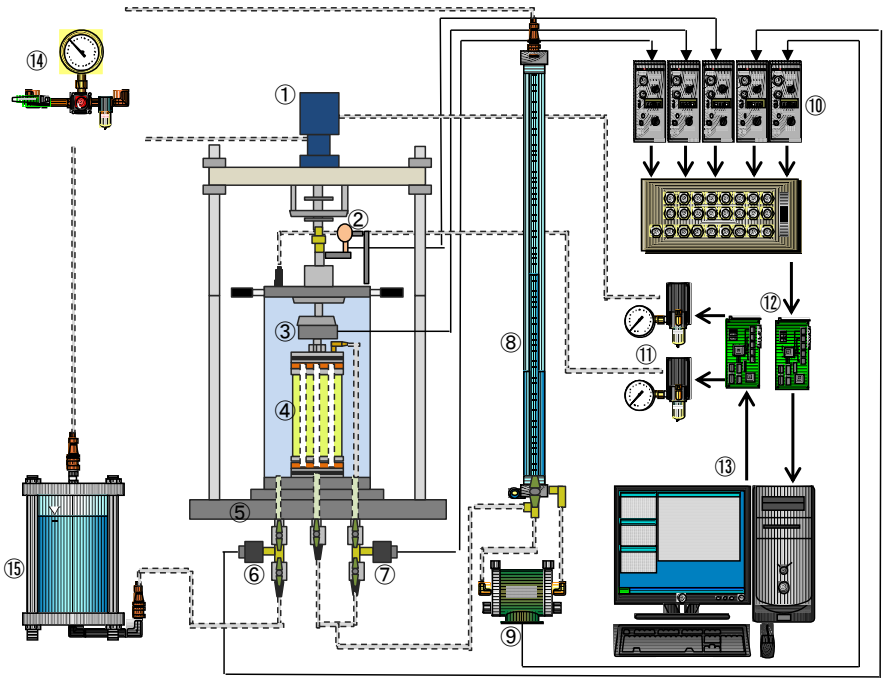

① Two-chamber type bellofram cylinder ② Dial gauge ③ Loadcell ④ Specimen ⑤ Loading table
⑥ Cell pressure gauge ⑦ pore water pressure gauge ⑧ double pipe burette
⑨ Differential pressure gauge ⑩ Strain amplifier ⑪ Electro-pneumatic converter ⑫ A / D conversion module
⑬ PC ⑭ Regulator ⑮ Water supply tank

Figure 3-13 Conventional triaxial apparatus for unfrozen soil test

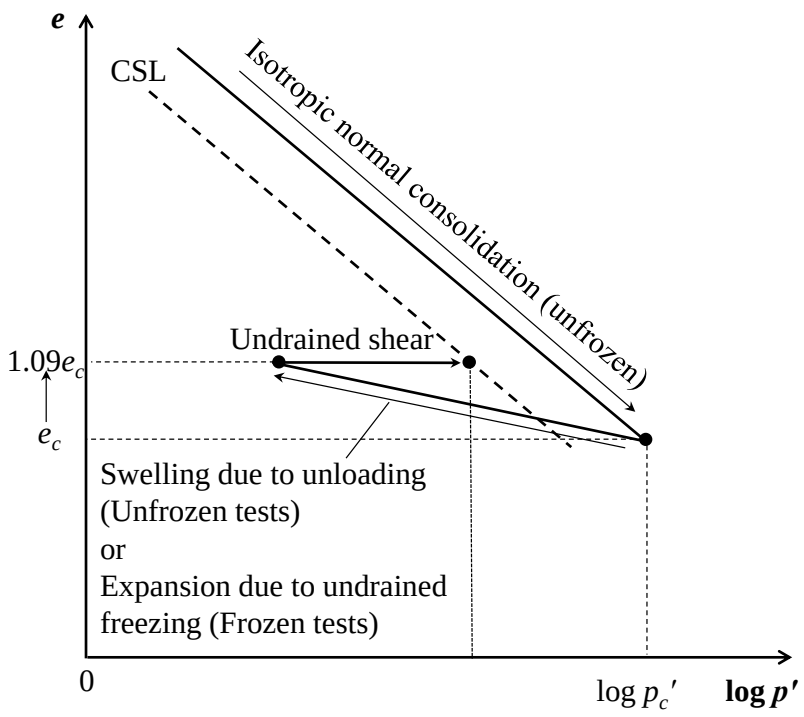

Figure 3-14 Illustration of the presumed e – log p' relationship during freezing or unloading

3.4. NUCLEAR MAGNETIC RESONANCE (NMR) MEASURING UNFROZEN WATER CONTENT IN FROZEN SOIL

It is known that water remains partially unfrozen at sub-0°C temperatures in soils (Williams, 1964; Smith and Tice, 1988; Andersland and Ladanyi, 2004; Watanabe and Wake, 2009). The unfrozen content can be significant for fine-grained soils with small pores. The unfrozen water content can be probed by a few different methods; among them, application of nuclear magnetic resonance (NMR) is known to be an accurate and reliable method. In this method, pulse application of a magnetic field induces voltage in its perpendicular direction, and the decay is monitored. As the decay in solid water (ice) is much faster than in liquid water, the decay curve can be readily decomposed into parts corresponding to each phase, and the amount of each phase can be quantified (Ishizaki et al., 1996). The present study used an NMR analyzer by Oxford Instruments (Model MQC, as shown in **Figure 3-15**) and a pulse frequency of 23 MHz was adopted. The other conditions and processing methods are same as those described by Ishizaki et al. (1996) and Watanabe and Wake (2009).

Figure 3-15 The NMR analyzer by Oxford Instruments (Model MQC)

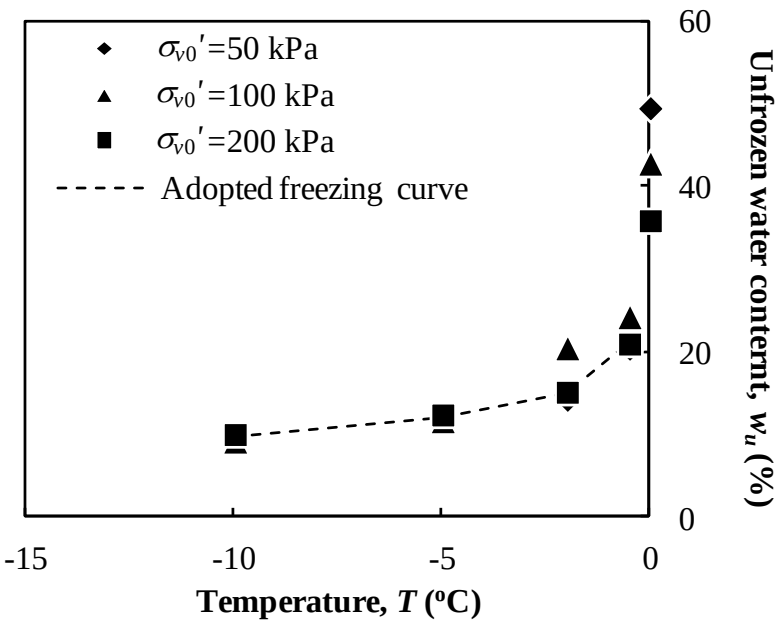

Figure 3-16 The freezing curve obtained from NMR tests

Three specimens, each preconsolidated one-dimensionally under σ_{v0}'=50, 100 or 200kPa and trimmed to 17.5mm in diameter and 25mm in height, were quickly frozen under unconfined states to -20°C. The temperature, *T*, was then raised in steps to -10, -5, -2 and -0.5°C, at which 24 hours of equilibration time was allowed and then NMR was applied in a cold room to measure the unfrozen water content, w_u. This temperature history is designed to be similar to that in the triaxial tests, as a w_u-*T* relationship, or freezing curve, can be hysteretic. This NMR test was performed by Dr. Tokoro's research group of National Institute of Technology, Tomakomai College. **Figure 3-16** shows the

deduced relationships for all the specimens. Despite the difference in the water content at unfrozen states, the freezing curve is fairly unique (the anomalous w_u values at -2 and -0.5^{o}C for the σ_{v0}'=100kPa sample might have been obtained by frosting of the sample container; they are ignored here). Although some specimens were eventually subjected to a higher isotropic effective stress of 400kPa in the triaxial tests, the subsequent calculation of the unfrozen water content at each temperature is conducted by assuming this curve is still valid.

4. BEHAVIOR OF REFERENCE UNFROZEN SAMPLES

In this chapter, the mechanical behavior of unfrozen samples which provides a reference for analysis of frozen behavior is focused on. The stress-strain relationships and effective stress paths of the reference unfrozen samples with three different preconsolidation pressures including over-consolidated and normally consolidated states at a same strain rate will be presented, with representative soil constants derived. Meanwhile, for unfrozen specimens normally consolidated to p_c' of 400 kPa, the mechanical behaviors of normally consolidated and over-consolidated unfrozen soils are discussed in terms of three orders of strain rates (i.e. 0.1, 0.01 and 0.001%/min). For p_c' of 400 kPa, same tests were also conducted in the apparatus for the frozen soil tests (i.e. the temperature-controlled apparatus), and a comparison of results obtained in the temperature-controlled apparatus and the conventional triaxial apparatus will be made to assess the compatibility between them.

4.1. STRESS-STRAIN RELATIONSHIPS AND EFFECTIVE STRESS PATHS OF REFERENCE UNFROZEN SAMPLES

In Series (ii), the specimens consolidated to p_c'=100, 200 and 400 kPa were subjected to undrained triaxial compression at +24°C. For over-consolidated (OC) specimens, they were unloaded to swell by a volumetric strain corresponding to 9% void ratio increase prior to undrained shear, resulting in an over-consolidation ratio (OCR) of 4.0-6.7. For specimens consolidated to p_c'=400 kPa, they were unloaded to p'=100 kPa with void ratio increased by 9%, having OCR of 4.0. The process was similar for specimens consolidated to p_c'=200 and 100 kPa which were subsequently unloaded to p'=36 kPa and 15 kPa having OCR of 5.6 and 6.7, respectively. **Figure 4-1(a)** shows the observed state paths in these tests from the set up to the end of undrained shear (as listed in **Table 3-4** in the previous chapter, specimens with p_c'=100 kPa and 200 kPa were all sheared at the strain rate of 0.01%/min while specimens with p_c'=400 kPa were sheared at three different strain rates). While the initial states, off the isotropic compression line, reflect the K_0-preconsolidation history, the subsequent isotropic consolidation brought the state onto a well-defined isotropic Normal Compression Line (NCL). The parallel Critical State Line (CSL) was also well-defined after the undrained shear. Here the critical state of the specimen under shear was referred to the state at the axial strain of 20% or the final strain it actually reached when it was less than 20%. By definition, the stress changes were very limited when the axial strain reached the critical state. The representative soil constants for the NCL, CSL and unloading-reloading line (URL) estimated are listed as follows: N=2.08 and λ=0.20 (for NCL), Γ=1.94 and κ=0.05 (for URL), which are the incept at p'=1 kPa and the slope respectively for NCL and URL with p' in natural logarithmical (i.e. ln) scale. The undrained effective stress paths from the normal and over-consolidated states at the axial strain rate of 0.01%/min are shown in **Figure 4-1(b)** (behaviors at the axial strain rate of 0.1 and 0.001%/min will be presented in the following paragraph).

A value of 1.08 was estimated for the Critical State parameter, *M*. **Figure 4-1(c)** shows the relationship of the deviator stress, *q*, and the axial strain, ε_a ,with regard to the maximum effective consolidation pressure, p_c', and the state of either normally consolidation or over consolidation. Figure 4-1(c) clearly shows that shearing behavior of Kasaoka Clay is affected by the maximum effective consolidation pressure. At a same axial strain rate of 0.01%/min, the deviator stress-axial strain curve of the specimen with higher p_c' is located above that of the one with lower p_c' regardless of whether the specimen is normally consolidated or not. The strength of over-consolidated specimen turned out to be greater than that of normally consolidated one. This fits the common knowledge of Critical State theory that both normally and over-consolidated specimens of same p_c' share an identical yield surface and the effective stress path should go towards the CSL vertically in ideal condition, which suggests a smaller strength for over-consolidated specimens with smaller p'. Because of the positive / negative excess pore water pressure generated in the course of undrained shearing of normally consolidated / over-consolidated specimens, the stress paths of the specimens turned out to be as shown in **Figure 4-1(b)**.

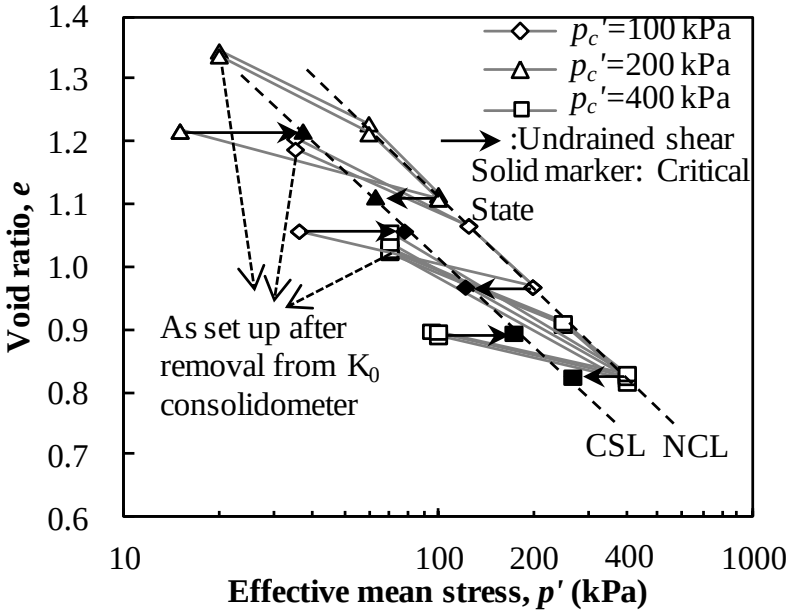

(a)

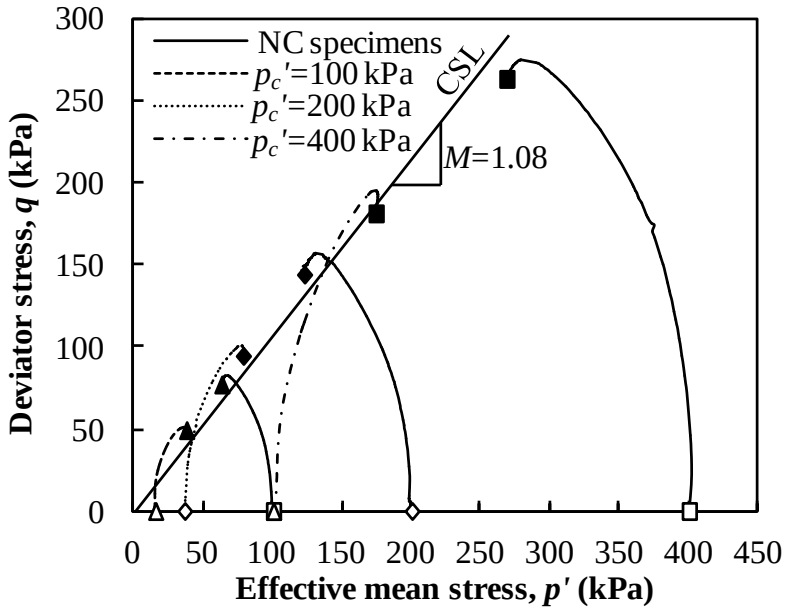

(b)

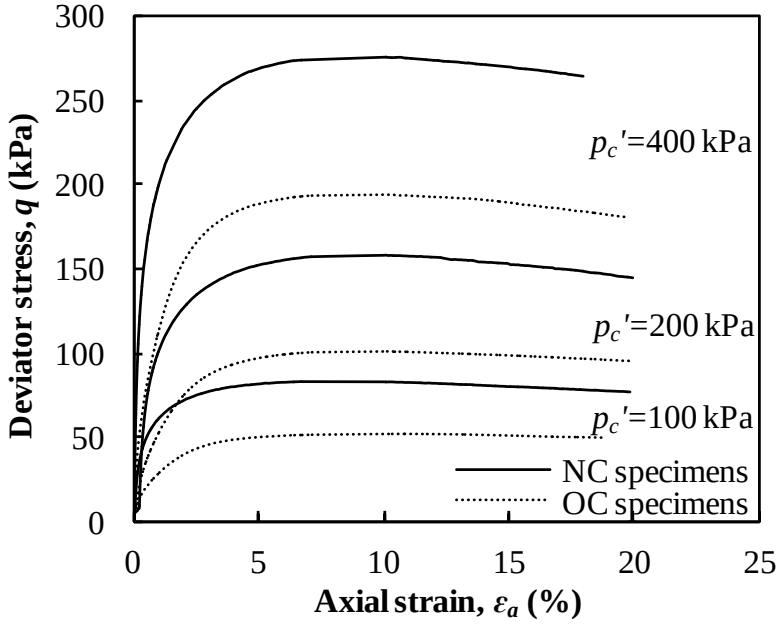

(c)

Figure 4-1 Presentations of unfrozen test results in terms of: (a) e – p' paths, (b) q – p' paths and (c) stress-strain curves

For p_c'=400 kPa, three orders of strain rates were applied both in the over-consolidated and normally consolidated tests (ii-1~6 in **Table 3-4**). **Figures 4-2(a)** and **(b)** show the stress-strain curves and the effective stress paths for the OC specimens. Almost no visible effect of strain rate is seen on the stress-strain relationship for this particular reconstituted soil, although many clays, including natural ones, tend to exhibit some degrees of rate-dependency even at over-consolidated states (e.g. Vaid and

Campanella, 1977; Graham et al., 1983; Zhu and Yin, 2000). Only the effective stress paths were slightly different, and this may be because the pore water pressure transducer response is not catching up with the generated excess pore water pressure due to a system compliance. This is a common feature in undrained triaxial tests, but the 'apparent' effective stress paths eventually converges as the rate of pore water pressure change slows down towards the Critical state and does not affect the strength interpretation. **Figures 4-3(a)** and **(b)** shows the stress-strain curves and effective stress paths for the NC specimens. As the behavior is more plastic than for the OC specimens, the strain-rate effect is somewhat stronger. Although the data are not fully consistent, the observed trend broadly agrees the conventional knowledge that a larger strength is associated with larger strain rates (e.g. Richardson and Whitman, 1963; Yin et al., 2002). The behavior against the strain rate of 0.001%/min was ductile and ultimately resulted in relatively large strength at large strains. For this clay, the strain-rate dependency of the shear behavior is relatively small even at normal consolidated states, and almost negligible at OCR=4.

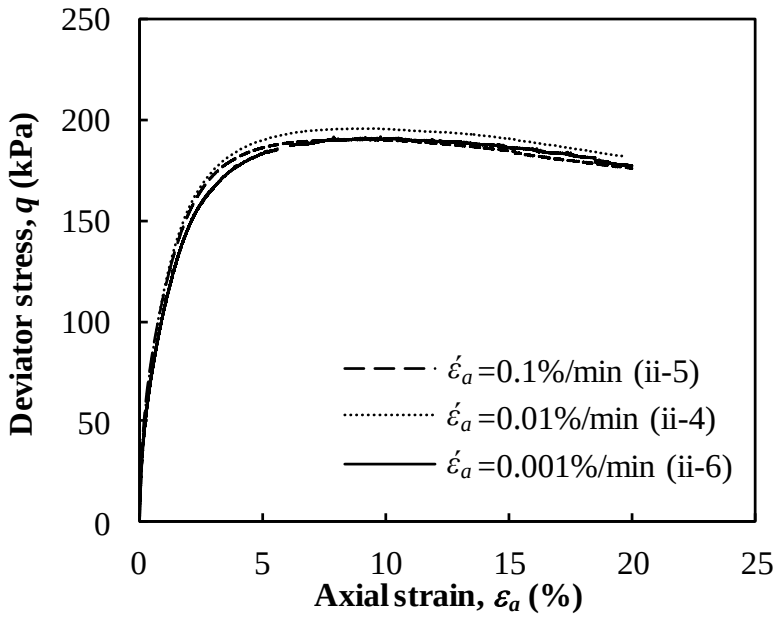

(a)

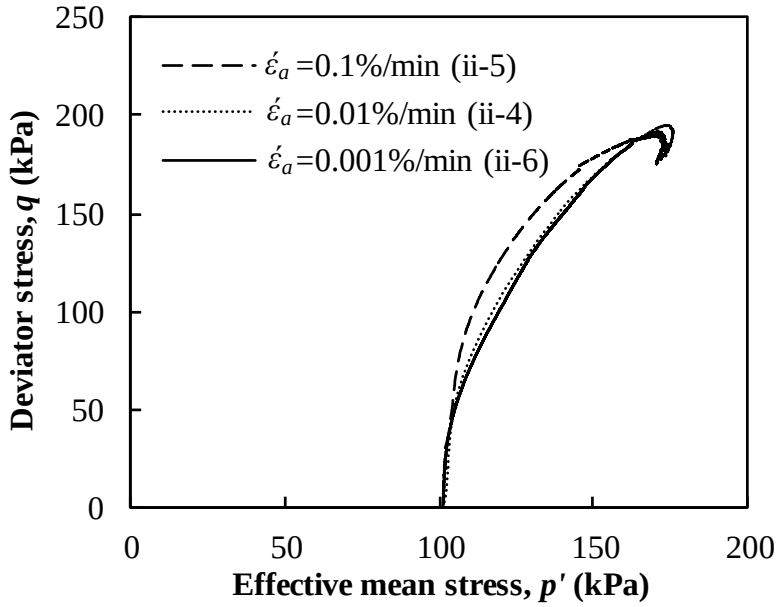

(b)

Figure 4-2 Contrast of unfrozen OC specimens' behavior (p_c' = 400 kPa) undrained sheared at different axial strain rates in terms of: (a) Stress-strain relationships and (b) Effective stress paths

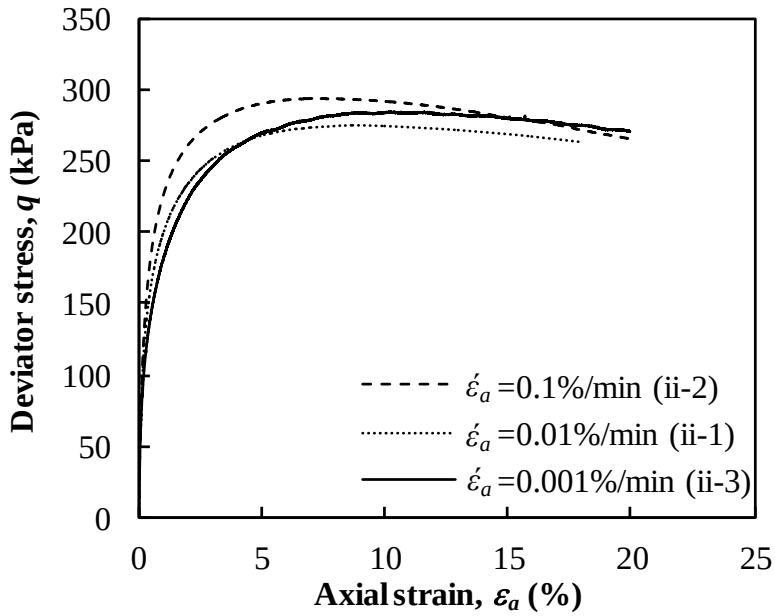

(a)

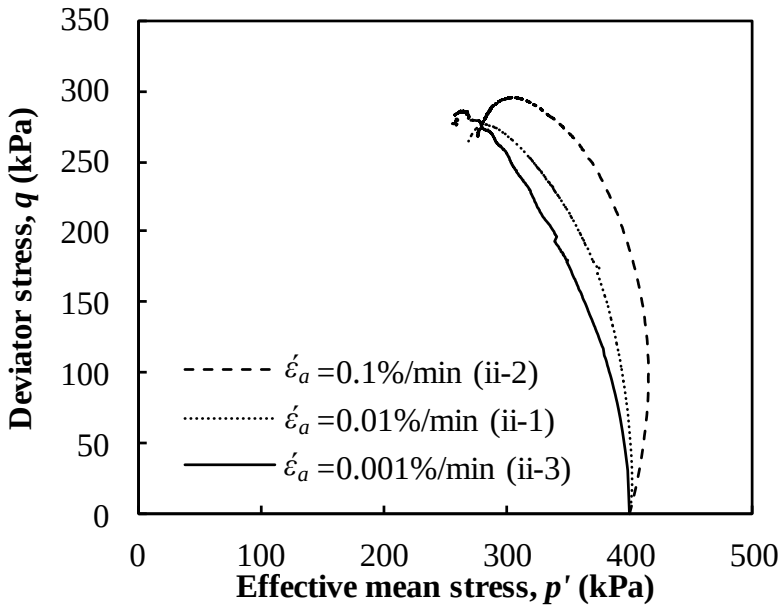

(b)

Figure 4-3 Contrast of unfrozen NC specimens' behavior (p_c' = 400 kPa) undrained sheared at different axial strain rates in terms of: (a) Stress-strain relationships and (b) Effective stress paths

4.2. COMPARISON OF UNFROZEN TESTS CONDUCTED IN TEMPERATURE-CONTROLLED APPARATUS AND CONVENTIONAL TRIAXIAL APPARATUS

The unfrozen tests were referred to for interpreting the behavior of the frozen specimens. However, the frozen and unfrozen tests were conducted on specimens with two different sizes (30mm and 50mm diameters) in two different machines (the temperature-controlled cell shown in **Figure 3-3** and the conventional triaxial apparatus shown in **Figure 3-10**), as explained earlier. To confirm the comparability between the two machines, two identical pairs of tests were performed in them (ii-5 and ii-11, p_c'=400 kPa and strain rate of 0.1%/min; ii-4 and ii-12, p_c'=400 kPa and strain rate of 0.01%/min). The stress-strain curves and the effective stress paths for strain rate of 0.1%/min were shown in **Figures 4-4(a)** and **(b)**, respectively. The results are considered consistent if it is taken into account that they were conducted in different machines with different specimen sizes; the difference of q is 3% at the peak and 7% at the 20% axial strain in the case of the strain rate of 0.1%/min. The stress-strain curves and the effective stress paths for strain rate of 0.01%/min can also be seen consistent to a similar degree, as shown in **Figures 4-5(a)** and **(b)**. Nevertheless, direct comparison or random mixing of data obtained from different machines is avoided in the subsequent discussion lest this modest variability affects the conclusions. The main difference in each test pair derives from the initial compliance in the ii-11 and 12 results, representing the tests performed with the “plane-plane” ram-platen contact. As discussed earlier, this contact was improved in the later stage of the research.

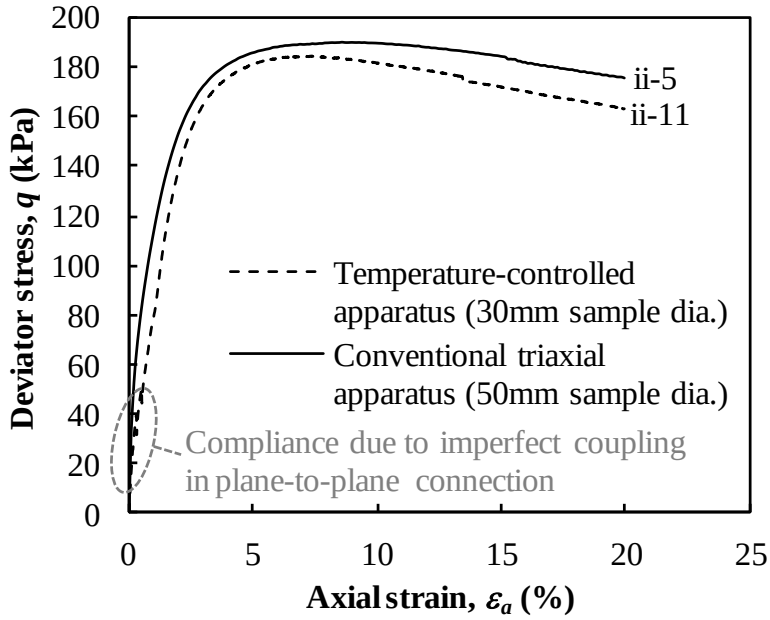

(a)

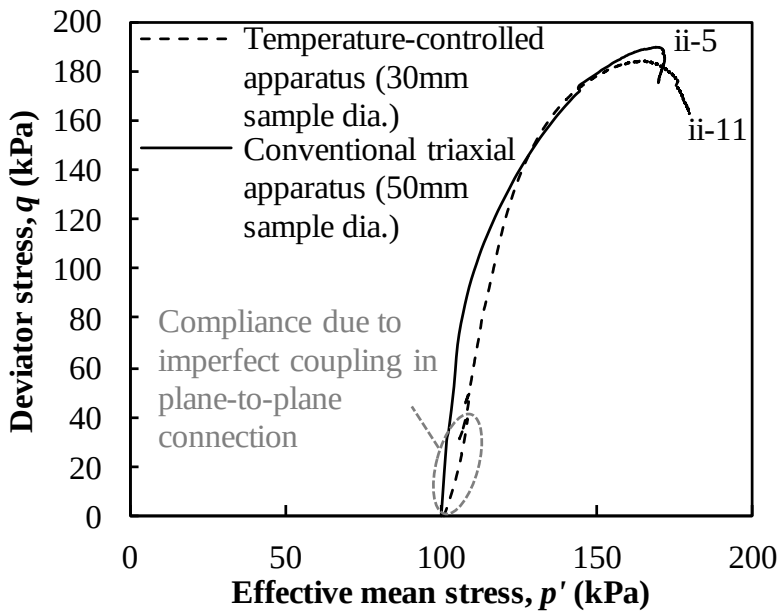

(b)

Figure 4-4 Comparison of unfrozen tests (ii-11 and ii-5) conducted in temperature-controlled apparatus and conventional triaxial apparatus in terms of: (a) Stress-strain relationships and (b) Effective stress paths

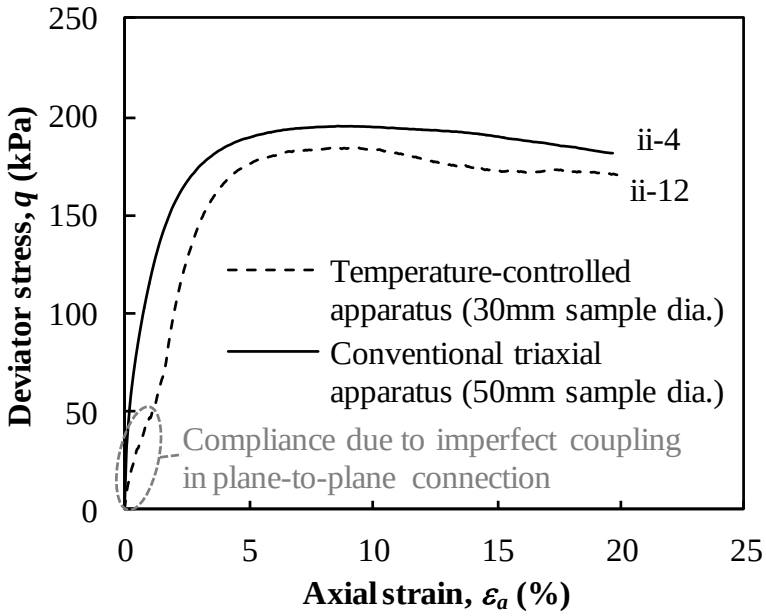

(a)

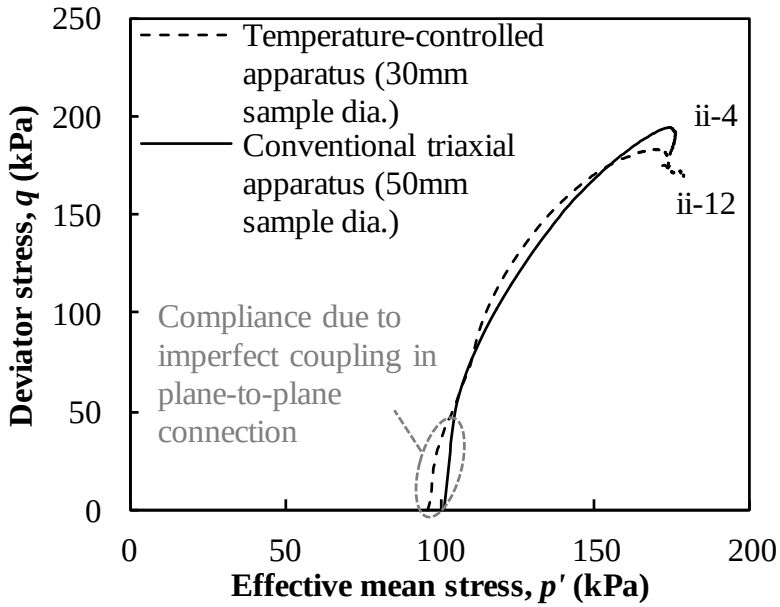

(b)

Figure 4-5 Comparison of unfrozen tests (ii-12 and ii-4) conducted in temperature-controlled apparatus and conventional triaxial apparatus in terms of: (a) Stress-strain relationships and (b) Effective stress paths

5. STRENGTH CHARACTERISTICS OF FROZEN SAMPLES

In this section, the strength characteristics of frozen clay samples are discussed. Firstly, the stress-strain curves for different temperatures, axial strain rates and maximum effective consolidation stress before freezing, p_c', are presented. Interpreting the results with those for the unfrozen over-consolidated (OC) clay specimens which were deliberately controlled to experience very similar, if not same, consolidation histories and strain histories as applied to the frozen specimens, the effective stress paths followed by the frozen samples are probed on the basis of Ladanyi and Morel's (1990) postulate. Envisaged effective stress paths of frozen clay are deduced for a case of full freezing of the pore water. The shear behavior and strength at critical states are discussed afterwards. The effects of temperature and axial strain rate in constant-condition and varying-condition tests are analyzed, leading to an overall interpretation on general effects of temperature and axial strain rate. Finally, in light of the obtained CSLs of the frozen samples, the effect of pore ice/water pressure on shear strength of frozen soil is explored by newly-designed test series.

5.1. STRESS-STRAIN RELATIONSHIPS AND ENVISAGED EFFECTIVE STRESS PATHS OF FROZEN SAMPLES

5.1.1. Stress-strain relationships of frozen samples and repeatability check for them

The specimens consolidated to p_c'=100, 200 and 400 kPa were tested at three freezing temperatures (-2, -5 and -10°C) at the strain rate of 0.01%/min (Series (i)). The stress-strain curves exhibited generally ductile behavior, as shown in **Figure 5-1**. The curves are clearly divided into three groups by temperature and the strength consistently increased with an increase in p_c'. The deviator stresses in the tests with lower temperature and lower pre-freezing effective stress (i.e. p_c'), or i-16 (T=-10°C, p_c'=200 kPa), i-20 (T=-5°C, p_c'=100 kPa) and i-21 (T=-10°C, p_c'=100 kPa), were observed to decrease once and then increase again at the strain of 3-4%. This feature may be attributed to a brittle failure of ice bonding, which is more likely to occur under lower temperature and smaller confining pressure (Sayles, 1973; Andersland and Ladanyi, 2004). Note that the cell pressure was kept constant (=200 kPa back pressure + p_c') during freezing and, for a same volumetric expansion, the reduction of the 'effective stress' was smaller when freezing occurred from smaller p_c' (see **Figure 4-1**). It follows that the corresponding rise in the pore ice pressure was smaller, leading to more brittleness in the ice. The subsequent deviator stress increases can be explained by the internal granular friction taking on the stress (Ting et al., 1983).

For p_c'=400 kPa, three orders of strain rates were applied for frozen specimens at T=-2, -5 and -10°C (i-1~13 in **Table 3-1**). The stress-strain curves, some of which were included in **Figure 5-1**, seemed again to be generally ductile, as shown in **Figure 5-2**. The curves are clearly divided into three groups

by temperature and the strength consistently increased with an increase in axial strain rate. Some stress-strain curves for the slowest strain rate were not quite smooth due to the fact that slight fluctuations in testing temperature compromises the stress-strain data quality for the slowest loading (i.e. 0.001%/min) period, for which a 5% strain interval represents 4 days.

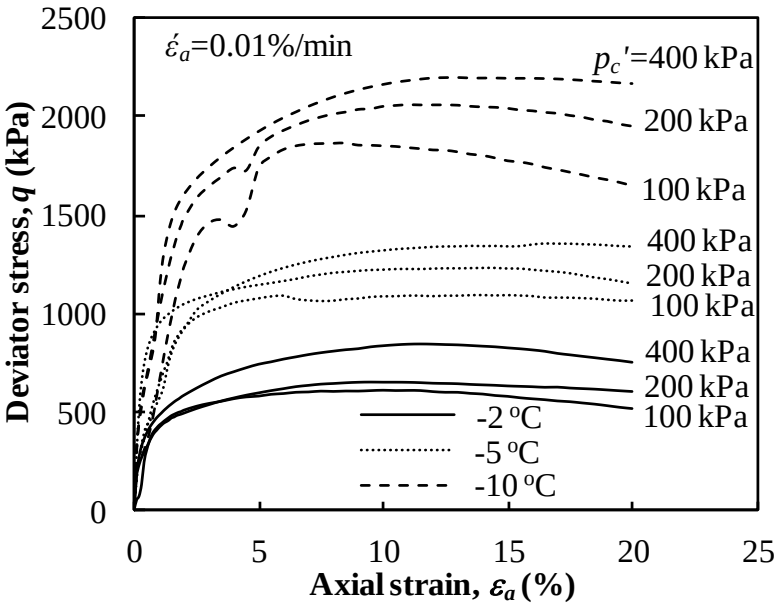

Figure 5-1 Stress-strain relationships in frozen specimens observed for constant temperatures at strain rate of 0.01%/min

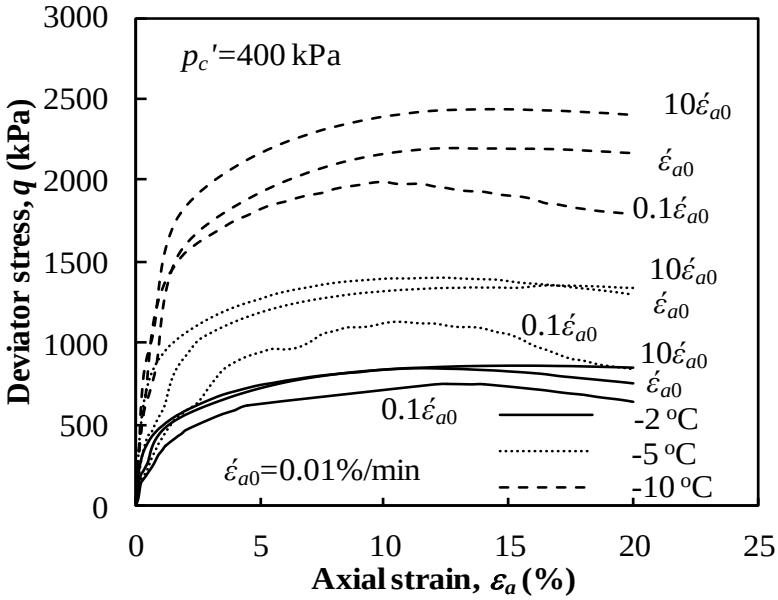

Figure 5-2 Stress-strain relationships in frozen specimens observed for constant temperatures and axial strain rates for p_c'= 400 kPa

Duplicate tests were performed to verify the repeatability and accuracy in this test program. **Figure 5-3(a)** shows the stress-strain curves of duplicate tests for T=-2°C and $\acute{\varepsilon}_a$=0.1%/min with the "plane-plane" ram-platen contact which has been illustrated in **Figure 3-7(a)**. The results matched very well. Lesser but still acceptable degree of consistency was also observed with the "ball point-plane" ram-platen contact, as shown by the stress-strain curves of i-10(pt) and i-11(pt) in **Figure 5-3(b)**. The stress-strain curves of i-1(pl) and i-11(pt) held close peak strengths. If the deviator stress of the specimen at the axial strain of 20% is defined as critical state (CS) shear strength, after which there is very limited stress changes in most test cases, almost same CS shear strengths of the aforementioned i-1(pl) and i-11(pt) could be observed. The strength obtained from both contact arrangements can thus be given a credit, while the ball point-platen contact generally alleviated the aforementioned initial compliance.

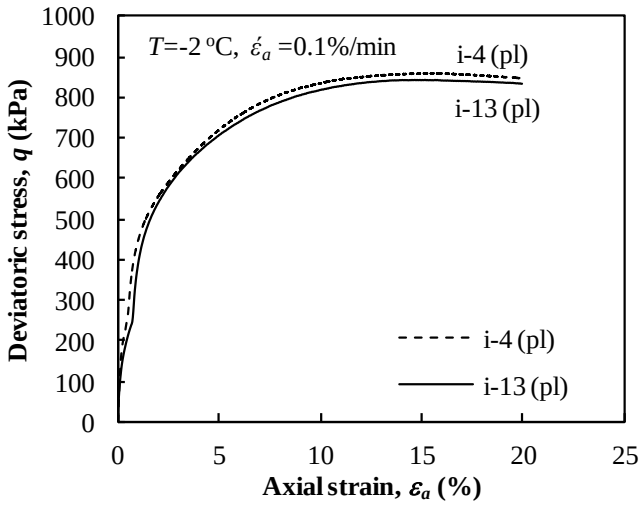

(a)

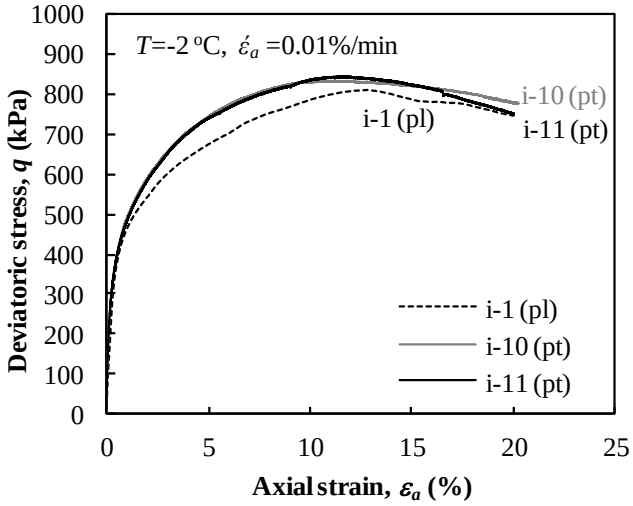

(b)

Figure 5-3 Contrast of stress-strain curves of duplicate tests: (a) with T=-2°C, $\acute{\varepsilon}_a$=0.1%/min and "plane-plane" (pl) ram-platen contact; (b) with T=-2°C, $\acute{\varepsilon}_a$=0.01%/min and different ram-platen contact forms ("plane-plane" or "ball point-plane" (pt))

5.1.2. Deduced effective stress paths for frozen soils under shear

As previously mentioned, the void ratio of the OC specimens in unfrozen tests was deemed to increase by 9% (Line OC in **Figure 5-4(a)**) under controlled unloading before undrained shear (Line CD). However, the frozen specimens under comparison did not expand exactly by the same magnitude, as the pore water froze only partially. The expansion coefficient of the void ratio, *f*, due to undrained freezing is expressed by:

$$f = 1.09 - 0.09 w_u / w_c \tag{1}$$

where w_c is the total water content at p_c' prior to freezing (measured after the test) and w_u is the unfrozen water content estimated from the interpreted relationship shown in **Figure 3-13**. The actual void ratio of the frozen specimens is fe_c, corresponding to point A in **Figure 5-4(a)**. According to Ladanyi and Morel's (1990) postulate, the effective mean stress, p', in the frozen specimen is same as those of the unfrozen specimen unloaded to a same void ratio of fe_c, given that they share same strain histories all through consolidation and shear. By projecting point A to the CSL, which had been established for the unfrozen specimens, p' in the frozen specimen at the critical state (point B) was estimated. The difference of p' between Points B and D (or D') is the correction necessary for the unfrozen water content. Note that q is measurable even in the frozen tests all through the shear, thus allowing mapping of B and D' in the q: p' space. The deviator stress at the strain of 20% in the stress-strain relationship was adopted as the deviator stress at the Critical State, as introduced earlier. The path connecting C to D' or A to B may be established by referring to the unfrozen q (defined q') at a common axial strain (and hence radial strain under undrained conditions), as schematically illustrated in **Figure 5-4(b)**, by following Ladanyi and Morel's postulate.

In ideal case of full freezing of pore water, a same p' value was assumed against the same axial strain (and hence same radial strain under the undrained condition) for both frozen and unfrozen tests. The 'effective stress paths' of frozen soils at the same strain rate were thus envisaged as shown in **Figure 5-4(c)**. The dotted segment in the stress path for T=-10°C, p_c'=100 kPa (i.e. the leftmost curve) represents a corrected part which was considered affected by temporary abnormal performance of the data acquisition system during the test.

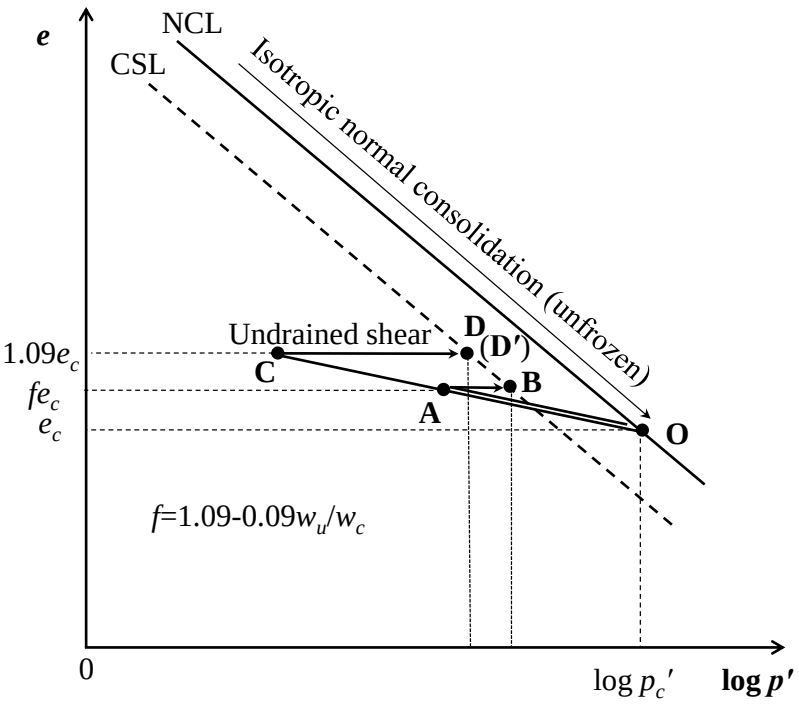
e
NCL
CSL
Isotropic normal consolidation (unfrozen)
Undrained shear
D
(D′)
1.09e_c
C
B
fe_c
A
e_c
O
f=1.09-0.09w_u/w_c
0
log p_c'
log p'

(a)

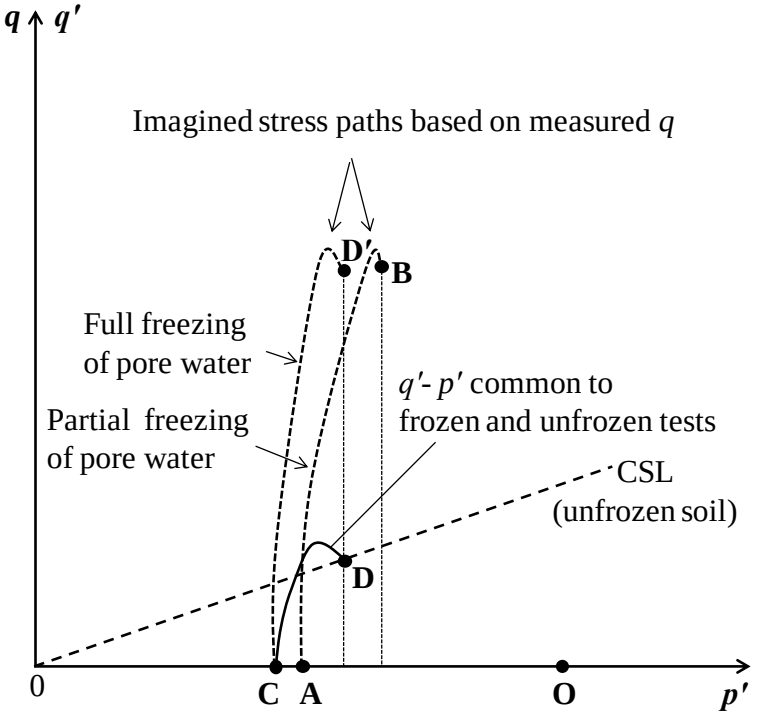
q q′
Imagined stress paths based on measured q
D′
B
Full freezing
of pore water
q′- p′ common to
frozen and unfrozen tests
Partial freezing
of pore water
CSL
(unfrozen soil)
D
0
C
A
O
p′

(b)

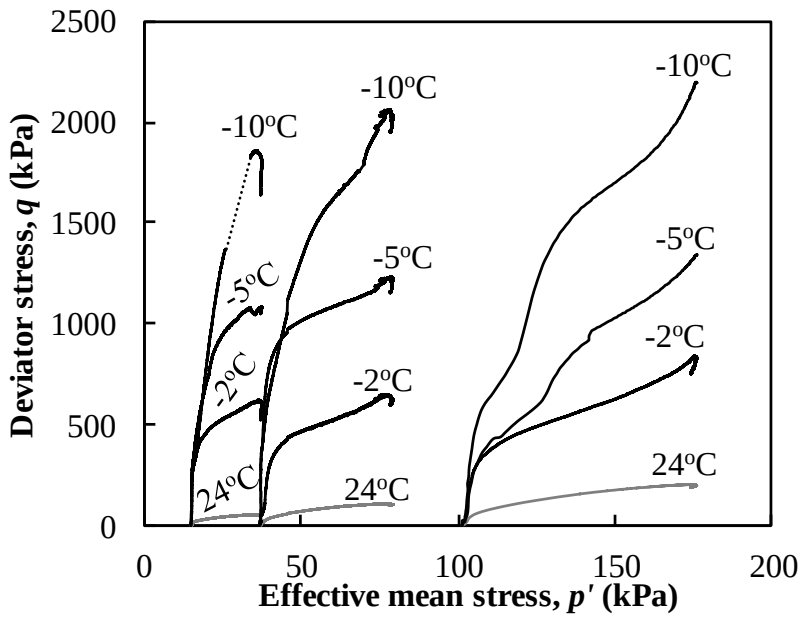

(c)

Figure 5-4 Illustrations of mapping effective stress path in frozen sample and estimated stress paths: (a) illustration of *e*-log *p′* relationship throughout the frozen soil test; (b) illustration of mapping the imagined stress paths based on measured *q*; (c) estimated effective stress path in case of full freezing of pore water

5.2. SHEAR BEHAVIOR AND STRENGTH AT CRITICAL STATES

The CSLs deduced in the above way for the strain rate of 0.01%/min are shown in the *q*:*p′* plane in **Figure 5-5(a)**. The CS strengths at p'≈50 kPa for T=-5°C and $\acute{\varepsilon}_a$=0.1%/min, and at p'≈200 kPa for T= -5°C and $\acute{\varepsilon}_a$=0.001%/min were not consistent with the general trends discussed in the next section, and need further deliberations with a more comprehensive test program. The CS strength at the strain rate of 0.01%/min increased linearly with *p′*. The existing literature mostly discusses the effects of confining stress only as total stress applied after freezing. The new interpretation here, on the contrary, takes account of the presumed inter-particle stress (i.e. effective stress) that remains in the soil skeleton as a result of initial consolidation, freezing expansion and shear. The slope, M_f, and intercept, c_f, of the CSLs increased broadly linearly with a decrease in the temperature below 0°C, as shown in **Figure 5-5(b)**. For frozen states, the resistance of ice gives rise to *q* intercept at *p′* =0 even at the critical states, where *q′*, defined for unfrozen states, is zero. The change of the CSL slope due to temperature may reflect effects of confinement on pore ice itself, as the pore ice/water pressure is larger for the tests with larger *p′* by the reason discussed earlier in this chapter. This possibility would be examined later in this chapter (i.e. section 5.4) by reducing the cell pressure after the freezing.

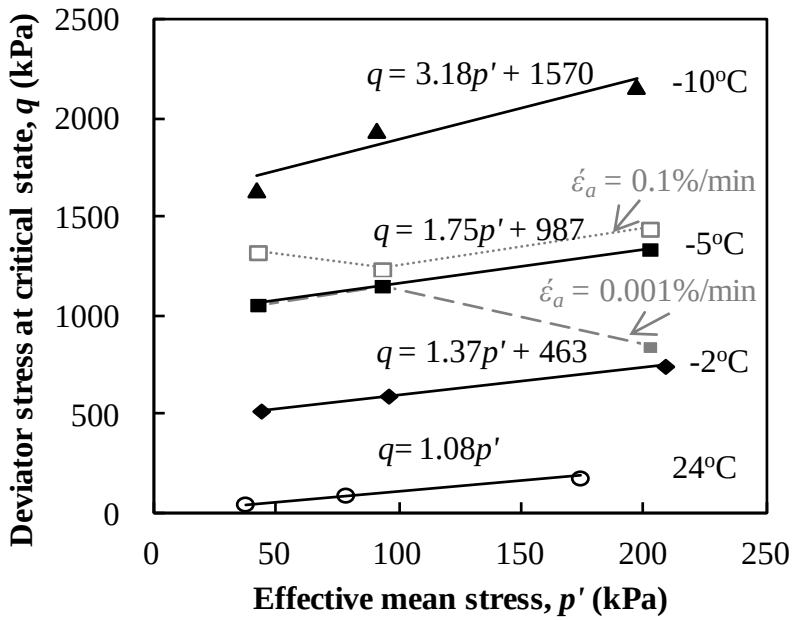

(a)

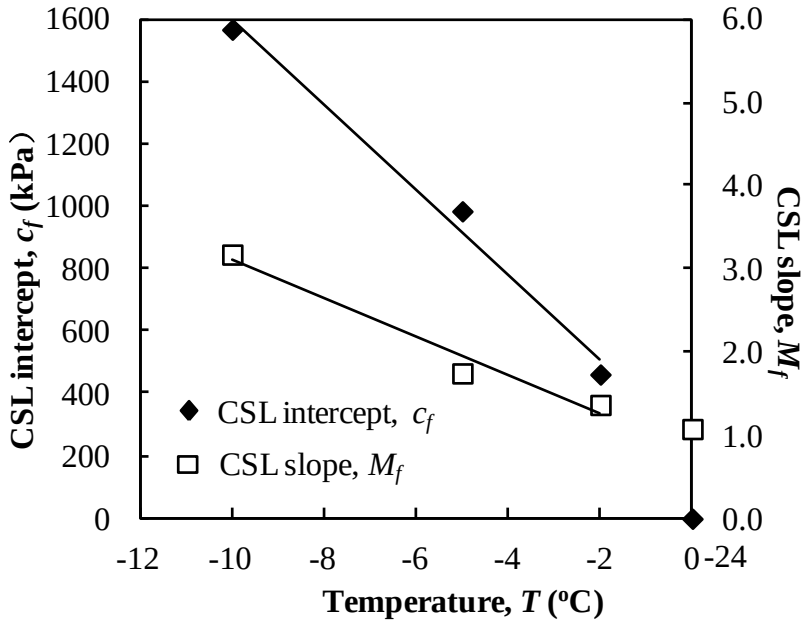

(b)

Figure 5-5 Shear behaviors of frozen samples: (a) Critical State Lines for axial strain rate of 0.01%/min (Critical State points at strain rate of 0.1 and 0.001%/min for -5°C also shown); (b) Temperature effects on the slope and intercept of the CSLs

5.3. GENERAL EFFECTS OF TEMPERATURE AND STRAIN RATE ON STRENGTH AND INTERPRETATIVE FRAMEWORK

5.3.1. Temperature and strain rate effects in constant-condition tests

The experimental results obtained from Series (i) reveal relationships of the shear strength with temperature and axial strain rate. As **Figure 5-6(a)** shows, at a same axial strain rate and p_c'=400 kPa, the peak undrained shear strength of the frozen sample increased linearly with a decrease in temperature over the range -10 to -2°C. With higher axial strain rates, the slope of the trend line is steeper. This temperature dependency of shear strength is in line with, for example, Yamamoto and Springman's (2014) results on reconstituted ice-rich frozen silty gravel sampled from a rock glacier between -3.0 and -0.3^{o}C. **Figure 5-7(a)** shows the comparison of results from their study and this study. The peak strength in the warmer temperature range also showed a similarly linear temperature dependency in their work. The magnitude of the slope of trend line increased with an increase in the strain rate, which agrees with the founding in this study. Haynes and Karalius (1977) conducted unconfined compression tests on frozen Fairbanks silt with a temperature range of -56.7 to 0°C and also observed more pronounced effects of temperature at higher strain rates. Their results are reanalyzed in terms of strain rate instead of machine speed used in their paper, as shown in **Figure 5-7(b)**. Yang et al. (2015) found that the ultimate compression strength of undisturbed naturally frozen silts increased with decreasing temperature raging from -0.7 to -11.6^{o}C with a linear trend as shown in **Figure 5-7(c)**. Their data were slightly scattered probably due to naturally frozen samples having less uniform ice distribution.

Table 5-1 Summary of soil types and testing conditions in previous studies and this study

Publication	Soil type	Specimen shape	Strain rate (%/min)	Temperature (^{o}C)	Testing method
Yamamoto and Springman (2014)	Silty gravel	Cylinder	0.006~0.3	-3~ -0.3	Triaxial
Haynes and Karalius (1977)	Fairbanks silt	Dumbbell	24~2400	-56.7~ 0	Unconfined
Yang et al. (2015)	Naturally frozen silt	Cylinder	6	-11.6~ -0.7	Unconfined
This study	Kasaoka Clay	Cylinder	0.001~0.1	-10~ -2	Triaxial

Table 5-1 summarizes the differences in soil types and testing conditions in previous studies as well as this study. As reflected by **Figure 5-7**, temperature dependency of shear strength of frozen soil in these studies turned out linear regardless of different soil types and testing condition. This study's data sets are unique, however, in that they allow direct comparison of the strain-rate effects between frozen and unfrozen specimens with identical strain paths and states in the soil skeleton (including the

consolidation, expansion and undrained, constant-volume shear history, although the expansion amount differed slightly due to the unfrozen water content). In the tested ranges, the peak undrained shear strength, c_u, is normalized by that at a given temperature (for example -2°C in **Figure 5-6(a)**) to form a fairly unique relationship. The critical state (CS) strengths were shown in **Figure 5-6(b)** in contrast to the peak strengths. For strain rates of 0.1 and 0.01%/min, the CS strength was just slightly smaller than the peak strength, while it was visibly smaller for 0.001%/min. While the mechanism for this is not totally clear, soils' response against slow loading is dominated by creep/relaxation (e.g. Arenson et al., 2007), and this may become gradually more relevant after the peak shear strength is mobilized.

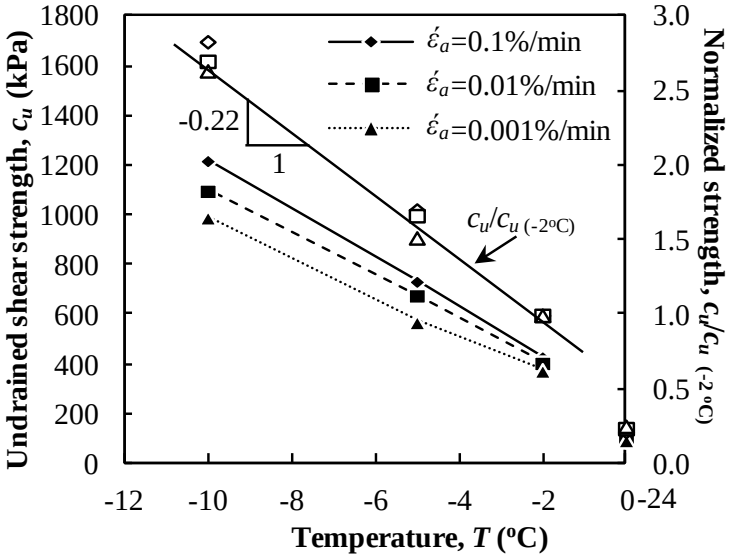

(a)

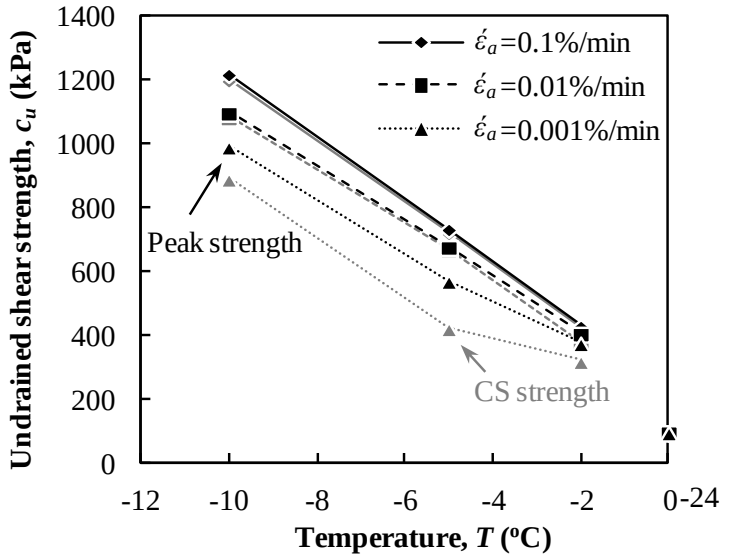

(b)

Figure 5-6 Relationships between shear strength and temperature for p_c' =400 kPa: (a) in terms of peak strength as well as normalized one; (b) in terms of CS strength as well as peak strength

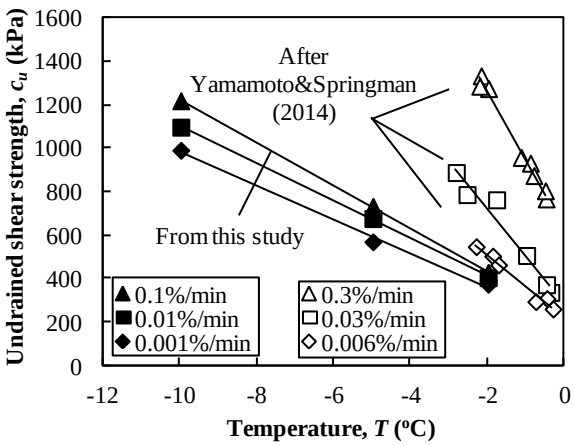

(a)

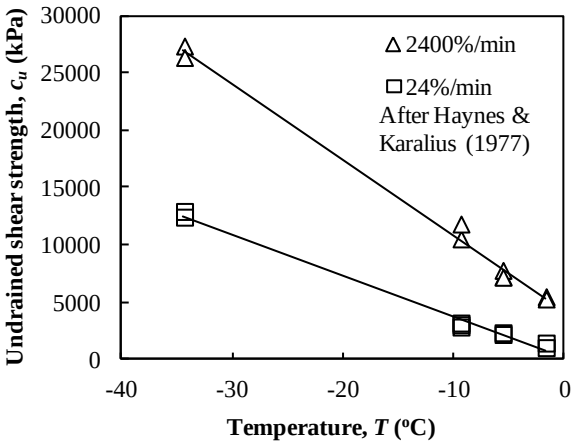

(b)

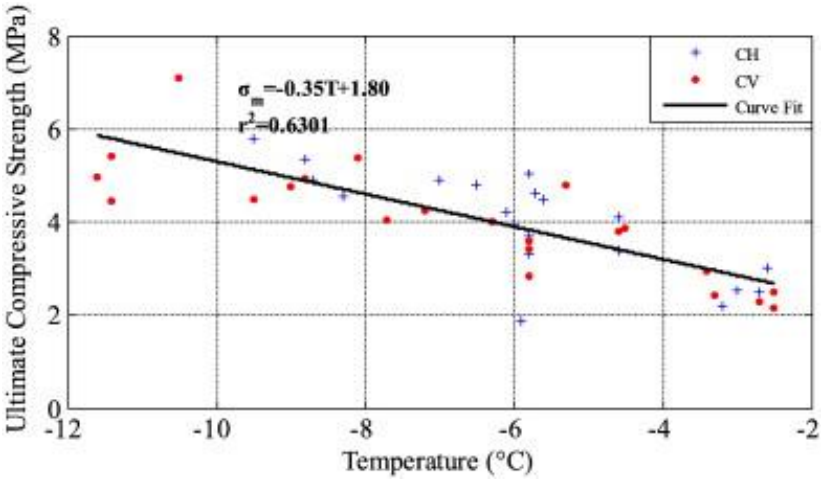

(c)

Figure 5-7 Results on shear strength vs. temperature for frozen soil: (a) Comparison of undrained shear strength with Yamamoto and Springman's (2014) study; (b) Results reproduced after Haynes and Karalius (1977); (c) Ultimate compressive strength vs. temperature for seasonally frozen silt specimen machined horizontally (CH) and vertically (CV) (from Yang et al., 2015)

The c_u value for unfrozen states at +24°C is plotted against 0°C in **Figure 5-6**, assuming that c_u is constant above the freezing temperature. Although the temperature above 0°C is still known to affect the mechanical properties of soils (e.g. Cekerevac and Laloui, 2004; Abuel-Naga et al., 2006; Tsutsumi and Tanaka, 2012), the effect is considerably small compared to that below the freezing temperature. Recalling the earlier discussion on **Figure 4-2**, the unfrozen (+24°C) OC specimens exhibited almost no visible strain-rate effects. Comparing to the identical-state unfrozen reference sample unambiguously indicates that the strain-rate effect is fully due to pore water freezing.

Figure 5-8(a) shows that, at a same temperature, the shear strength of the frozen clay linearly increased with a logarithmic increase in the strain rate. While it also appears linear in a log-log scale for the tested range of 0.001-0.1%/min as shown in **Figure 5-8(b)**, Li et al. (2004) found that the unconfined compressive strength of a frozen clay with medium dry density increased with a different trend against $\dot{\varepsilon}_a$ of 0.1%/min or greater. This may be due to change of ice response from ductile to brittle, and the trend seen in **Figure 5-8(a)** should not be extrapolated to a faster rate. The slope of the trend lines is steeper at lower temperatures. In a normalized form (by c_u at 0.1%/min, for example), again, a broadly unique relationship is obtained as shown in **Figure 5-8(a)**, indicating roughly ~9% increase per log cycle of strain rate for the peak strength. Summarizing the above normalization, the peak undrained shear strength, c_u can be expressed by the following equation for the investigated ranges:

$$\frac{c_u(T,\dot{\varepsilon})}{c_u(T_0,\dot{\varepsilon}_0)} = \left[\alpha_T(T-T_0)+1\right]\left[\alpha_{\dot{\varepsilon}}\log\left(\frac{\dot{\varepsilon}}{\dot{\varepsilon}_0}\right)+1\right] \qquad (T,\ T_0 < T_f) \qquad (2)$$

where T_0 and $\dot{\varepsilon}_0$ are a reference temperature and a reference strain rate, which may be arbitrarily chosen within the tested range (e.g. T_0 = -2°C and $\dot{\varepsilon}_0$ = 0.1%/min as shown in **Figures 5-6** and **5-8(a)** in this study), respectively, α_T and $\alpha_{\dot{\varepsilon}}$ are the slopes in the normalized c_u line in **Figures 5-6** and **5-8(a)**, respectively, and T_f is the freezing temperature. A similar relationship also broadly holds for the undrained CS strength.

The nature of temperature effects on the strength is further explored in **Figure 5-9**, which compares the CSL intercepts from **Figure 5-5(b),** interpreted as ice cohesion component, c_f, in the CS strength of the frozen clay, with compressive ice strength reported in the literature. Zhang et al.'s (2012) results for unconfined condition have a similar trend as for the CSL intercepts, suggesting that the "ice cohesion" is compatible with the pore ice strength. However, results from Rist and Murrell (1994) show very different trends under large total stress (5 MPa). The present study's tests involved the cell pressure of 600 kPa (for p_c'=400 kPa) at maximum and the ice phase pressure is thought to be smaller than this, thus explaining the agreement with Zhang et al.'s (2012) results. Note, however, that an ice

crystal can take anisotropic microstructures depending on how it is formed, and attention is here drawn only to broad comparisons.

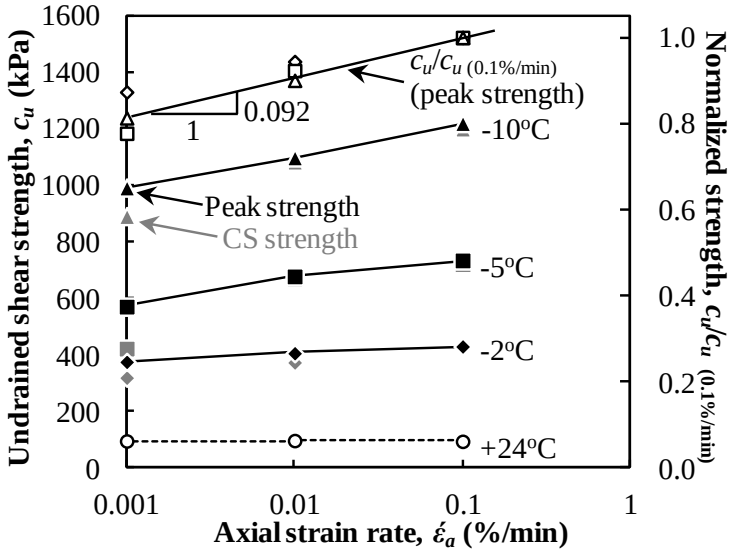

(a)

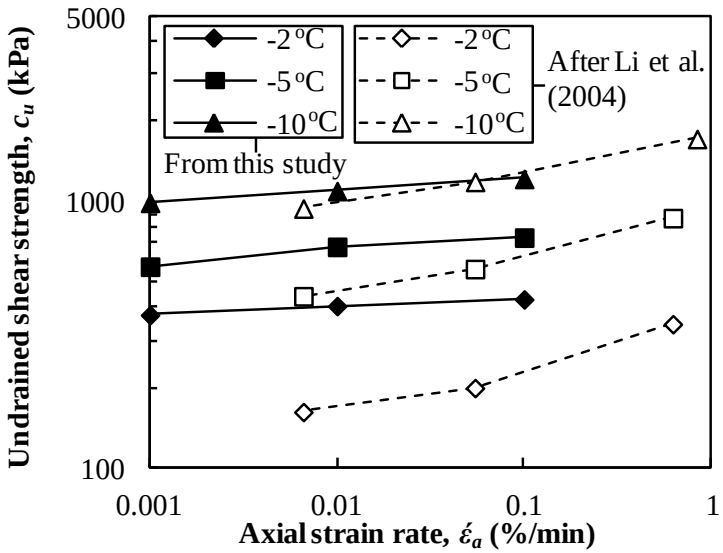

(b)

Figure5-8 Relationships between shear strength and strain rate: (a) for p_c' =400 kPa; (b) Comparison to results after Li et al. (2004) in log-log scale

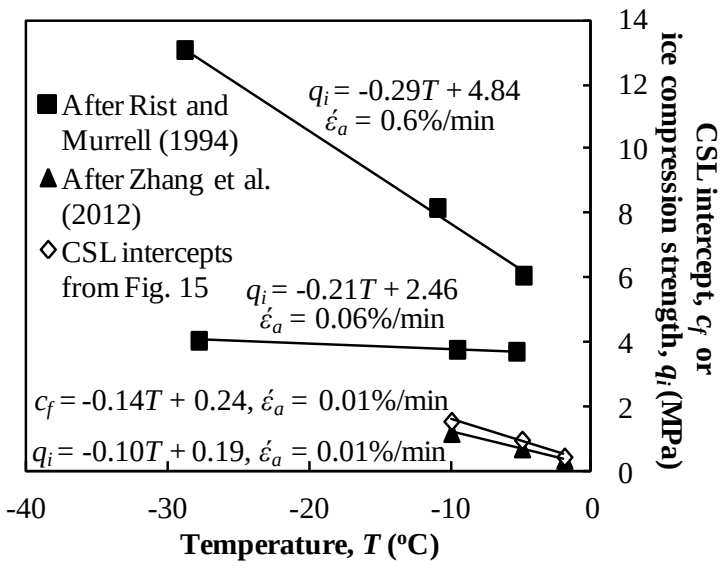

Figure 5-9 Temperature effect on the CSL intercept in this study and on ice compression strength in literature (confining pressure of 5 MPa in Rist and Murrell, 1994, and unconfined condition in Zhang et al., 2012)

5.3.2. Temperature and strain rate effects in varying-condition tests

In most real situations, the ambient temperature varies with time going. Knowledge of the response of frozen soil to general changes of temperature is desired. As complementary tests to the constant-temperature tests conducted in Series (i), varying-temperature tests described in Section 3.3 were carried out (Series (iii)). The test paths for constant- and varying- temperature tests are illustrated in **Figure 5-10**.

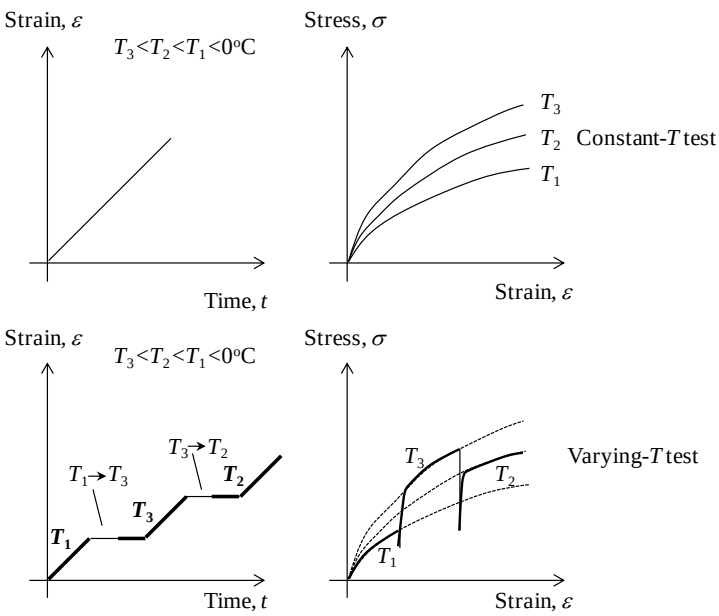

Figure 5-10 Illustrations of test paths for constant- and varying- temperature tests

From the varying-temperature tests (Series iii-1 and 2), the stress-strain relationships with the starting temperature of -5°C and -10°C at the axial strain rate of 0.01%/min are shown in **Figures 5-11(a)** and **(b)**, respectively. In **Figure 5-11(a)** representing test iii-1, the order of testing temperatures for each incremental axial strain of 5% was -5°C, to -10°C, to -2°C and back to -5°C. In contrast, the order of testing temperatures of test iii-2 was -10°C, to -5°C, to -2°C and back to -10°C, as shown in **Figure 5-11(b)**. The interruption of loading upon a temperature change and ensuing hold for the new temperature equilibrium led to a stress relaxation in this transition period. A stress jump or drop was observed as the loading was resumed with a new, different temperature. This temperature dependency seems to be unique to frozen soil compared to unfrozen soil. Burghignoli et al. (2000) found that the deformability and strength of the unfrozen clayey soil were relatively independent of temperature in the investigated temperature range of 20°C to 60°C. The temperature dependency of frozen soil can thus be attributed to the existence of ice inclusion and ice content variation (referring to the freezing curve in **Figure 3-16**) with different freezing temperature. It can be seen that at strains larger than 5%, where the behavior is almost fully plastic, the stress-strain of the varying-temperature tests traveled along those of the corresponding constant-temperature tests. The stress-strain relationships from the constant-temperature tests serve as bounding backbone curves for the tests under generally changing temperature.

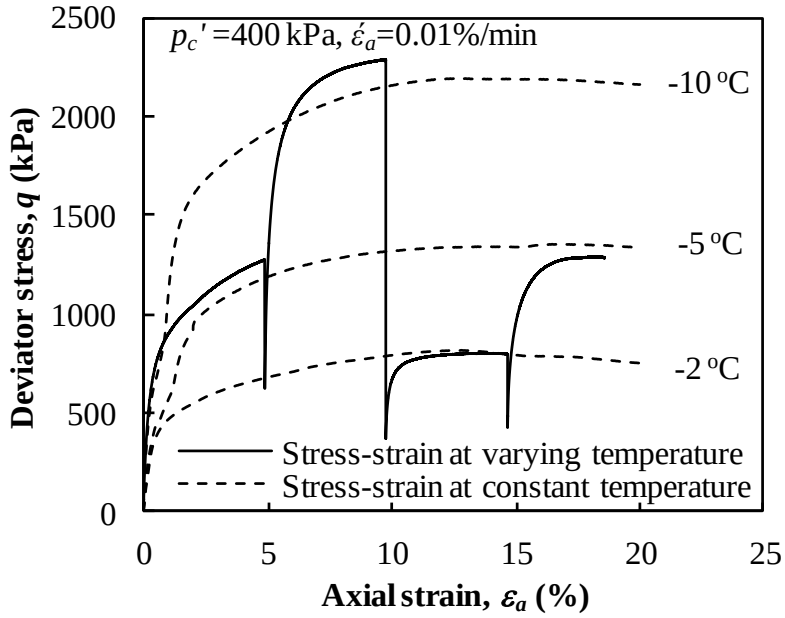

(a)

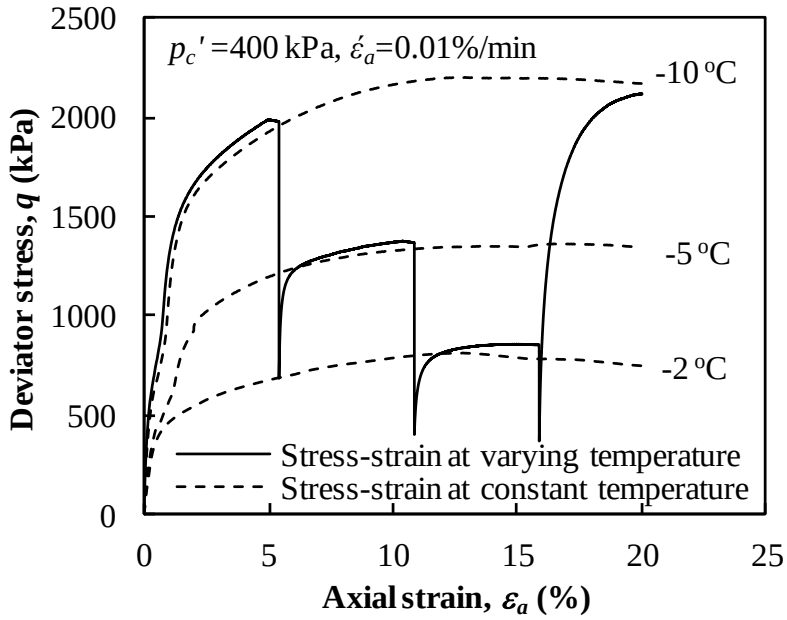

(b)

Figure 5-11 Stress-strain relationship in constant- and varying-temperature tests (a) With the starting temperature of -5°C (iii-1); (b) With the starting temperature of -10°C (iii-2)

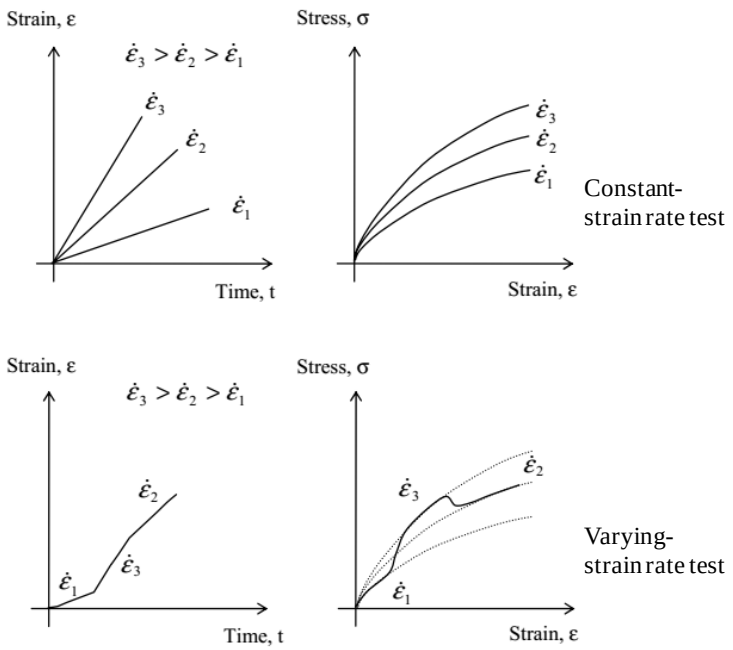

Figure 5-12 Illustrations for test paths for constant- and varying- strain rate tests (modified from Sorensen, 2006)

Constant strain rate triaxial compression tests were performed for unfrozen and frozen tests as already described, in which the axial strain rate was kept constant throughout the test. The strain rate effect on the strength of unfrozen and frozen samples has been summarized. When the behaviors for different strain rates are compared, the possible variation of samples and time consumed by the low strain rate tests (and hence potential long-term drifts of the transducers) are concerned. In this context, Richardson and Whitman (1963) proposed an approach of applying stepwise change of strain rate in a single test for unfrozen soil, which can be used to estimate the immediate strain rate effect. The stress-strain curves can be obtained from interpolation by connecting the portions of curves for the same strain rate. **Figure 5-12** illustrates the test paths for constant- and varying- strain rate tests. However, few attempts of this approach of varying strain rate in a single test were made in past studies of frozen soils. Similar to the previous varying-temperature tests, varying-strain rate tests (iii-3 and iii-4) were carried out in this study.

As for the varying-strain rate test at -2°C, the switching between axial strain rates after every strain interval of 5% was conducted in an order of 0.01, 0.001, 0.1 and back to 0.01%/min. The obtained stress-strain relationship is shown in **Figure 5-13(a)**. The strain rate effect on the stress strain behavior in strain range 5-10% was difficult to distinguish due to uneven portion caused by fluctuation of temperature in the slowest strain rate. At this slowest loading (i.e. 0.001%/min) period, a 5% strain interval represents 4 days. Immediately after an abrupt increase of strain rate by 100 times at the strain of 10%, the stress-strain path was seen to jump upwards and exhibit an initially stiff response. Then almost fully plastic behavior was observed until the subsequent stepwise strain rate

change. When the strain rate was reduced back to the initial strain rate at the strain of 15%, a downward stress drop was observed. The stress-strain path in strain range 15-20% can be roughly regarded to rejoin the extrapolation of the path for the strain rate of 0.01%/min. However, it has to be admitted that the overall response in this varying-strain rate test turned out to be stronger than those in the corresponding constant-strain rate tests at each stage, beginning with a stiffer deformation behavior than that of the corresponding constant-strain rate tests. As the consistency seen in the other tests in this research program indicates reasonable reproducibility of the specimens (see **Figure 5-3**), the reason for this response needs further deliberation by additional tests. Although direct comparison of the deviator stresses between the two test series (i.e. constant- and varying strain rate tests) here is difficult, the strain-rate effect, as represented by the relative shift of the stress, can be compared in a normalized form shown in **Figure 5-13(b)**, in which the maximum deviator stress, q_{max}, at 0.1%/min was taken as 1, separately for varying- and constant-rate series. By normalization to remove the impact of the unknown factors affecting the overall response, the stress-strain curves in the initial common stage (i.e. 0.01%/min) agree between the two series, thus allowing evaluating the relative shifts of q upon rate changes. 7-11% changes of the deviator stress were seen for 10-fold changes in the strain rate in the varying-rate series, as compared to the ~9% changes seen for c_u from the constant-rate tests (**Figure 5-8(a)**). The curve from the varying-strain rate test joined those from the constant-strain rate tests at corresponding rates after transient stages of a few percent strain.

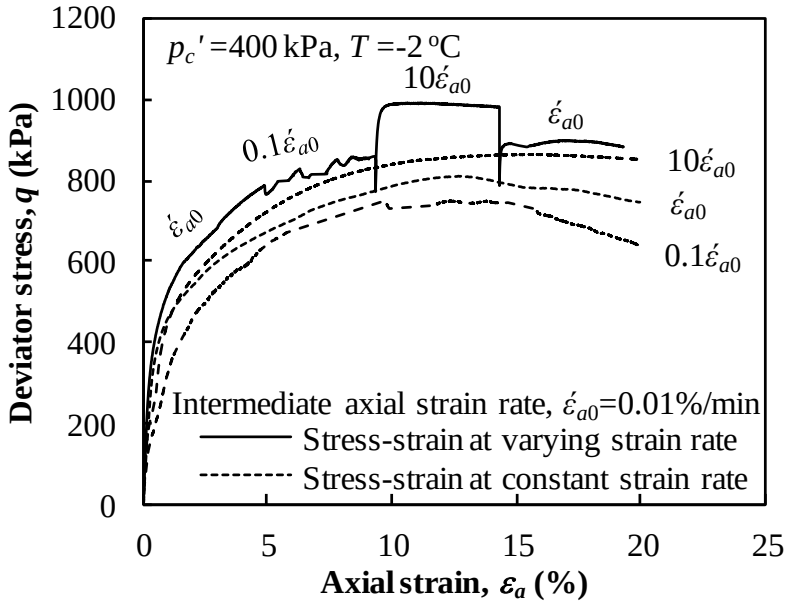

(a)

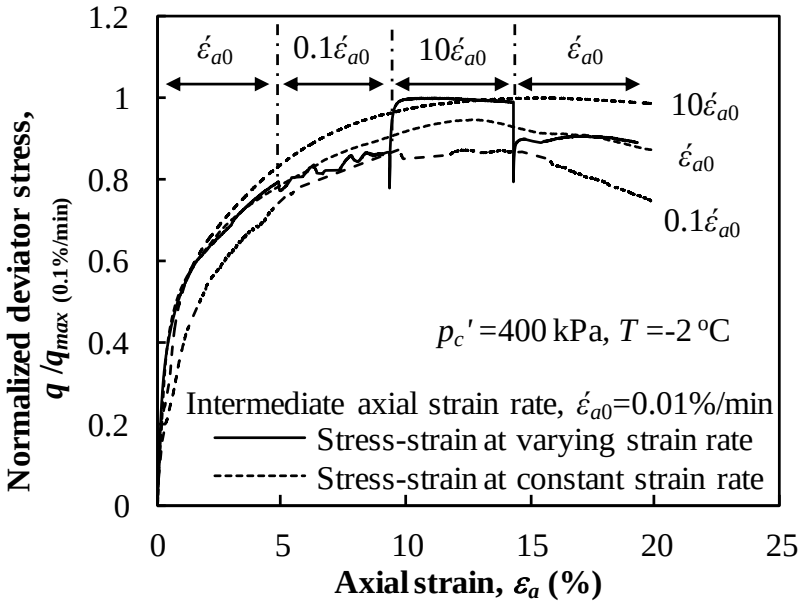

(b)

Figure 5-13 Stress-strain relationship in constant-strain rate tests (i-1, 4 and 7) and varying-strain rate test (iii-3) (a) As measured; (b) Normalized at the peak

For the case of varying-strain rate tests at T=-5°C, distinct strain rate effects were seen for each stepwise strain rate change from **Figure 5-14(a)**. Especially, the strain rate effect was observed in the first strain rate change from 0.01%/min to 0.001%/min, which was ambiguous to distinguish for varying-strain rate tests at T=-2°C. One reason for this improvement is that the temperature fluctuation

around -5°C for shear stage at 0.001%/min was minimized by careful control to sustain the exactly same testing temperature. Compared to the stress-strain behaviors in the corresponding constant-strain rate tests, the shear behavior turned again to be stronger at each stage of varying-strain rate tests except for the coinciding path in the initial strain range 0-3%. In a normalized form shown in **Figure 5-14(b)**, the intermediate stages (i.e. 0.001 and 0.1%/min) approach well to the corresponding stress-strain at constant strain rate.

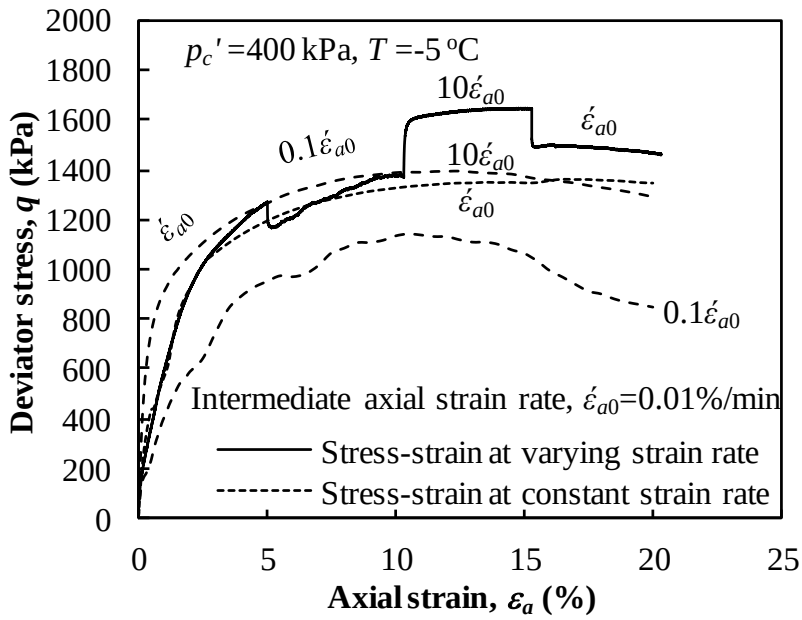

(a)

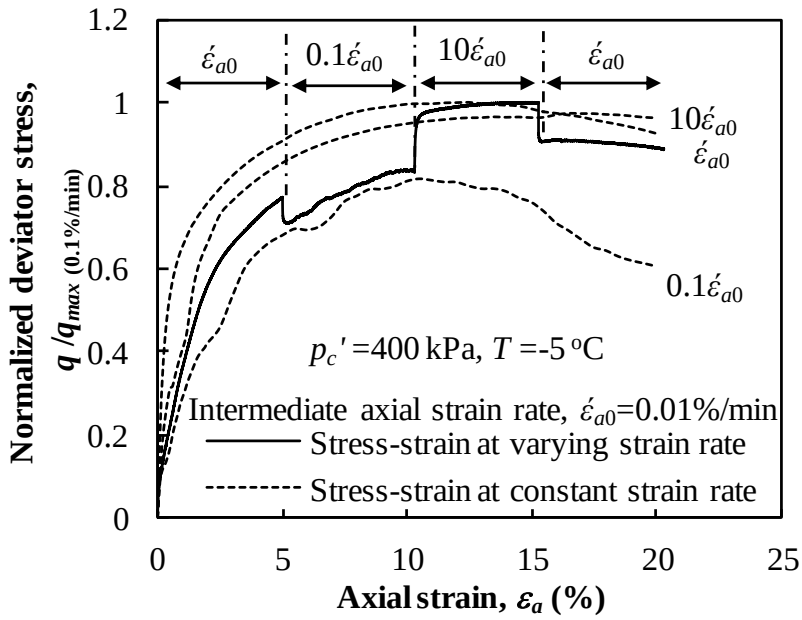

(b)

Figure 5-14 Stress-strain relationship in constant-strain rate tests (i-2, 5 and 8) and varying-strain rate test (iii-4) (a) As measured; (b) Normalized at the peak

The comparisons drawn for the constant- and varying- strain rate tests at -2°C and -5°C suggest a potentially unique stress-strain backbone relationship for a given strain rate, at least when the strain is larger than 5% and the behavior is broadly plastic. Although any further definitive conclusion warrants further tests, this feature is potentially captured by the isotach theory (e.g. Šuklje, 1957; Leroueil, 2006) proposed for unfrozen clays, in which the stress state is uniquely defined by the current strain and its rate (Leroueil et al., 1985; Vaid and Campanella, 1977).

The features of temperature and strain rate effects revealed by tests at constant- and varying-conditions in terms of temperature and strain rate are relatively simple to formulate and will be useful in developing a general rate-dependent thermo-mechanical model for frozen clays.

5.4. EFFECT OF PORE ICE/WATER PRESSURE ON SHEAR STRENGTH OF FROZEN SOIL

In **Figure 5-5**, the deviator stress at the critical state exhibited a linear relationship with the effective mean stress and the CSL slope also seemed to have a linear relationship with temperature. The variation of the CSL slope due to temperature may be attributed to the confinement on pore ice itself. Note that the reduction of the effective stress was smaller for smaller p_c' condition for the same volumetric strain due to swelling (equivalent to freezing) in **Figure 4-1**, which may suggest that the larger value of p_c' led to a larger pore ice/water pressure, u, after freezing. Here pore ice/water pressure is regarded as a synthesized pressure from pore ice and pore water. The lower temperature may reinforce the pore ice/water confining effect due to the increased ice content. According to this mechanism, the pore ice pressure may play a role in determining how much deviator stress the pore ice can sustain at critical state, in addition to that sustained by the soil skeleton (i.e. effective mean stress). As shown in **Table 5-2**, corresponding to different values of p_c', pore ice/water pressure varies in an obvious manner if it is calculated by subtracting effective mean stress from total stress.

Table 5-2 Pressure and stress at the beginning of the shear for tests with various p_c'

	p_c'=100kPa	p_c'=200kPa	p_c'=400kPa
Total stress (cell pressure)	300kPa	400kPa	600kPa
Effective mean stress	15kPa	36kPa	100kPa
Pore ice/ water pressure	**285kPa**	**364kPa**	**500kPa**

In order to discuss the effect of pore ice/water pressure on the CS strength, additional frozen soil tests (i.e. Series (iv)) were carefully designed and conducted. As illustrated in **Figure 5-15**, unlike the test

series (i), represented as "NC" frozen soil test here, Series (iv) decreased the cell pressure after the specimen was frozen and stabilized into a stable temperature (i.e. Step 3 in **Figure 5-15**). Frozen specimens undergoing decrease of cell pressure after being frozen are defined as "OC" frozen soil here. Since only the cell pressure varies from 600 kPa to 400 kPa or 200 kPa while the skeleton of the frozen sample including pore ice content and void ratio are largely identical, same effective mean stress, p' can be taken, which is 100 kPa in case of p_c'=400 kPa. In this sense, the "OC" specimens were not over-consolidated in terms of the soil skeleton stress, because p' is identical before and after decreasing the cell pressure. When a cell pressure p of 400 kPa or 200 kPa is adopted, the pore/ice pressure u equals to 300 kPa or 100 kPa, respectively. The new cell pressure was kept for 24 hours before undrained shear at an axial strain rate of 0.01%/min was applied to the specimen.

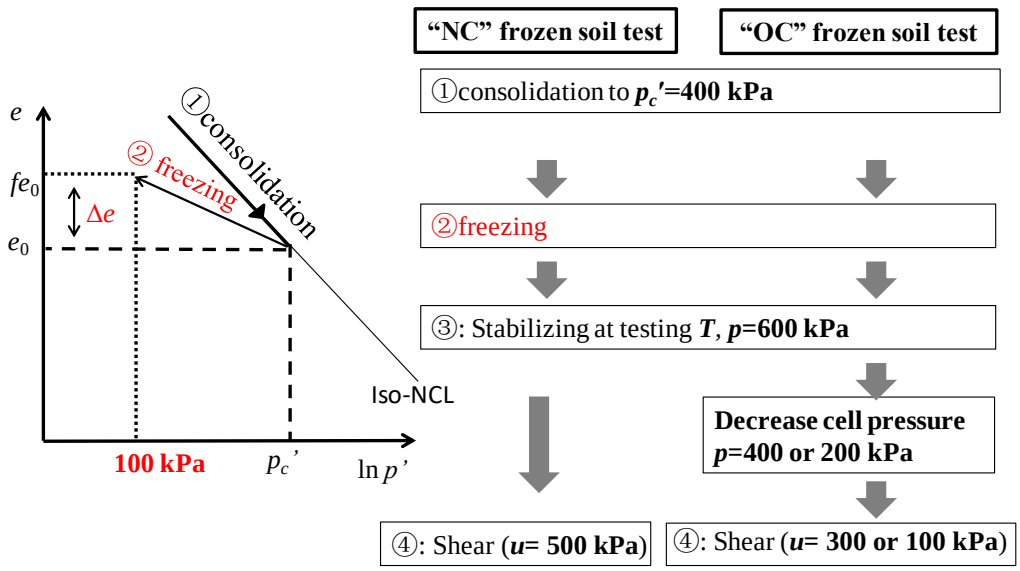

Figure 5-15 Illustration and flow chart of test procedures for "NC" and "OC" frozen soil test

The stress-strain curves of "OC" specimens (u=100kPa and 300kPa) and "NC" specimen (u=500kPa) at -2, -5 and -10°C are shown in **Figures 5-16**, **5-17** and **5-18**, respectively. In **Figure 5-18**, the test with u=300kPa showed a strain-hardening stress-strain curve which was quite different from the other tests. The stress-strain curves in this test as well as the two "OC" tests for T=-2°C (see **Figure 5-16**) turned out to be with noise and not quite smooth. The presented curves of these tests have been processed by deleting the abnormal data points. In the test with T=-10°C and u=500kPa, the undrained shear process was interrupted for once at the axial strain of about 7%, which made the deviator stress have a sudden jump when the shear was resumed as shown in **Figure 5-18**. Taking into account the impact of these noises and the unexpected disturbance, the stress-strain curves for each temperature can be considered very close, especially for T=-5°C. The axial strain at which the deviator stress reached the peak strength for each test is summarized in **Table 5-3**. Except for the test with T=-10°C and u=300kPa having a strain at peak of 16.7%, all the stress-strain curves reached the peak at an

axial strain range 11-14%. The stress-strain curve of "OC" tests showed negligible dependency on the pore ice/water pressure.

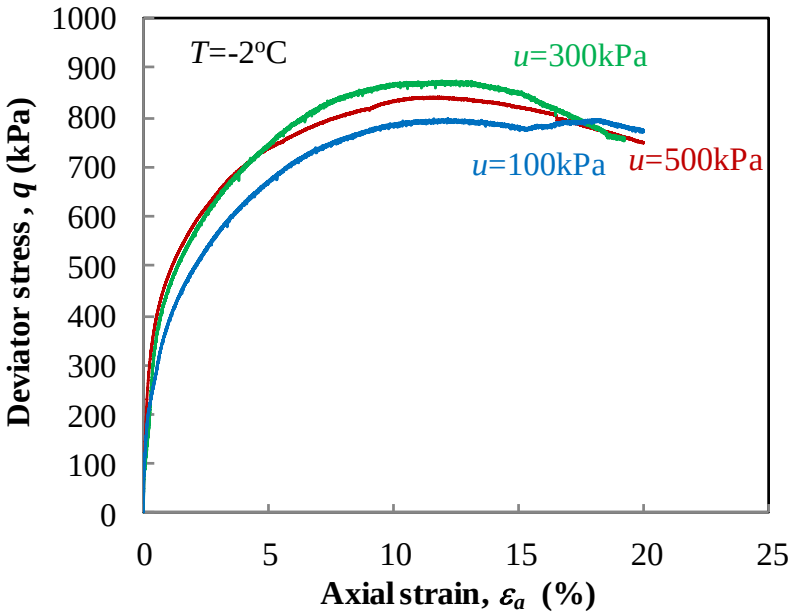

Figure 5-16 Stress-strain curves of frozen soil with different pore water/ice pressures at T=-2°C

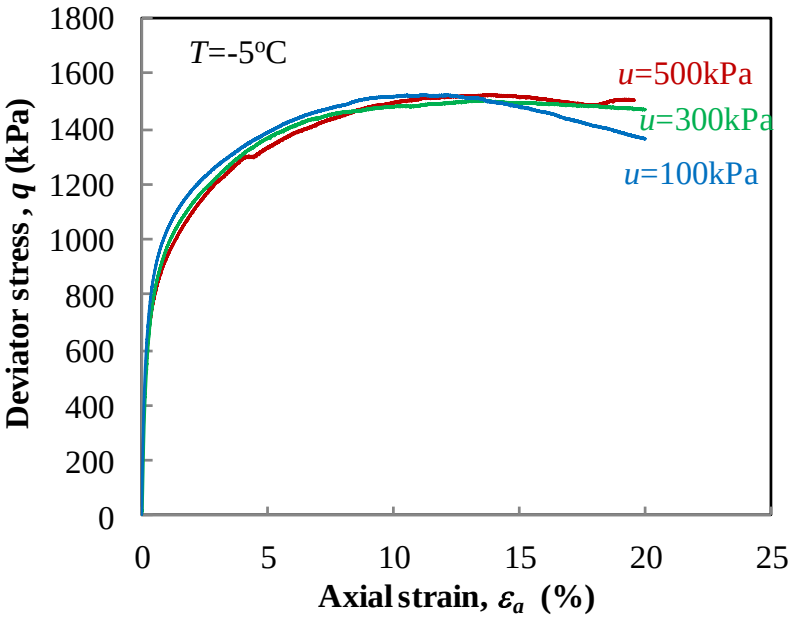

Figure 5-17 Stress-strain curves of frozen soil with different pore water/ice pressures at T=-5°C

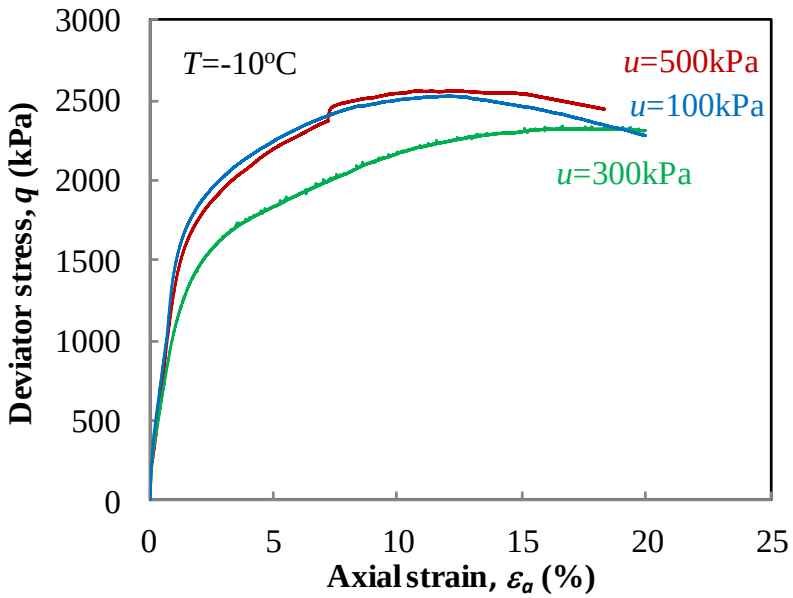

Figure 5-18 Stress-strain curves of frozen soil with different pore water/ice pressures at T=-10°C

Table 5-3 Peak strength and the corresponding axial strain for each test

T= -10°C	Peak strength (kPa)	Strain for peak	T= -5°C	Peak strength (kPa)	Strain for peak	T= -2°C	Peak strength (kPa)	Strain for peak
500	2558	10.8%	500	1526	13.9%	500	842	11.7%
300	2342	16.7%	300	1504	13.6%	300	873	11.9%
100	2533	12.1%	100	1525	11.1%	100	797	12.2%

Figure 5-19 plots the CS strength against the pore ice/water pressure. For T=-5°C, specimens with u=300 and 500kPa had very close critical state (CS) strength while the specimen with u=100kPa showed slightly lower CS strength. For T=-10°C, specimens with u=100 and 300kPa had relatively close CS strength while the specimen with u=500kPa showed slightly higher CS strength. However, for T=-2°C, the "OC" specimens and the "NC" one all had fairly close CS strength although noises occurred during shear of "OC" specimens. Summarizing the general trend in **Figure 5-19,** it can be concluded that the pore ice/water pressure may have a negligible effect on the CS strength for the investigated temperatures, hence the CSL slope seen in **Figure 5-5**. The temperature effect on CSL slope may be attributed to ice content other than the associated ice pressure. The fact that the volumetric ice content influences the angle of friction (equivalent to CSL slope) was revealed by Arenson and Springman (2005b).

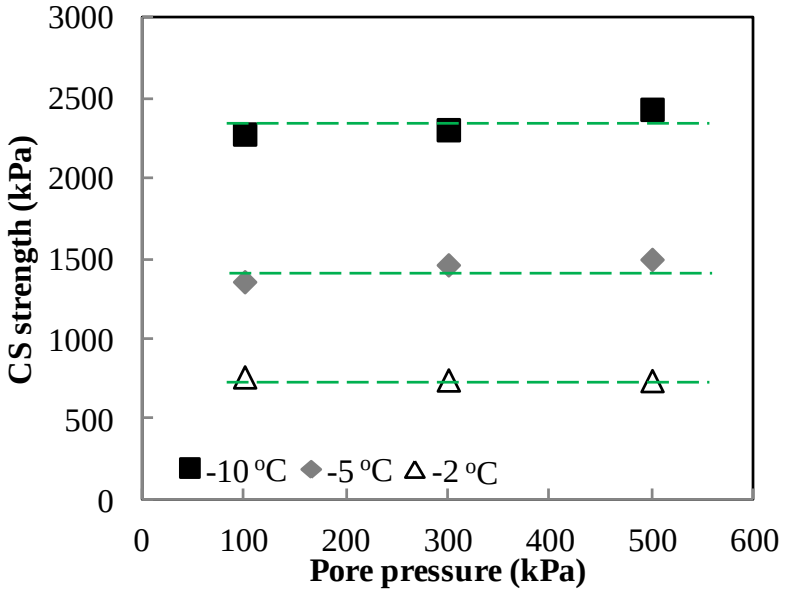

Figure 5-19 Relationship of critical state strength and pore water/ice pressure

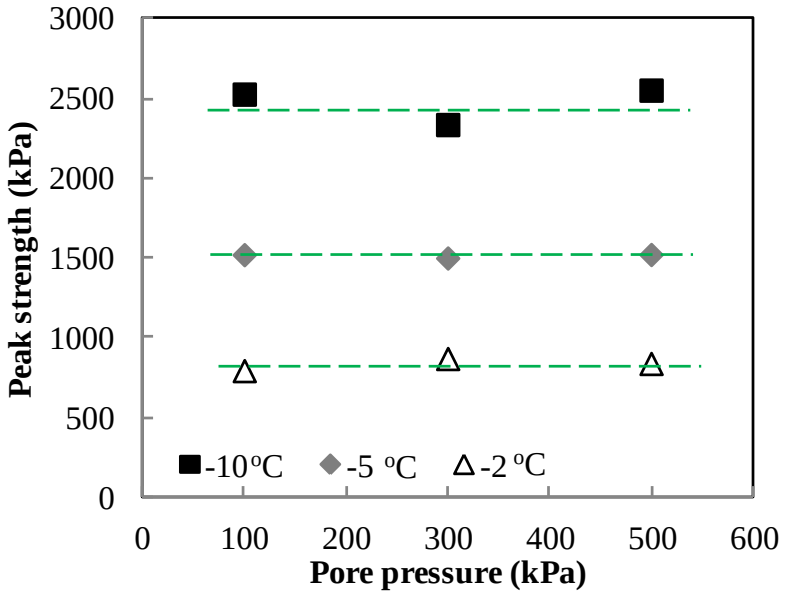

Figure 5-20 Relationship off peak strength and pore water/ice pressure

The negligible dependency on pore ice/water pressure also can be seen for the peak strength-pore ice/water pressure relationship, as shown in **Figure 5-20**. In other words, the shear strength of the tested frozen soil which was isotropically normally consolidated prior to freezing has little dependence on the magnitude of total stress applied after freezing. In past studies, some researchers (e.g. Lai et al., 2010) studied the effect of the confining pressure on the shear strength of frozen soil with specimens which were prepared without knowing the consolidation histories prior to freezing.

Lai et al. (2010) found that the strength of frozen silt increased with increasing confining pressure (in a range less than 10MPa), which was also applied after freezing. The different trend revealed by Lai et al. (2010) may be due to the dilation-induced strengthening under high confining pressure (Andersland and Ladanyi, 2004). In the investigated total confining pressure ranging from 200kPa to 600kPa, the magnitude of confining pressure applied after freezing may have little significance on the shear strength of NC specimens.

6. STIFFNESS CHARACTERISTICS OF FROZEN SOIL

In this chapter, the stiffness characteristics of frozen soil will be the focus of discussion. As previously mentioned, the external measurement of axial strain is inevitably faced with errors, which exert a considerable impact to the accuracy of stiffness of either unfrozen or frozen soils. In the frozen soil test series, gap sensors were employed to measure the small range deformation at the initial stage of shearing. A nondestructive testing method mainly focused on measurement of stiffness is introduced in this chapter. Different temperatures and axial strain rates were applied in order each time after the specimen was loaded and unloaded in the quasi-elastic strain range. From the nondestructive test of frozen soil, the stiffness at three orders of axial strain rates and three temperatures was obtained and compared with those from the monotonic loading tests with shearing to axial strain of 20% in the earlier series. The effects of temperature and strain rate on stiffness of frozen soil are investigated.

6.1. NONDESTRUCTIVE TESTING ON ESTIMATING THE STIFFNESS OF FROZEN SOIL

To measure the stiffness repeatedly for different temperatures and axial strain rates in a single test, the specimen was loaded to a very small strain. Throughout the test, the specimen was sustained to be close to the initial condition (i.e. frozen under isotropic stress). This approach is defined as nondestructive testing method in this study. The nondestructive test took similar steps as the aforementioned frozen soil test series (i), but the strain rate and the temperature were varied repeatedly for a specimen with p_c'=400kPa between the small-strain shearing. The procedures and sequences of each probe of loading-unloading in quasi-elastic range are listed in **Table 6-1**. After the specimen froze at -15°C, it was firstly warmed up to -10°C and kept for 24 hours. Then axial compression was applied at a strain rate of 0.01%/min until an externally measured axial strain of 0.025%. The specimen was then unloaded to the original isotropic state by lifting up the loading ram to initial position. At least 3 cycles of loading and unloading were applied before another strain rate was applied, and the above 0.025%-strain probe was repeated at strain rates of 0.01, 0.1 and then 0.001%/min in order. To confirm that the specimen's state had not changed significantly after these steps, one more cycle of loading and unloading for each strain rate was carried out and the results were compared to the earlier ones. After these loadings at -10°C were done, a new temperature was set in the cell and kept for 24 hours. The 0.025%-strain probes were repeated for the new temperature. The order of stages was set from -10°C to -5°C and finally to -2°C, in a similar way to the earlier tests, in which the specimens warmed up from -15°C to the testing temperatures, which make the results from this test with nondestructive probes comparable to the past individual tests in Series (i), (iii) and (iv).

Table 6-1 Procedures and orders of probes carried out at different temperatures and strain rates

Temperature was set at -10°C and kept for 24 hours after stabilization					
Sequence of probe	T (°C)	strain rate (min/%)	subsequence	Time for loading (min)	ε_{tl} (%)*
1	-10	0.01	No.1	2.5	0.0026
2	-10	0.01	No.2	2.5	0.0026
3	-10	0.01	No.3	2.5	0.0025
4	-10	0.01	No.4	2.5	0.0030
5	-10	0.1	No.1	0.25	0.0026
6	-10	0.1	No.2	0.25	0.0024
7	-10	0.1	No.3	0.25	0.0025
8	-10	0.001	No.1	25	0.0030
9	-10	0.001	No.2	25	0.0030
10	-10	0.001	No.3	25	0.0026
11	-10	0.1	Check	0.25	0.0026
12	-10	0.01	Check	2.5	0.0027
Temperature was set at -5°C and kept for 24 hours after stabilization					
Sequence of probe	T (°C)	strain rate (min/%)	subsequence	Time for loading (min)	ε_{tl} (%)
13	-5	0.01	No.1	2.5	0.0036
14	-5	0.01	No.2	2.5	0.0036
15	-5	0.01	No.3	2.5	0.0042
16	-5	0.1	No.1	0.25	0.0040
17	-5	0.1	No.2	0.25	0.0035
18	-5	0.1	No.3	0.25	0.0043
19	-5	0.001	No.1	25	0.0036
20	-5	0.001	No.2	25	0.0042
21	-5	0.001	No.3	25	0.0043
22	-5	0.1	Check	0.25	0.0036
23	-5	0.01	Check	2.5	0.0042
24	-5	0.001	Check	25	0.0038
Temperature was set at -2°C and kept for 24 hours after stabilization					
Sequence of probe	T (°C)	strain rate (min/%)	subsequence	Time for loading (min)	ε_{tl} (%)
25	-2	0.01	No.1	2.5	0.0026
26	-2	0.01	No.2	2.5	0.0048
27	-2	0.01	No.3	2.5	0.0044
28	-2	0.01	No.4	2.5	0.0036
29	-2	0.1	No.1	0.25	0.0040
30	-2	0.1	No.2	0.25	0.0040
31	-2	0.1	No.3	0.25	0.0040
32	-2	0.001	No.1	25	0.0040
33	-2	0.001	No.2	25	0.0032
34	-2	0.001	No.3	25	0.0029
35	-2	0.1	Check	0.25	0.0040
36	-2	0.01	Check	2.5	0.0032
37	-2	0.001	Check	25	0.0028

Note: * ε_{tl} denotes the linear threshold strain defined later in Section 6.1.1.

6.1.1. The stiffness characteristics at *T*=-10°C

At *T*=-10°C, four rounds of 0.025%-strain probe were performed at the strain rate of 0.01%/min, then three rounds at 0.1%/min and finally three at 0.001%/min. Each probe at the strain rate of 0.001%/min took 25 minutes for loading. After these probes were finished, one probe at 0.1%/min and one at 0.01%/min were repeated to confirm that the specimen still exhibited the same stiffness as the beginning. Each probe at 0.1%/min and 0.01%/min took 0.25 minute and 2.5 minutes for loading, respectively. Taking into account that three probes at 0.001%/min had just been done before these two probes at faster strain rates, one more probe at 0.001%/min was not repeated at *T*=-10°C, which was repeated for *T*=-5°C and -2°C.

Figure 6-1 shows the deviator stress increment plotted against the axial strain for strains up to 0.025% obtained from the external measurements in the first probe. The axial strain obtained from semi-local measurements of the gap sensors was much less than that obtained by the external measurements, resulting in the stress-strain curve plotting above that from external measured strain. This is mainly because the external measurement incorporates system compliance. To evaluate the soil stiffness at small strain accurately, the axial strain obtained from the gap sensors are used hereafter.

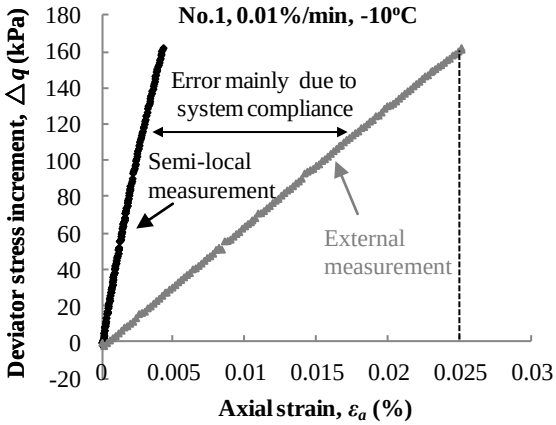

Figure 6-1 the deviator stress increment plotted against the axial strain obtained from the external measurements and the semi-local measurements of gap sensors

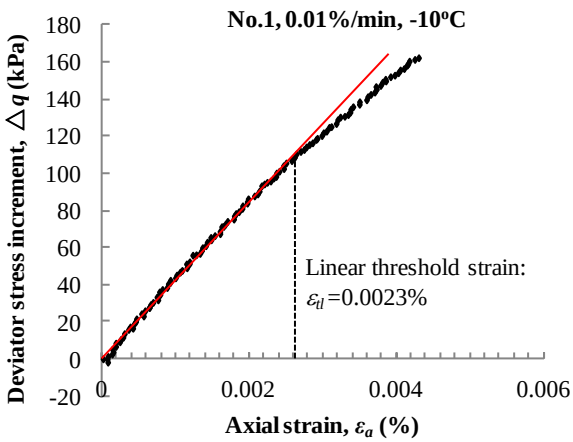

Figure 6-2 small-range stress-strain curve and linear threshold strain for the probe No.1 at 0.01%/min and -10°C

In the stress-strain curve based on strains from the gap sensors in Figure **6-1**, nonlinearity can be seen as shown in Figure **6-2**. The strain point from which the curve deviates from the linear portion is defined as linear threshold strain, ε_{tl}. The linear threshold strains for each probe was estimated from the stress-strain curve and listed in the last column in **Table 6-1**. It is found that the linear threshold strains for -10°C and -5°C were nearly equal to 0.003% and 0.004%, respectively, irrespective of the strain rate. However, the linear threshold strain for -2°C varied in a range from 0.003% to 0.005%. The reasons for this are unknown. For unfrozen reconstituted soils, it is reported that the linear threshold strain varies with plasticity from about 0.001% for low-plasticity soils to about 0.01% for plastic clays (Georgiannou et al. 1991; Lo Presti, 1989). Kasaoka clay can be regarded as high-plasticity clay whose plasticity index is 34%. A linear threshold strain of 0.01% can be estimated, which is twice or more of that for frozen Kasaoka clay in the temperature range of -10°C to -2°C.

Figure 6-3 plots the deviator stress increment against the axial strain for the strain rate of 0.01%/min. To compare the magnitude of stiffness for each probe, an identical reference axial strain was set as 0.002%, which is less than the linear threshold strains for all testing temperatures. Linear Regression analyses of stress-strain relationships were made over this reference axial strain of 0.002%. Good linearity was exhibited for each probe and consistent magnitudes of the stiffness were observed for the four probes and the one repeated at last. The shear stiffness at 0.01%/min for T=-10°C was estimated to be G_0=1.4 GPa on average, although the magnitude of the stiffness had a slight trend to decrease. This slightly decreasing trend was also observed for strain rate of 0.1%/min and warmer temperatures, which will be described later, as shown in **Table 2**.

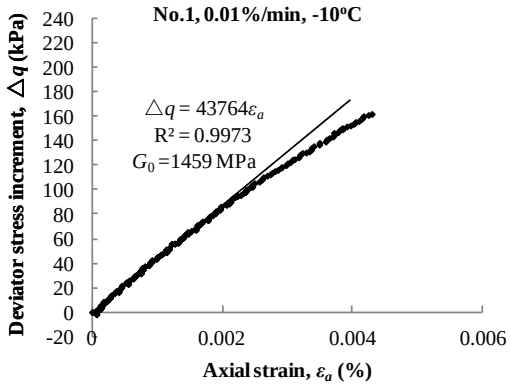

(a)

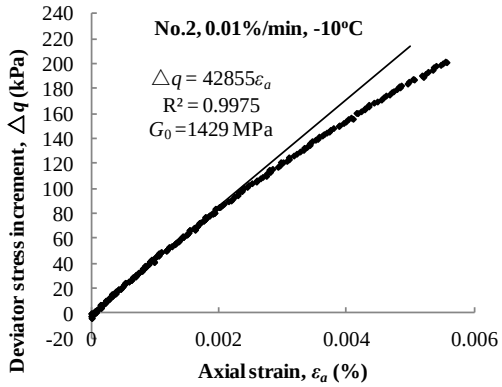

(b)

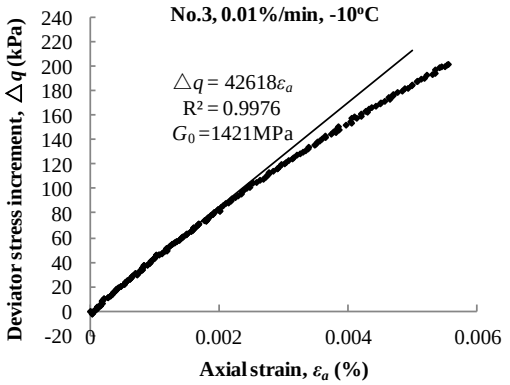

(c)

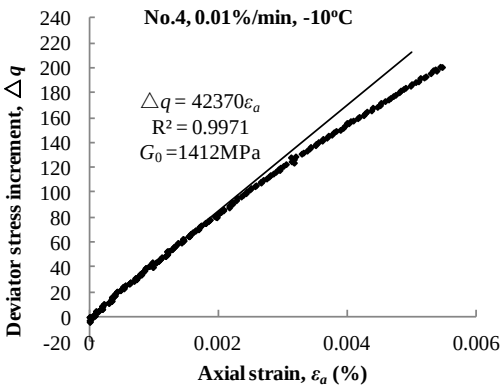

(d)

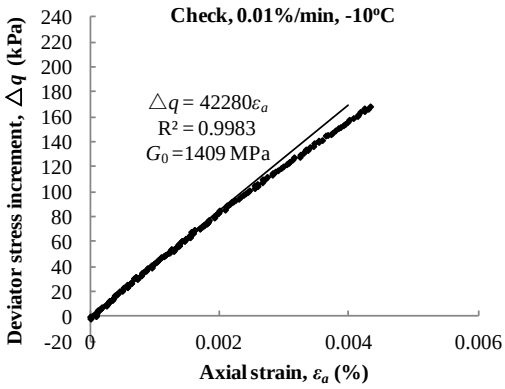

(e)

Figure 6-3 Small-range stress-strain behavior for each 0.025% probe at 0.01%/min at -10°C

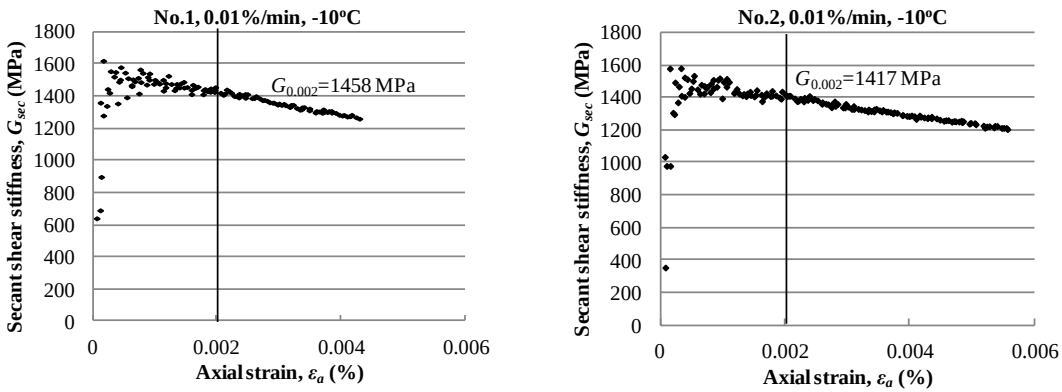

(a)

(b)

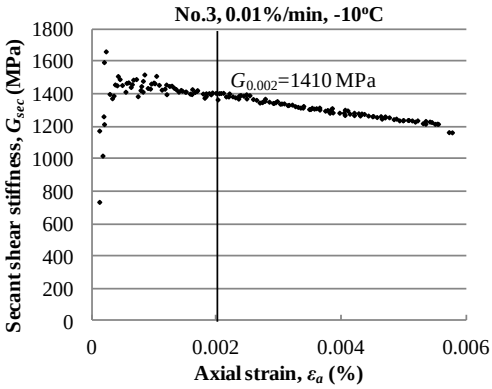

(c)

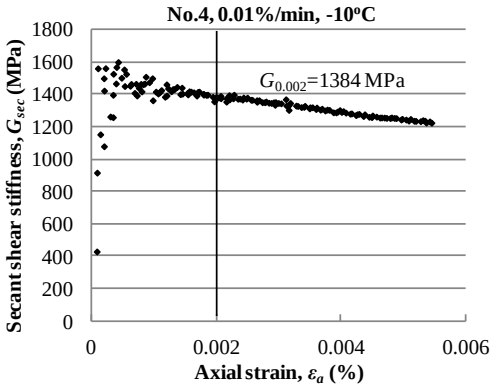

(d)

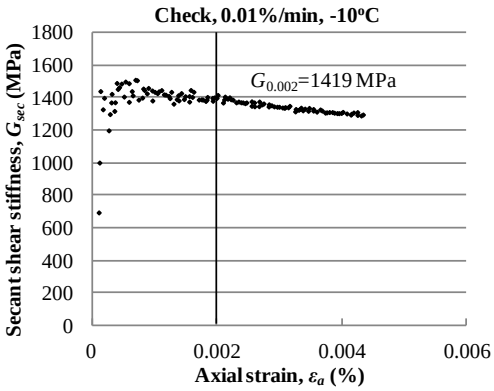

(e)

Figure 6-4 Secant shear stiffness against axial strain at 0.01%/min at -10°C

Table 6-2: List of the parameters derived from least-squared fitted lines of stress-strain curves for the 0.025% probes (the bold-font values represent data with relatively low linearity)

		0.01%/min		0.1%/min		0.001%/min	
		G_0 (MPa)	R^2	G_0 (MPa)	R^2	G_0 (MPa)	R^2
-10°C	No.1	1459	0.9973	1781	0.9983	1242	0.9978
	No.2	1429	0.9975	1732	0.9986	1301	0.9979
	No.3	1421	0.9976	1676	0.9984	1354	0.9976
	No.4	1412	0.9971	-	-	-	-
	Check	1409	0.9983	1784	0.9980	-	-
	Average	1426		1743		1299	
-5°C	No.1	893	0.9953	986	0.9986	745	0.9943
	No.2	890	0.9936	972	0.9986	799	0.9934
	No.3	872	0.9948	971	0.9961	804	0.9910
	Check	857	0.9968	932	0.9980	792	0.9959
	Average	878		965		785	
-2°C	No.1	464	0.9923	518	0.9929	442	0.9901
	No.2	**396**	**0.9119**	523	0.9996	454	0.9922
	No.3	**438**	**0.9237**	528	0.9975	476	0.9946
	No.4	463	0.9879	-	-	-	-
	Check	491	0.9934	539	0.9977	445	0.9922
	Average	473		527		454	

The secant stiffness is taken from the secant line connecting the origin and the point at a certain axial strain. The relationship between the secant stiffness and axial strain for 0.01%/min is plotted in **Figure 6-4**. Note that the horizontal axis representing the axial strain is expressed in a linear scale in this figure, in contrast to a log scale which is more conventional. Scatter was observed at the beginning of the probe, due to the limitation of precision of the gap sensors. From **Figures 6-4(a)-(e)**, a general trend can be observed, namely, all of the stress-strain behaviors tend to exhibit a short plateau after the initial scatter and before the secant stiffness degradation. This plateau should have been more evident if the scatter could be eliminated. The plateau is representative of linear stress-strain behavior, and the secant shear stiffness on this plateau can be taken as the initial shear stiffness. The linear threshold strain separates the plateau and the start of stiffness degrading, which equal to approximately 0.003% (referring to **Table 6-1**). Wang et al. (2007) found such plateaus when they studied the stiffness characteristics of artificially frozen soils subjected to K_0 consolidation before freezing. In their studies, a linear threshold strain of about 0.05% was estimated. One reason for the overestimated linear threshold strain is that they used traditionally external measurement for axial strain inevitably incorporating system compliance.

In the earlier individual tests in Series (i), (iii) or (iv), the stress-strain relationships in small strain ranges based on outputs of the gap sensors can be used to confirm the compatibility of the shear stiffness values obtained above. **Figure 6-5** presents the comparison of stress-strain curves at the strain rate of 0.01%/min and T=-10°C between the probing test and the past tests of iii-2 (pl) and iv-9 (pt). The test iii-2 (pl) representing the varying-temperature test, of which T=-10 °C was firstly set and shear was carried out for axial strain of 0-5%. The plane-plane platen-ram contact (pl), which was different from the ball point-plane contact employed in the probing test, might be the reason causing a smaller stiffness value in test iii-2. Similar phenomenon is also seen in Figure 5-3, in which the stress-strain in strain 0-20% of tests with plane-plane platen-ram contact was slightly beneath that of tests with ball point-plane contact. The platen-ram contact in the test iv-9 (pt) was in ball point-plane form, which was same as that in the probing test. The stress-strain curves of iv-9 (pt) and the probing test almost overlapped, which shows good consistency.

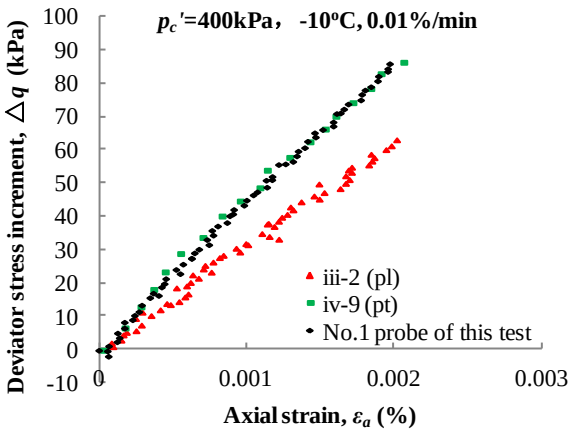

Figure 6-5 Comparison of stress-strain curves at 0.01%/min and -10°C between the probing test and the past tests of iii-2 (pl) and iv-9 (pt)

Figure 6-6 plots the deviator stress increment against the axial strain for the strain rate of 0.1%/min. The applied strain rate was so large that the data acquisition system could only obtain a limited number of data points, which were much less than those for slower strain rates. The regressed initial shear moduli were very close between the probes, but showed a gradually decreasing trend from probe No.1 to No.3, which had an approximate value of G_0 =1.7 GPa. **Figure 6-6(d)** representing the probe for final check at 0.1%/min, intervened by the ensuing three probes at strain rate of 0.001%/min, showed a shear modulus value approximate to those of probes No.1 to No.3. The relationship between the secant stiffness and axial strain for 0.1%/min is plotted in **Figure 6-7**. From **Figures 6-6** and **6-7**, continuous probes and one intervened probe for check showed good consistency on repetition.

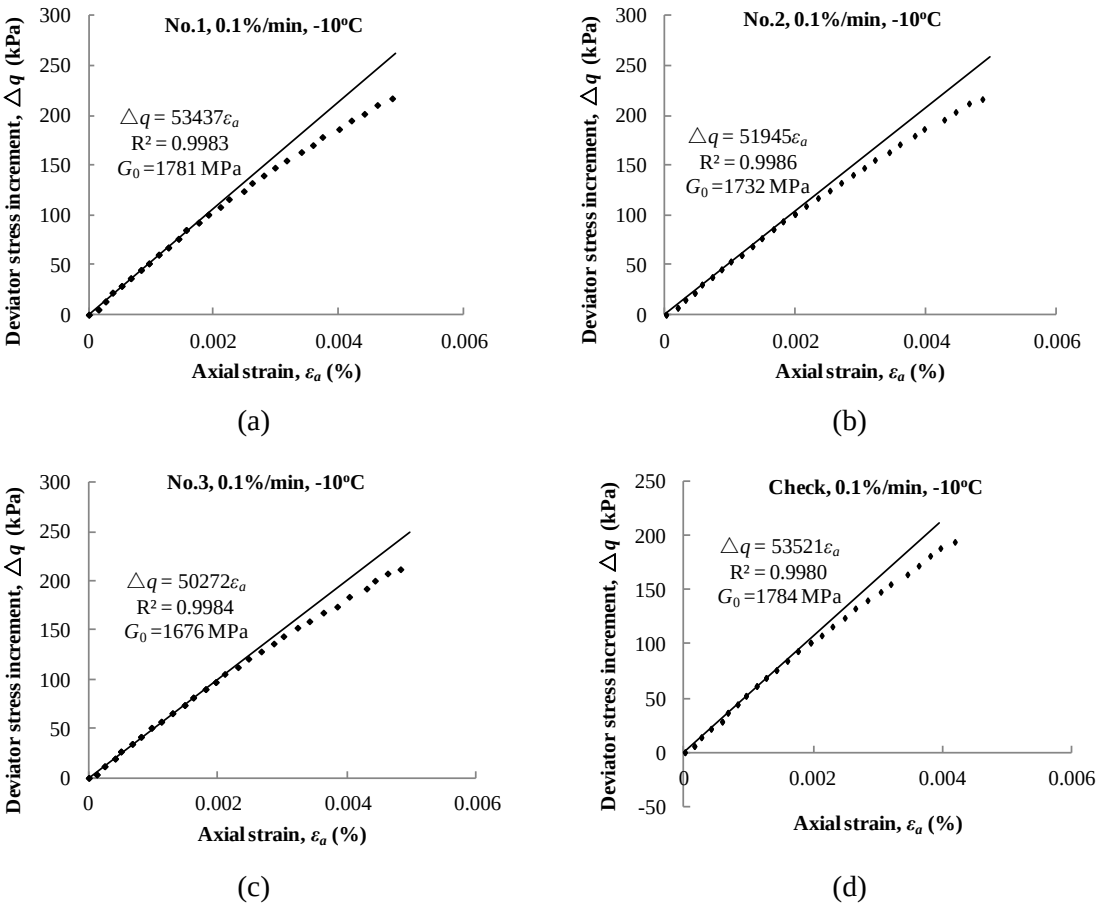

Figure 6-6 Small-range stress-strain behavior for each 0.025% probe at 0.1%/min at -10°C

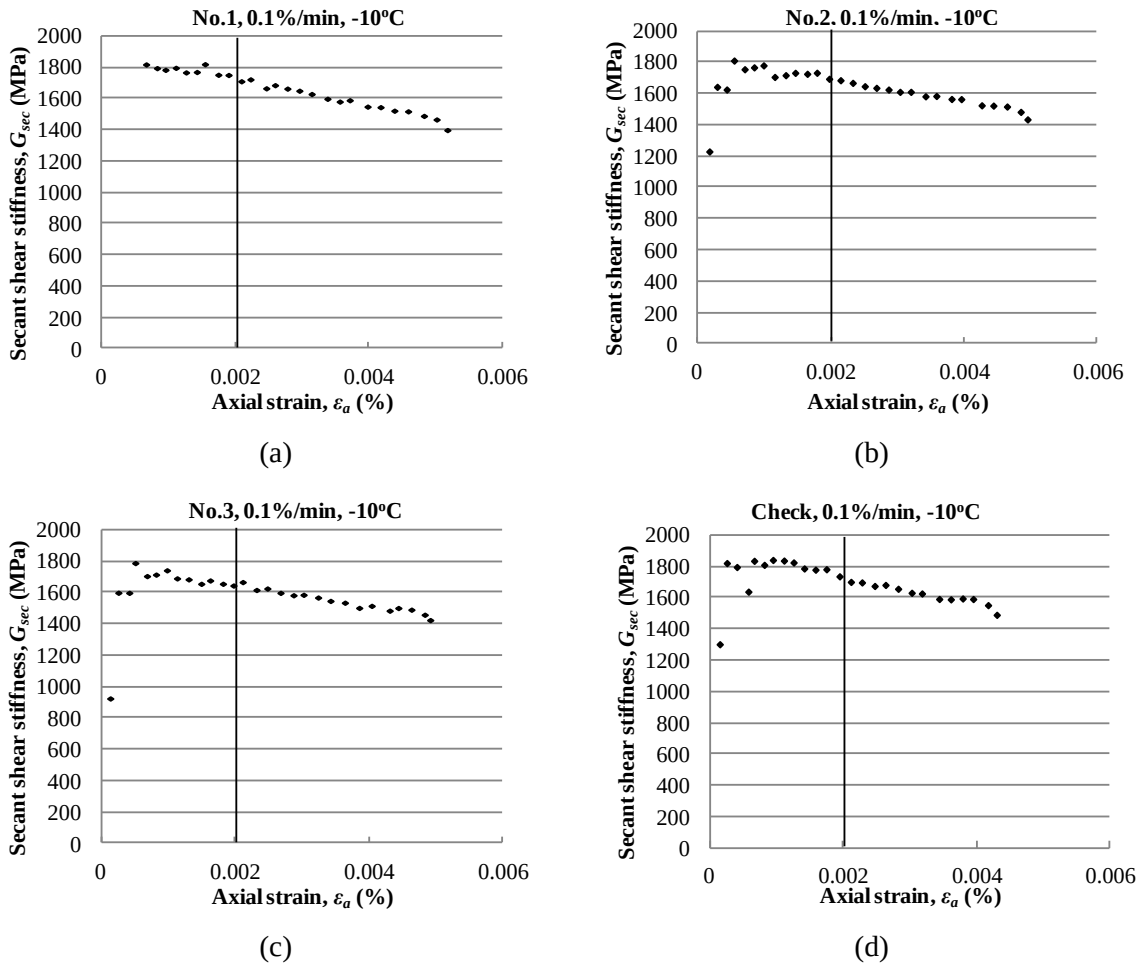

Figure 6-7 Secant shear stiffness against axial strain at 0.1%/min at -10°C

Figure 6-8 plots the deviator stress increment against the axial strain for the strain rate of 0.001%/min. The regressed initial shear moduli had a rough value of G_0 =1.3 GPa for three consecutive probes, although a gradually increasing trend from probe No.1 to No.3 could be observed. This increasing trend was opposite to those seen for the previous faster strain rates of 0.01%/min and 0.1%/min. The reason for this is unknown and need to be confirmed by duplicate tests. The relationship between the secant stiffness and axial strain for 0.001%/min is plotted in **Figure 6-9**. Good consistency among repeated probes was also confirmed here.

From the results at three orders of axial strain rates, it is found that duplicate probes for the same temperature and strain rate were largely consistent. Hereafter, the small strain behavior for one certain condition of temperature and strain rate will be represented by the result of the first probe. **Figure 6-10** shows the stress-strain curves for the three axial strain rates at T=-10°C from probe No.1. Distinct strain rate effect can be observed in strain ranges less than 0.005%. **Figure 6-11(a)** plots the secant shear stiffness against axial strain for first probe for three axial strain rates at -10°C. To look into the

stiffness degradation clearly, the secant stiffness is normalized by the derived initial shear stiffness and axial strain is in a logarithmic scale in **Figure 6-11(b)**. The degradation portions for strain rate of 0.1%/min and 0.01%/min are overlapped well while the stiffness degradation for 0.001%/min exhibits a slower rate.

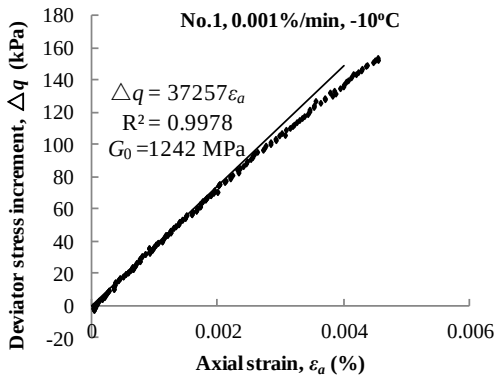

(a)

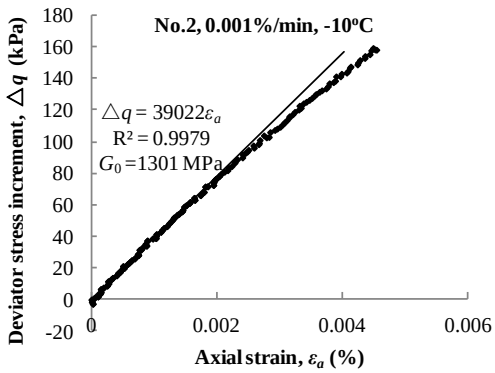

(b)

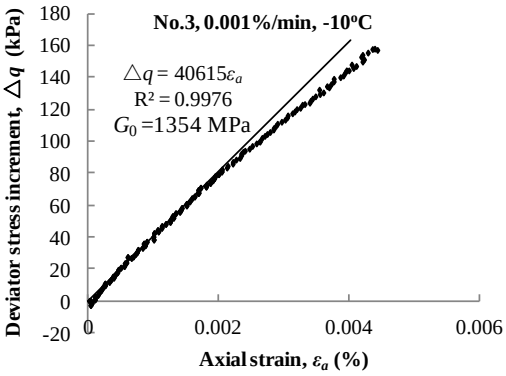

(c)

Figure 6-8 Small-range stress-strain behavior for each 0.025% probe at 0.001%/min at -10°C

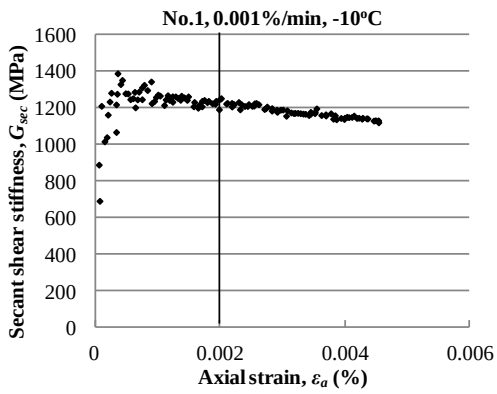

(a)

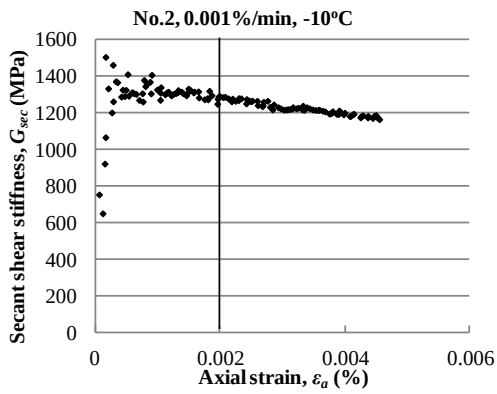

(b)

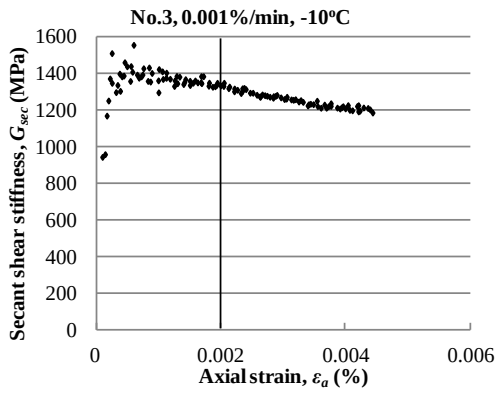

(c)

Figure 6-9 Secant shear stiffness against axial strain at 0.001%/min at -10°C

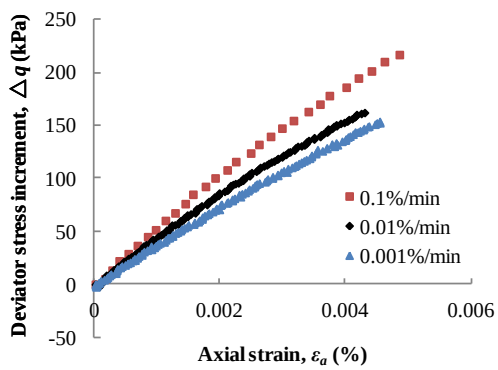

Figure 6-10 Comparison of mall-range stress-strain behaviors for first probe at three strain rates at -10°C

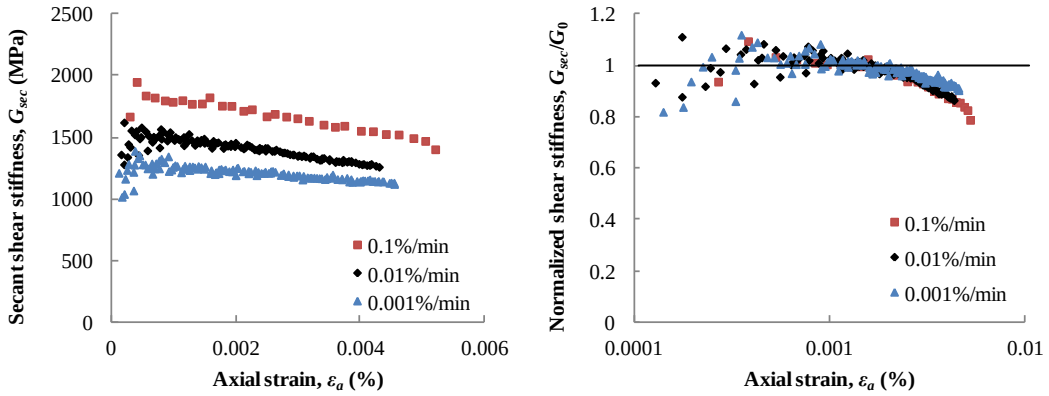

(a) (b)

Figure 6-11 Secant shear stiffness against axial strain for first probe for three axial strain rates at -10°C (a) with absolute value of stiffness and linear scale for axial strain (b) with normalize stiffness and logarithmic scale for axial strain

6.1.2. The stiffness characteristics at *T*=-5°C

At *T*=-5 °C, three rounds of 0.025%-strain probe were performed at the strain rate of 0.01%/min, then three rounds at 0.1%/min and finally three at 0.001%/min. After these probes, one additional probe for each strain rate of 0.1%/min, 0.01%/min and 0.001%/min was repeated to confirm that the stiffness characteristics remained unchanged due to the repeated loadings. The stress-strain curves of the first round 0.025%-strain probe for each strain rate is plotted in **Figures 6-12(a)**, **(b)** and **(c)**. The comparison of the stress-strain curves for three strain rates in **Figure 6-12(d)** shows the distinct strain rate effect for small strain range at -5°C. The stress-strain curves for the rest of the probes are not presented here. Instead, the derived shear stiffness and corresponding R-squared values for the stress-strain curves of these probes are listed in **Table 6-2**. Comparing the probes from No.1 to No.3, for the strain rate of 0.01%/min and 0.1%/min, the derived shear stiffness had a trend of descending while the trend was ascending for 0.001%/min. This is in agreement with the case at *T*=-10 °C. This phenomenon needs to be further investigated. **Figure 6-13(a)** shows the secant shear stiffness against axial strain for first probe for three axial strain rates at -5°C. The normalized secant shear stiffness against the derived G_0 is shown in **Figure 6-13(b)** in the logarithmic scale of axial strain. The stiffness degradation trends were seen roughly same for the three axial strain rates at -5°C.

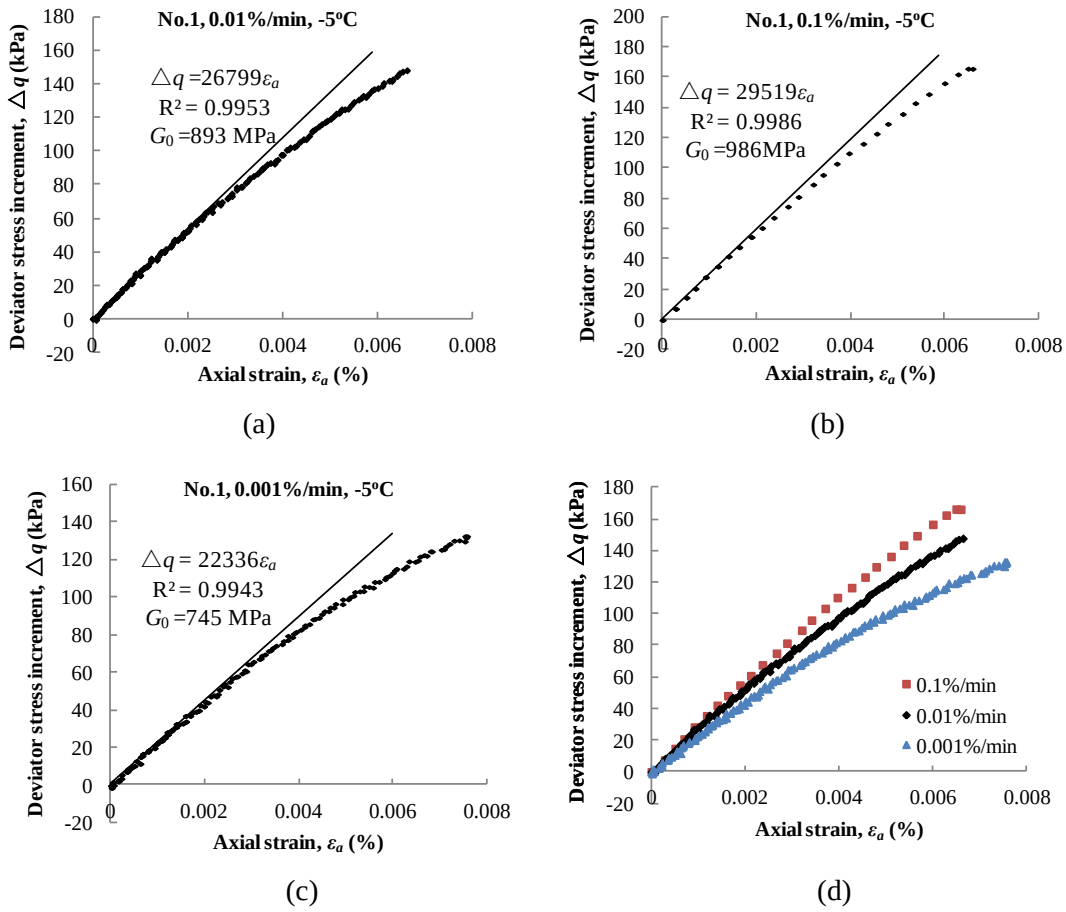

Figure 6-12 Small-range stress-strain behavior for first probe at strain rate of (a) 0.01%/min (b) 0.1%/min and (c) 0.001%/min at -5°C, and (d) the comparison between three strain rates

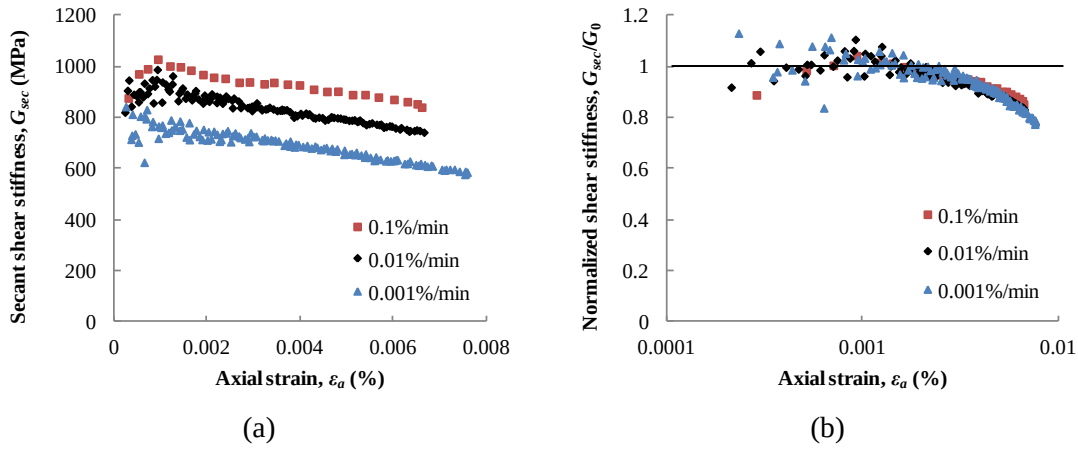

Figure 6-13 Secant shear stiffness against axial strain for first probe for three axial strain rates at -5°C (a) with absolute value of stiffness and linear scale for axial strain (b) with normalize stiffness and logarithmic scale for axial strain

Comparisons of stress-strain curves at -5 °C between the probing test and the earlier test series are drawn as shown in **Figure 6-14**. From **Figure 6-14(a)** and **(c)**, results of past tests for the strain rates of 0.01%/min and 0.001%/min well coincided with the 0.025% probes, suggesting that great consistencies were observed. The initial stiffness of test iii-4 in **Figure 6-14(a)** was slightly higher. It is because that one of the two gap sensors malfunctioned and the stress-strain curve was plotted based on the semi-local strain of one lateral side of the specimen. For the strain rate of 0.1%/min shown in **Figure 6-14(b)**, the past test i-12 (pt) showed a smaller shear stiffness than the probing test. Minor eccentricities in load application in i-12(pt) was confirmed by the slight but visible difference of two gap sensor outputs and observed tilting of specimen after test, which limits the reliability of the measured initial stiffness. Cuccovillo and Coop (1997) reported similar observation in measuring the small strain behavior of unfrozen sands in the triaxial cell.

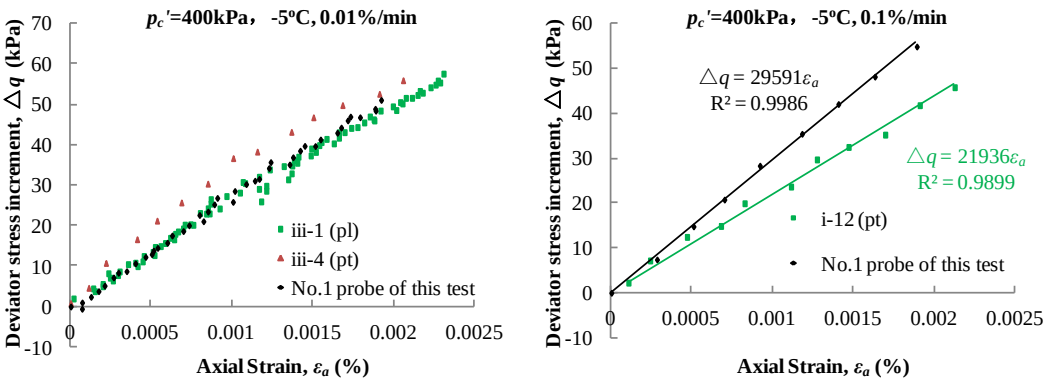

(a) (b)

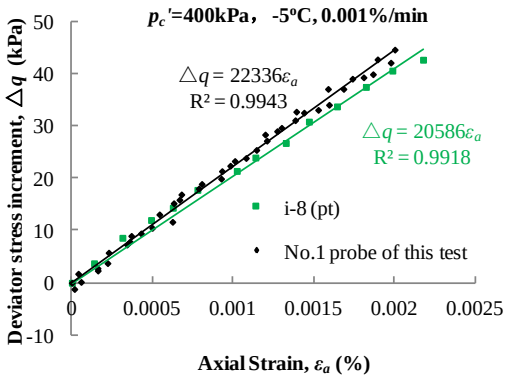

(c)

Figure 6-14 Comparison of stress-strain curves at -5 °C between the probing test and the past tests for the strain rate of (a) 0.01%/min (b) 0.1%/min and (c) 0.001%/min

6.1.3. The stiffness characteristics at T=-2°C

At T=-2 ^{o}C, same 0.025%-strain probes were performed at the strain rate of 0.01%/min, 0.1%/min and 0.001%/min. The stress-strain curves of the first round 0.025%-strain probe for each strain rate is plotted in **Figures 6-15(a)**, **(b)** and **(c)**. The comparison of stress-strain curves for the three strain rates in **Figure 6-15(d)** shows a convergence of strain rate effect between strain rate of 0.01 and 0.001%/min. The results for the rest of the probes are also listed in **Table 6-2** including the derived shear stiffness and corresponding R-squared values for the stress-strain curves of these probes. The results in probes No.2 and No.3 at strain rate of 0.01%/min appeared to be scattered according to their R-squared values. **Figures 6-16(a)** and **(b)** plots the strains obtained from the two gap sensors against the external strains which was controlled at constant strain rate. Severe scatter can be seen in 0-0.002% external strain for probe No.2 and 0.004%-0.006% external strain for probe No.3. It may be attributed to malfunctioning of gap sensors due to some unknown reasons. Comparing the probes from No.1 to No.3, the derived shear stiffness had a trend of ascending for all the three strain rates. This is different from the cases at T=-10 ^{o}C and -5 ^{o}C. It might be because it was easier for a warmer frozen specimento accumulate plastic residual strain after unloading even for faster strain rates (Wang et al. 2014). **Figure 6-17(a)** shows the secant shear stiffness against axial strain for first probe for three axial strain rates at -2°C. The normalized secant shear stiffness against the derived G_0 is shown in **Figure 6-17(b)** in the logarithmic scale of axial strain. The stiffness degradation trends were seen slightly deviated at the end of the strain for the three axial strain rates, which might suggest a possibly unique behavior for cases at -2°C most approaching to the freezing temperature in this study.

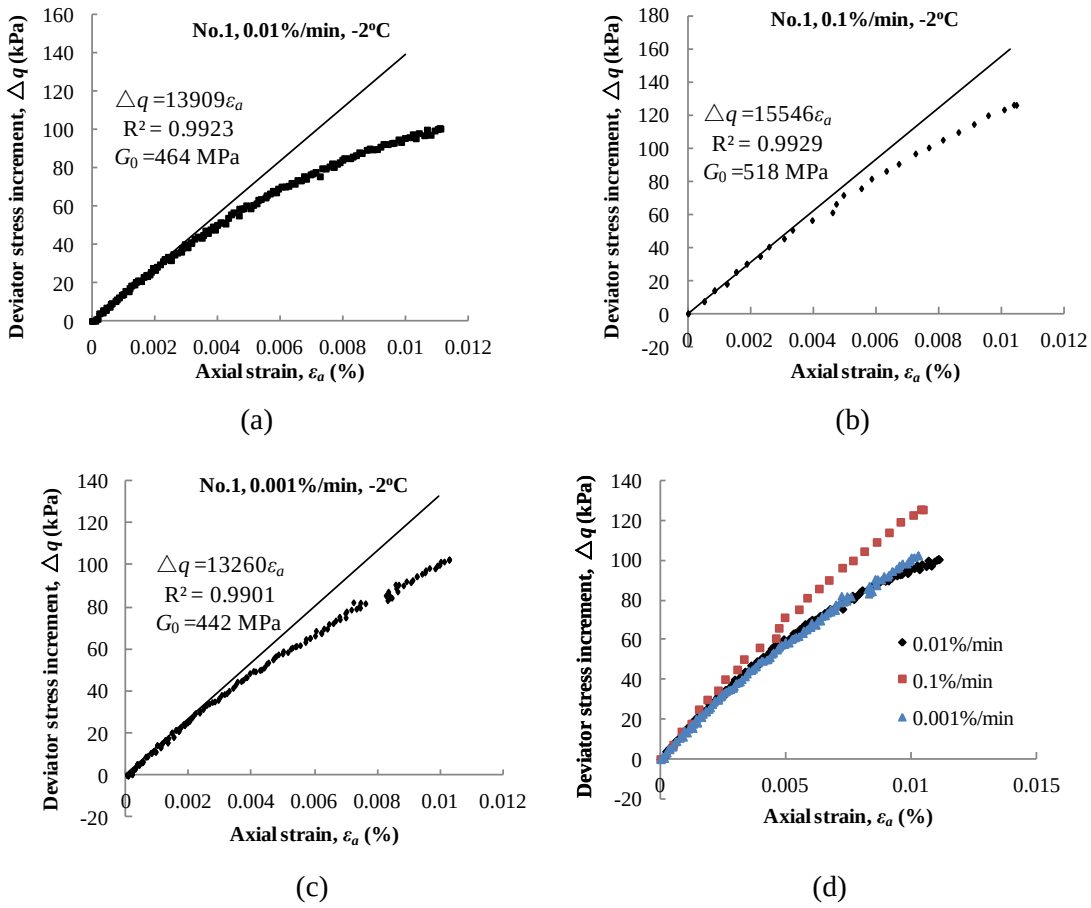

Figure 6-15 Small-range stress-strain behavior for first probe at strain rate of (a) 0.01%/min (b) 0.1%/min and (c) 0.001%/min at -2°C, (d) the comparison for three strain rates

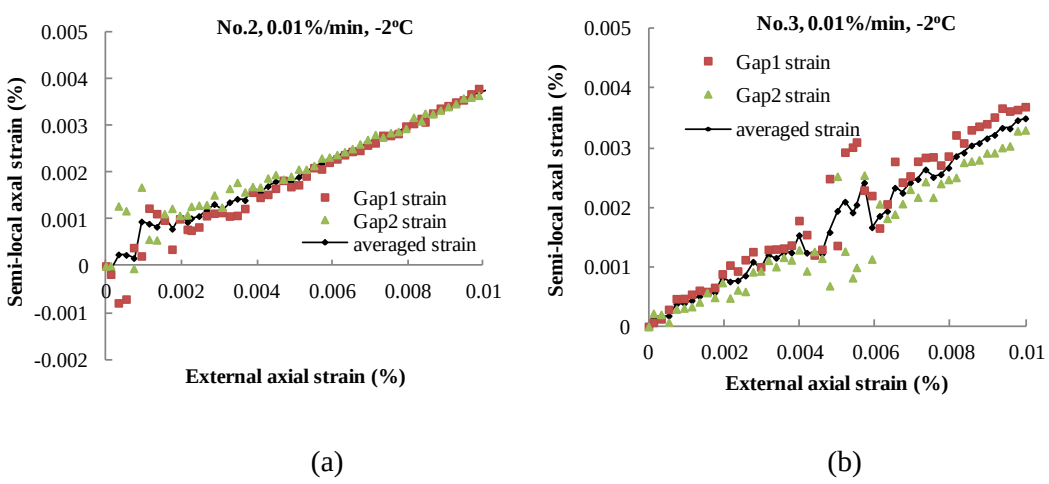

Figure 6-16 Comparison of strains obtained between from the two gap sensors against the external strains at 0.01%/min and -2°C: (a) for probe No.2 (b) for probe No.3

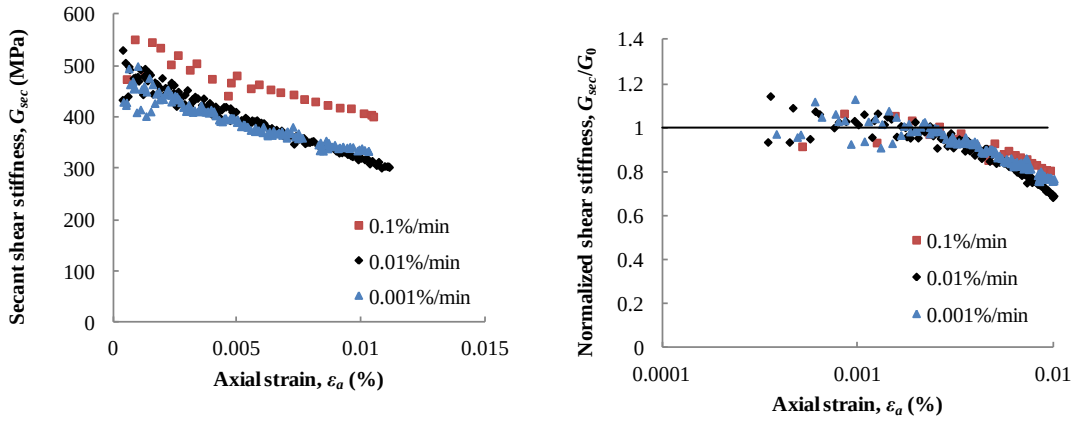

(a) (b)

Figure 6-17 Secant shear stiffness against axial strain for first probe for three axial strain rates at -2°C (a) with absolute value of stiffness and linear scale for axial strain (b) with normalize stiffness and logarithmic scale for axial strain

Figure 6-18 presents the comparison of stress-strain curves at the strain rate of 0.01%/min and *T*=-2 °C between the probing test and the earlier tests i-11 (pt) and iii-3 (pl). The test iii-3 (pl) representing the varying-strain rate test, of which the strain rate of 0.01%/min was firstly set and shear was carried out for axial strain of 0-5%. The consistency to the probing test is satisfactory although a slightly smaller stiffness was observed. The platen-ram contact in the test i-11 (pt) was same as adopted in the probe loading test. In the test i-11 (pt), only the strain obtained from gap sensor 2 output was available to present the small strain behavior (the on-specimen metal target corresponding to gap sensor 1 fell off the specimen during shearing). Uniform straining, confirmed by parallelism between the top cap surface and the specimen base observed after the i-11 (pt), allows the results based on the gap sensor 2 output to compare with that of the probing test. Great consistency can be seen from their overlapped stress-strain curves although limited number of data points was available in the range of 0.002% for the test i-11 (pt).

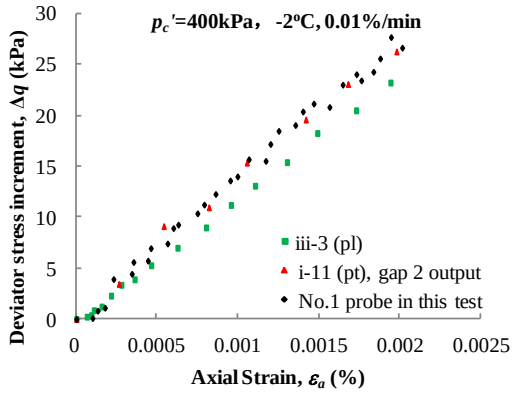

Figure 6-18 Comparison of stress-strain curves at 0.01%/min and -2 °C between the probing test and the earlier tests i-11 (pt) and iii-3 (pl)

In summary, the multiple probes for each condition (i.e. at fixed temperatures and strain rates) were consistent and exhibited repeatability. The results of the probes fit well most of the past results in Series (i), (iii) and (iv) for different temperatures and strain rates. The compatibility and reliability can be thus confirmed.

6.2. EFFECTS OF TEMPERATURE AND STRAIN RATE ON STIFFNESS OF FROZEN SOIL

The 0.025%-probes at three orders of strain rates for three freezing temperatures were carried out for one same frozen clay specimen. For the same strain rate, the effect of temperature on the shear stiffness of frozen clay can be shown in **Figure 6-19**. Similar to the strength characteristics, the shear stiffness, averaged from the multiple probes of the same condition, increased linearly with the decrease in temperature. The temperature dependency of the shear stiffness tended to be more pronounced for faster strain rates. The magnitudes of this temperature dependency for the axial strain rates of 0.01%/min and 0.001%/min were close while visibly lower than that for 0.1%/min. There are few studies which quantitatively evaluated the temperature dependency of the shear stiffness in conventional compression tests, and even fewer for the small-strain levels explored in this study. From the perspective of dynamic tests, Wang et al. (2006) applied ultrasonic technology to study the mechanical properties of frozen soils and revealed that the dynamic shear modulus increased with decreasing temperature, as shown in **Figure 6-20**. A certain degree of linearity of temperature dependency of dynamic shear modulus could be observed in the temperature range of -10 °C to -2 °C. The stiffness based on wave velocity showed larger values and stronger temperature effect than that from probing tests in triaxial compression. Besides the soil type, one reason for this is that in the dynamic measurement the wave travels through the shortest path made by interlocking of soil particles resulting in larger stiffness modulus (Maqbool, 2005). Although direct comparison between

the results of Wang et al. (2006) and this study is difficult because of the different soils, strain rates and modes of shearing, the linear trend of temperature effect on shear stiffness can be confirmed.

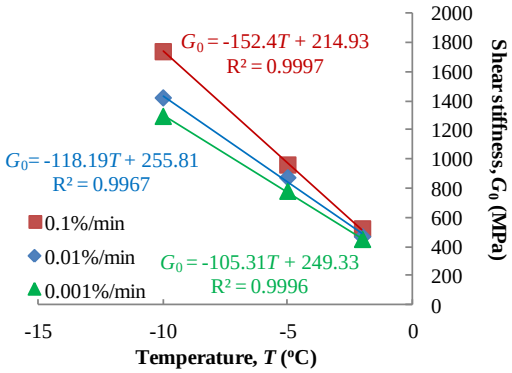

Figure 6-19 Relationship of shear stiffness of frozen clay with the freezing temperature

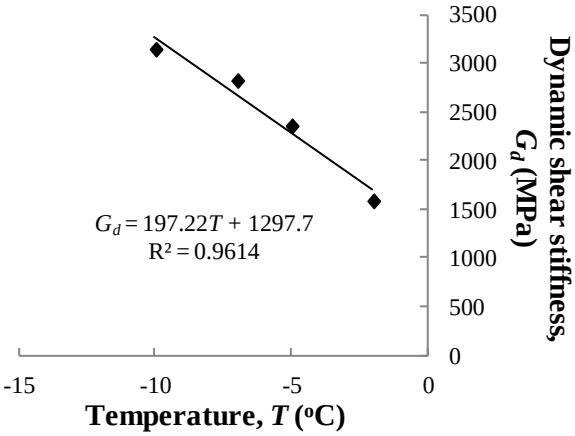

Figure 6-20 Relationship between dynamic shear modulus and temperature for Harbin Clay (data from Wang et al. 2006)

For unfrozen soil, the initial shear stiffness is much smaller, as shown in **Table 6-3**. **Table 6-3** lists the stiffness values of unfrozen clays from past studies having similar conditions (mainly based on I_P and p') as those in this study (data extracted from Vardanega and Bolton, 2013). The initial stiffness values of the listed unfrozen clays, despite the fact that all heavily over-consolidated and hence having much greater stiffness than normally consolidated specimens at same p' values, range in the order of 100 to 200 MPa, while those for frozen Kasaoka clay range from 400 to 1800 MPa for temperature -2 to -10°C seen in **Figure 6-19**. This difference in stiffness reflects the freezing effect and significant contribution of ice to the stiffness of frozen soils.

Table 6-3 list of soil properties and stiffness values of unfrozen clays

Publication	Apparatus	Test label*	w (%)	e_0	I_P	p' (kPa)	G_0 (MPa)
Georgiannou et al., 1991	Triaxial	Pietrafitta Clay I-TX	42	1.20	30	320	164
Yimsiri, 2001	Triaxial	London Clay I (D-1)	20	0.57	36	410	105
		London Clay I (D-2)	20	0.55	36	410	97
Gasparre, 2005	Triaxial	London Clay II (t13)	25	0.69	33	502	105

Note:* The short acronyms in the Test label column are descriptors used in the original publications.

For the same temperature, the effect of strain rate on the shear stiffness of frozen clay is shown in **Figure 6-21(a)**. It can be observed that for T =-5 °C, the shear stiffness of the frozen clay increased quite linearly with the logarithmic increase of strain rate. For T =-2°C and -10°C, the log-linearity became less pronounced by referring to the R-squared values. Because only three orders of strain rates were applied, fitting the data points to explore the relationship between shear stiffness and axial strain rate becomes a matter of judgment. Parameswaran (1980) conducted uniaxial unconfined compression tests on frozen saturated Ottawa sand at temperatures between -2 and -15 °C and found the initial tangent modulus increased logarithmically with the strain rate (see **Figure 6-22**). In his study, the initial tangent modulus was evaluated for strains less than 1%, which were obtained by conventional external displacement measurement. Inspired by their finding, an attempt was made to fit the data obtained within very small strain levels, of which reliability was proved earlier, by power regression analysis, as shown in **Figure 6-21(b)**, providing a slightly better fitting than **Figure 6-21(a)**. Lee et al. (2016) observed that the increments of deformation moduli, E_{50} derived from uniaxial compression test, gradually decreased and then converged to a certain value with the increase in loading rate for frozen sand. The threshold loading rate was 1.43%/min according to their results. Although it is the frozen clay that was tested in this study, any extrapolation of shear stiffness with strain rate larger than 0.1%/min is still uncertain. Unlike frozen soils, rate effects are considered to be relatively unimportant at very small strain levels in unfrozen soils (Clayton¸ 2011). It is reported by Tatsuoka and Shibuya (1992) and Tatsuoka et al. (1994) that stiffness was almost independent of strain rate for strains less than 0.001% in testing stiff clays and soft clays.

This chapter reported the small-strain stiffness characteristics of frozen clay consolidated to p_c'=400 kPa prior to freezing. To validate the small-strain behavior revealed in this chapter at a wider stress state, tests on frozen clay with p_c'=100 kPa and 200 kPa are desired in the future.

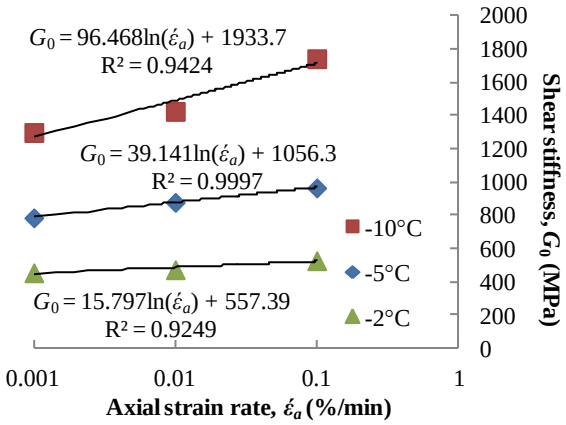

(a)

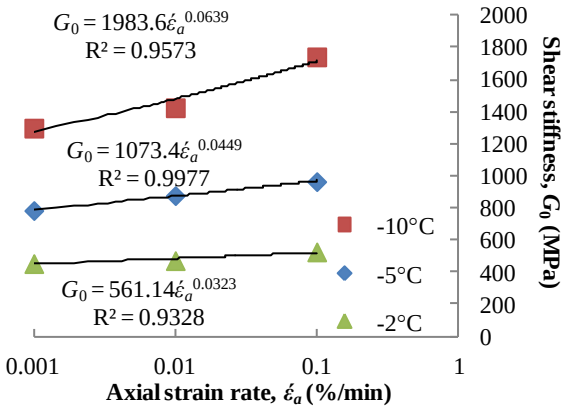

(b)

Figure 6-21 Relationship of shear stiffness of frozen clay with the axial strain rate with (a) logarithmic regression analysis and (b) power regression analysis

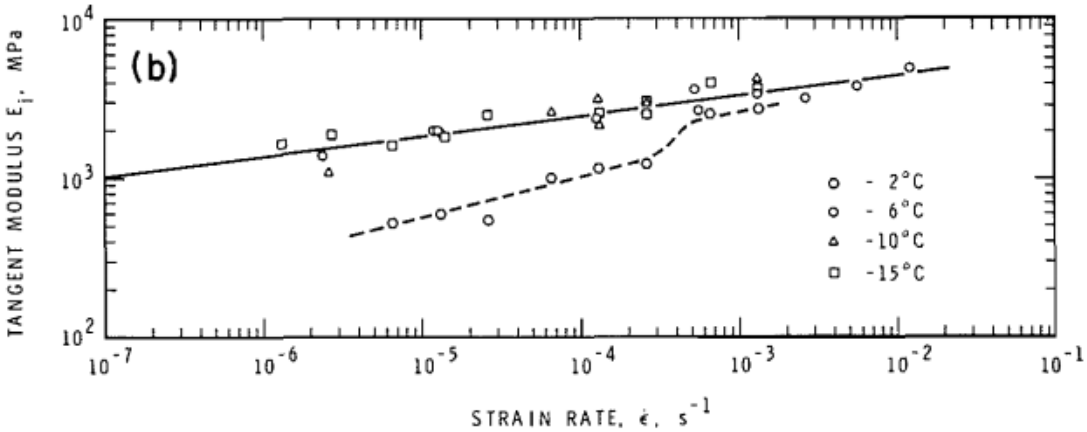

Figure 6-22 Variation of initial tangent modulus with nominal strain rate for frozen sand (log-log scale) (from Parameswaran, 1980)

7. CONCLUSIONS AND RECOMMENDATIONS

Towards development of a mechanical model that can be part of multi-physical analysis of frozen soils, a program of systematic frozen-unfrozen parallel tests at different temperatures and strain rates was conducted. Focusing on one-substance (water) and two-phase (solid and liquid) pore conditions, reconstituted plastic clay samples were tested. The interpretation, based on Ladanyi and Morel's (1990) postulate on the unique relationship between the inter-particle "effective" stress and the strain path, led to a variety of new insights and renewed understanding of the conventional knowledge.

The following findings have been obtained from this study.

1. By adopting Ladanyi and Morel's (1990) postulate, which successfully explained frozen sands' shear strength and connecting it to unfrozen sand behavior in their work, critical state lines (CSLs) for clay specimens frozen undrained were mapped by referring to the shear behavior of unfrozen specimens sharing the same strain history as the frozen ones. This treatment essentially leads to fair comparison of frozen and unfrozen soils with a controlled common deformation and state history.

2. In applying the above concept, the unfrozen water content measured by nuclear magnetic resonance (NMR) was taken into account and the volume increase during undrained freezing was assessed.

3. With other conditions set identical, the shear strength linearly increased with a decrease in temperature for the range from -10°C to -2°C, and log-linearly increased with an increase in the strain rate for the range from 0.001%/min to 0.1%/min. The shear strength normalized by that at a given temperature, or by that at a given strain rate formed unique relationships against the strain rate or the temperature, respectively.

4. No clear strain-rate effect was observed for unfrozen over-consolidated reconstituted specimens. However, significant rheological behavior was exhibited for equivalent states with frozen pores. This is a direct indication of viscoplasticity deriving from existence of pore ice.

5. Consistency of stress-strain curves was observed at large strains under varying- and constant-temperature, and less clearly, under varying- and constant-strain rate. The latter observation, if further confirmed, may lead to isotach formulation of strain rate effects for the investigated range of strain rate (i.e. up to 0.1%/min), where the behavior is largely ductile.

6. Variations of pore ice/ water pressure controlled by reduction of confining pressure after freezing of frozen specimens have no obvious effect on critical state strength of frozen clay.

7. A nondestructive method of repeatedly loading frozen specimen is feasible to obtain the small-strain stiffness characteristics for various temperatures and axial strain rates. It is a novel attempt to

evaluate the initial stiffness based on internal (semi-local) strain measurements by static loading tests. Linear threshold strains for frozen clay in small strain range were confirmed, which seemed to be less than half of those of similar clay in the unfrozen state. In the investigated range of conditions, the shear stiffness, averaged from the multiple probes of the same condition, increased linearly with the decrease in temperature, and increased linearly with the logarithmic increase of strain rate.

Obviously much further experimental work is desired, as mentioned through this thesis, to describe the frozen and unfrozen soil behavior under a unified framework with smooth transition. The present study demonstrated how experimental program should be designed with careful considerations to the state history. Some directions for the future research are recommended as below:

The above conclusions are derived from a limited amount of experimental data. It should be noted that many factors, such as the soil type, grading of particles, initial water content, freeze-thaw cycles may be also important for the mechanical behaviors of frozen clay. Therefore, there is vacancy for further investigation to interpret the mechanical behavior of frozen soil. Meanwhile, as a reference the void ratio of normally consolidated unfrozen specimen was increased by 9% to simulate the full freezing of pore water. If the increase rate of void ratio can be adjusted to the actual void ratio change as that occurs in frozen soil for different temperatures, the mapping of envisaged effective mean stress path can discover a new insight into the internal stress state in frozen soil. Mechanical behaviors of frozen soil at near-zero temperature and frozen soil experiencing freeze-thaw histories are desired to investigate to solve transient moving boundary problems and bridge the understanding of unfrozen and frozen soil in a unified framework.

REFERENCES

[1] Aas, G. 1981. Laboratory determination of strength properties of frozen salt marine clay. Eng. Geol. 18(1): 67–78.

[2] Abuel-Naga, H.M., Bergado, D.T., Ramana, G.V., Grino, L., Rujivipat, P. and Thet, Y. 2006. Experimental evaluation of engineering behavior of soft Bangkok clay under elevated temperature. J. Geotech. Geoenvironmental Eng. 132(7): 902–910.

[3] Akili, W. 1971. Stress-strain behavior of frozen fine-grained soils. Highw. Res. Record No. 360. pp. 1–8.

[4] Al-Hunaidi, M.O., Chen, P.A., Rainer, J.H., and Tremblay, M. 1996. Shear moduli and damping in frozen and unfrozen clay by resonant column tests. Canadian Geotechnical Journal, 33(3): 510–514. doi:10.1139/t96-073

[5] Andersland, O.B. and Akili, W. 1967. Stress effect on creep rates of a frozen clay soil. Geotechnique 17(1): 27–39.

[6] Andersland, O.B. and Ladanyi, B. 2004. Frozen ground engineering. John Wiley & Sons.

[7] Arenson, L. U., Almasi, N., and Springman, S. M. 2003. Shearing response of ice-rich rock glacier material. In Eighth International Conference on Permafrost. AA Balkema, Zurich, Switzerland (pp. 39-44).

[8] Arenson, L.U., Johansen, M.M. and Springman, S.M. 2004. Effects of volumetric ice content and strain rate on shear strength under triaxial conditions for frozen soil samples. Permafr. Periglac. Process. 15(3): 261–271.

[9] Arenson, L.U. and Springman, S.M. 2005a. Triaxial constant stress and constant strain rate tests on ice-rich permafrost samples. Can. Geotech. J. 42(2): 412–430.

[10] Arenson, L.U. and Springman, S.M. 2005b. Mathematical descriptions for the behaviour of ice-rich frozen soils at temperatures close to 0 ^{o}C. Can. Geotech. J. 42(2): 431–442.

[11] Arenson, L. U., Springman, S. M., and Sego, D. C. 2007. The rheology of frozen soils. Applied Rheology, 17(1), 12147.

[12] Atkinson, J. H. 2000. Non-linear soil stiffness in routine design. Geotechnique. 50(5): 487–508

[13] Baker, T.H.W. 1976. Preparation of artificially frozen sand specimens. Pap. Div. Build. Res. Natl. Res. Counc. Can. (682): 15 pp.

[14] Baker, T. H. W. 1979. Strain rate effect on the compressive strength of frozen sand. Engineering Geology. 13(1-4): 223–231.

[15] Bragg, R.A. and Andersland, O.B. 1981. Strain rate, temperature, and sample size effects on compression and tensile properties of frozen sand. Eng. Geol. 18(1): 35–46.

[16] Burghignoli, A., Desideri, A., and Miliziano, S. 2000. A laboratory study on the thermomechanical behaviour of clayey soils. Canadian Geotechnical Journal, 37(4), 764-780.

[17] Casini, F., Gens, A., Olivella, S. and Viggiani, G. M. 2014. Artificial ground freezing of a volcanic ash: laboratory tests and modelling. Environ. Geotechnics 3(3): 141–154.

[18] Cekerevac, C. and Laloui, L. 2004. Experimental study of thermal effects on the mechanical behaviour of a clay. International journal for numerical and analytical methods in geomechanics, 28(3), 209-228.

[19] Chamberlain, E., Groves, C. and Perham, R. 1972. The mechanical behaviour of frozen earth materials under high pressure triaxial test conditions. Geotechnique 22(3): 469–483.

[20] Choi, H. W. 2011. An experimental study on the unconfined compression strength and split tensile strength properties to freezing temperature and loading rate of frozen soil. MSc Thesis.

[21] Clayton, C. R. I. 2011. Stiffness at small strain: research and practice. Geotechnique 16 (1), 5-37.

[22] Cuccovillo, T. and Coop, M. R. 1997. The measurement of local axial strains in triaxial tests using LVDTs. Géotechnique, 47(1).

[23] Cuccovillo, T. and Coop, M.R. 1997. Yielding and pre-failure deformation of structured sands. Geotechnique, 47(3), 491-508.

[24] Eisenberg, M.A. and Yen, C. F. 1981. A theory of multiaxial anisotropic viscoplasticity. J. Appl. Mech, 48, 276-284.

[25] Fredlund, D. G. and Rahardjo, H. 1993. Soil mechanics for unsaturated soils. John Wiley & Sons.

[26] Fukuda, M. and Kinoshita, S. 1974. Permafrost at Mt. Taisetsu, Hokkaido and its climatic environment. Daiyonki kenkyu. 12(4): 192–202 (in Japanese).

[27] Gasparre, A. 2005. Advanced laboratory characterisation of London Clay. PhD thesis. Imperial College London, London.

[28] Georgiannou, V. N., Rampello, L. and Silvestri, F. 1991. Static and dynamic measurement of undrained stiffness of natural overconsolidated clays. Proc. 10th Eur. Conf. Soil Mech., Florence 1, 91-96.

[29] Ghoreishian Amiri, S. A., Grimstad, G., Kadivar, M., and Nordal, S. 2016. Constitutive model for rate-independent behavior of saturated frozen soils. Canadian Geotechnical Journal, 53(10), 1646-1657.

[30] Goodman, M.A. 1975. Mechanical properties of simulated deep permafrost. J. Eng. Ind. 97(2): 417–425.

[31] Goto, S., Tatsuoka, F., Shibuya, S., Kim, Y.S., and Sato, T. 1991: A simple gauge for local strain measurements in laboratory, Japanese Geotechnical Society Special Publication, 31(1), 169-180.

[32] Goughnour, R.R. and Andersland, O.B. 1968. Mechanical properties of a sand-ice system. ASCE, J. Soil Mech. Found. Div. 94(SM4): 923–950.

[33] Graham J, Crooks J H, Bell A L. 1983. Time effects on the stress-strain behaviour of natural soft clays[J]. Géotechnique, 33(3): 327-40.

[34] Haynes, F.D., Karalius, J.A. and Kalafut, J. 1975. Strain rate effect on the strength of frozen silt. USACRREL Res. Rep. 350, 27 pp.

[35] He, P., Zhu, Y., and Cheng, G. 2000. Constitutive models of frozen soil. Canadian geotechnical journal, 37(4), 811-816.

[36] Hohmann-Porebska, M. 2002. Microfabric effects in frozen clays in relation to geotechnical parameters. Appl. Clay Sci. 21(1): 77–87.

[37] Hooke, R.L., Dahalin, B.B. and Kauper, M.T. 1972. Creep of ice containing dispersed fine sand. J. Glaciol. 11(63): 327–336.

[38] Ishikawa, T., Tokoro, T. and Seiichi, M. 2015. Geohazard at volcanic soil slope in cold regions and its influencing factors. Jpn. Geotech. Soc. Spec. Publ. 1(1): 1–20.

[39] Ishizaki, T., Maruyama, M., Furukawa, Y. and Dash, J.G. 1996. Premelting of ice in porous silica glass. J. Cryst. Growth 163(4): 455–460.

[40] Jardine, R. J., Symes, M. J. and Burland, J. B. 1984. The measurement of soil stiffness in the triaxial apparatus. Geotechnique. 34(3): 323–340.

[41] Jiao, G.D. 2011. Dynamic characteristics of warm frozen soils under long-term cyclic loading. Ph.D. Thesis. Cold and Arid Regions Environmental and Engineering Research Institute. Lanzhou, China

[42] Joshi, R.C. and Wijeweera, H. 1990. Post peak axial compressive strength and deformation behavior of fine-grained frozen soils. In: Proc. of the 5th Canadian Permafrost Conference. Citeseer. pp. 317–325.

[43] Kawamura, S., & Miura, S. 2011. Stability evaluation of slope subjected to rainfall and freeze–thaw actions based on field monitoring. Advances in Civil Engineering (Online Access Journal), 2011, 14 pages.

[44] Kokusho, T. 1980. Cyclic triaxial test of dynamic soil properties for wide strain range, Japanese Geotechnical Society Special Publication, 20(2), 45-60.

[45] Ladanyi, B. 1972. An engineering theory of creep of frozen soils. Can. Geotech. J. 9(1): 63–80.

[46] Ladanyi, B. 1981. Mechnical behaviour of frozen soils. In: Proc. Int. Symp. on Mechanical Behavior of Structured Media. Calreton Univ., Ottawa, New York, B. pp. 205–245.

[47] Ladanyi, B. and Morel, J.-F. 1990. Effect of internal confinement on compression strength of frozen sand. Can. Geotech. J. 27(1): 8–18.

[48] Lai, Y., Yang, Y., Chang, X. and Li, S. 2010. Strength criterion and elastoplastic constitutive model of frozen silt in generalized plastic mechanics. Int. J. Plast. 26(10): 1461–1484.

[49] Lai, Y., Xu, X., Dong, Y. and Li, S. 2013. Present situation and prospect of mechanical research on frozen soils in China. Cold Regions Science and Technology 87: 6–18.

[50] Lee, J., Kim, Y. S., Chae, D. and Cho, W. 2016. Loading rate effects on strength and stiffness of frozen sands. KSCE Journal of Civil Engineering. 20(1): 208–215.

[51] Leroueil, S. 2006. Suklje's Memorial Lecture–The isotache approach: Where are we fifty years after its development by Professor Suklje. In: Proc. of European-Danube Conference on Geotechnical Engineering, Ljubljana. pp. 55–88.

[52] Li, H., Zhu, Y., Zhang, J. and Lin, C. 2004. Effects of temperature, strain rate and dry density on compressive strength of saturated frozen clay. Cold Reg. Sci. Technol. 39(1): 39–45.

[53] Li, N., Chen, F., Xu, B., & Swoboda, G. 2008. Theoretical modeling framework for an unsaturated freezing soil. Cold Regions Science and Technology, 54(1), 19-35.

[54] Liu, E., Lai, Y., Liao, M., Liu, X., & Hou, F. 2016. Fatigue and damage properties of frozen silty sand samples subjected to cyclic triaxial loading. Canadian Geotechnical Journal, 53(12), 1939-1951.

[55] Lo Presti, D. C. F. 1989. Proprieta dinamiche dei terreni. Atti delle conferenze di geotecnica di Torino, vol.2, pp.1-62.

[56] Ma, W. and Chang, X. 2002. Analyses of strength and deformation of an artificially frozen soil wall in underground engineering. Cold Reg. Sci. Technol. 34(1): 11–17.

[57] Maqbool, S. 2005. Effects of compaction on strength and deformation properties of gravel in triaxial and plane strain compression tests. PhD thesis. The University of Tokyo, Japan.

[58] Nishimura, S., Gens, A., Olivella, S. and Jardine, R.J. 2009. THM-coupled finite element analysis of frozen soil: formulation and application. Geotechnique 59(3): 159–171.

[59] Parameswaran, V. R. 1980. Deformation behaviour and strength of frozen sand. Canadian Geotechnical Journal. 17(1): 74–88.

[60] Parameswaran, V. R. and Jones, S. J. 1981. Triaxial testing of frozen sand. Journal of Glaciology, 27(95), 147-155.

[61] Perzyna, P. 1963. The constitutive equations for rate sensitive plastic materials. Q. Appl. Math. 20: 321– 332.

[62] Rist, M.A. and Murrell, S.A.F. 1994. Ice triaxial deformation and fracture. J. Glaciol. 40: 305–318.

[63] Richardson A.M. and Whitman R. V. 1963. Effect of strain-rate upon undrained shear resistance of a saturated remoulded fat clay. Geotechnique, 13(4): 310-324.

[64] Sayles, F. H. and Epanchin, N. V. 1966. Rate of strain compression tests on frozen Ottawa sand and ice. US Army CREEL, Tech. Note, Hanover.

[65] Sayles, F.H. 1973. Triaxial and creep tests on frozen Ottawa sand. In: Proc. Of the North American Contribution to the 2nd Int. Permafrost Conf., National Academy of Sciences, Washington, DC. pp. 384–391.

[66] Sayles, F.H. and Haines, D. 1974. Creep of frozen silt and clay. USACRREL Tech. Rep. 252.

[67] Sharma, S. S. and Fahey, M. 2003. Degradation of stiffness of cemented calcareous soil in cyclic triaxial tests. Journal of Geotechnical and Geoenvironmental engineering. 129(7): 619–629.

[68] Smith, M.W. and Tice, A.R. 1988. Measurement of the unfrozen water content of soils: A comparison of NMR (Nuclear Magnetic Resonance) and TDR (Time Domain Reflectometry) methods. In: Proc. of the 5th Int. Conf. on Permafrost, Trondheim, Norway. pp. 473–477.

[69] Šuklje, L. 1957. The analysis of the consolidation process by the isotache method. In: Proc. of the 4th Int. Conf. on Soil Mechanics and Foundation Engineering, London. pp. 200–206.

[70] Tatsuoka, F. & Shibuya, S. 1992. Deformation characteristics of soils and rocks from field and laboratory tests. Keynote Lecture. Proc. 9th Asian Conf. Soil Mech. Found. Engng, Bangkok2, 101–170.

[71] Tatsuoka, F., Sato, T., Park, C.-S., Kim, Y.-S., Mukabi, J. N., and Kohata, Y. 1994. Measurements of elastic properties of eeomaterials in laboratory compression tests, Geotechnical Testing Journal, GTJODJ, Vol. 17, No. 1, March 1994, pp. 80-94.

[72] Thomas, H. R., Cleall, P. J., Li, Y., Harris, C., and Kern-Luetschg, M. 2009. Modelling of cryogenic processes in permafrost and seasonally frozen soils. Geotechnique, 59(3), 173-184.

[73] Ting, J.M., Torrence Martin, R. and Ladd, C.C. 1983. Mechanisms of strength for frozen sand. J. Geotech. Eng. 109(10): 1286–1302.

[74] Tsutsumi, A. and Tanaka, H., 2011. Compressive behavior during the transition of strain rate. Soils and Foundations 51 (5), 813–822.

[75] Tsutsumi, A. and Tanaka, H. 2012. Combined effects of strain rate and temperature on consolidation behavior of clayey soils. Soils Found. 52(2): 207–215.

[76] Vaid Y P, Campanella R G. 1977. Time-dependent behavior of undisturbed clay. Journal of Geotechnical and Geoenvironmental Engineering, 103(ASCE 13065).

[77] Vardanega, P. J., & Bolton, M. D. 2013. Stiffness of clays and silts: Normalizing shear modulus and shear strain. Journal of Geotechnical and Geoenvironmental Engineering, 139(9), 1575-1589.

[78] Viggiani, G. and Casini, F. 2015. Artificial ground freezing: from applications and case studies to fundamental research. In: Proc. of the XVI ECSMGE: Geotechnical Engineering for Infrastructure and Development. pp. 65–92.

[79] Wang, D., Ma, W. and Chang, X. 2004. Analyses of behavior of stress–strain of frozen Lanzhou loess subjected to K0 consolidation. Cold Reg. Sci. Technol. 40(1): 19–29.

[80] Wang, D. Y., Zhu, Y. L., Ma, W., & Niu, Y. H. 2006. Application of ultrasonic technology for physical–mechanical properties of frozen soils. Cold Regions Science and Technology, 44(1), 12-19.

[81] Wang, D., Ma, W., Wen, Z. and Wu, Z. 2007. Stiffness of frozen soils subjected to K0 consolidation before freezing. Soils and foundations. 47(5): 991–997.

[82] Wang, D., Ma, W., Wen, Z. and Chang, X. 2008. Study on strength of artificially frozen soils in deep alluvium. Tunn. Undergr. Space Technol. 23(4): 381–388.

[83] Wang, Lina, et al. 2014. Accumulative plastic strain of frozen silt clay under cyclic loading. In: Applied Mechanics and Materials. Trans Tech Publications, p. 38-42.

[84] Wang, J. and Nishimura, S. 2015. Mechanical behavior of frozen clay under constant-and varying-temperature and strain rate shear. Jpn. Geotech. Soc. Spec. Publ. 1(2): 6–11.

[85] Watanabe, K. and Wake, T. 2009. Measurement of unfrozen water content and relative permittivity of frozen unsaturated soil using NMR and TDR. Cold Reg. Sci. Technol. 59(1): 34–41.

[86] Watson, G. H., Slusarchuk, W. A., and Rowley, R. K. 1973. Determination of some frozen and thawed properties of permafrost soils. Canadian Geotechnical Journal, 10(4), 592-606.

[87] Williams, P.J. 1964. Unfrozen water content of frozen soils and soil moisture suction. Geotechnique 14(3): 231–246.

[88] Xu, G. 2014. Hypoplastic constitutive models for frozen soil. Ph.D. dissertation, University of Natural Resources and Life Sciences, Vienna, Austria.

[89] Yamamoto, Y. and Springman, S.M. 2014. Axial compression stress path tests on artificial frozen soil samples in a triaxial device at temperatures just below 0 C. Can. Geotech. J. 51(10): 1178–1195.

[90] Yang, Z.J., Still, B. and Ge, X. 2015. Mechanical properties of seasonally frozen and permafrost soils at high strain rate. Cold Reg. Sci. Technol. 113: 12–19.

[91] Yimsiri, S. 2001. Pre-failure deformation characteristics of soils: Anisotropy and soil fabric. PhD thesis. Univ. of Cambridge, U.K.

[92] Yin J H, Zhu J G, Graham J. 2002. A new elastic viscoplastic model for time-dependent behaviour of normally and overconsolidated clays: theory and verification. Canadian Geotechnical Journal, 39(1): 157-173.

[93] Zhang, L., Li, Z., Jia, Q. and Huang, W. 2012. Experimental study on uniaxial compressive strength of reservoir ice. Trans. Tianjin Univ. 18: 112–116.

[94] Zhang, S., Du, H. and Harbor, J. 2016. The effect of confining pressure and water content on compressive strength and deformation of ice‐rich silty sand. Permafrost and Periglacial Processes.

[95] Zhang, T., Parsons, M.A. and Barry, R.G. 2006. Statistic of global permafrost distribution. Asian Conference on Permafrost. Lanzhou, China. pp. 7–8.

[96] Zhou, Y. W., Guo, D. X., Qiu, G. Q., Cheng, G. and Li, S. D. 2001. Geocryology in China. Permafrost and Periglacial Processes. 12(3): 315–322.

[97] Zhu J G, Yin J H. 2000. Strain-rate-dependent stress-strain behavior of overconsolidated Hong Kong marine clay[J]. Canadian Geotechnical Journal, 37(6): 1272-1282.

[98] Zhu, Y. and Carbee, D.L. 1984. Uniaxial compressive strength of frozen silt under constant deformation rates. Cold Reg. Sci. Technol. 9(1): 3–15.

LIST OF NOTATION

c_f: Intercept of the Critical State Line for frozen soil

c_u: Undrained shear strength

e: Void ratio

e_c: Void ratio after the normal consolidation

f: Expansion coefficient of the void ratio due to undrained freezing

K_0: Coefficient of earth pressure at rest

M_f: slope of the Critical State Line for frozen soil

P: Pressure

p': Effective mean stress

p_c': Maximum effective mean stress after the normal consolidation

p_i: Ice pressure

p_l: Liquid pressure

q: Deviator stress

q_{max}: Maximum deviator stress

q_i: Ice strength

s: Suction stress

T: Temperature

T_0: Reference temperature

T_f: Freezing temperature

w: Water content

w_u: Unfrozen water content

α_T: Slope in the normalized c_u line

$\alpha_{\dot{\varepsilon}}$: Slope in the normalized c_u line

ε_a: Axial strain

$\acute{\varepsilon}_0$: Reference strain rate

$\acute{\varepsilon}_a$: Axial strain rate

$\acute{\varepsilon}_{a0}$: Reference axial strain rate

σ: Total stress

σ_{li}: liquid water-ice water surface tension

σ_{v0}': Vertical effective preconsolidation pressure

σ_n: Net stress